Earthquake Performance of Long-Span Arch Culverts

December 2008

Research Report 366

Earthquake Performance of Long-Span Arch Culverts

G J Fairless, Opus International Consultants, Hamilton
D Kirkcaldie, Opus International Consultants, Wellington

NZ Transport Agency Research Report 366

ISBN 978-0-478-33472-2 (paperback)
ISBN 978-0-478-33471-5 (PDF)
ISSN:1173-3756 (paperback)
ISSN 1173-3764 (PDF)

Private Bag 6995, Wellington 6141, New Zealand
Telephone 64 4 894 5400; Facsimile 64 4 894 6100
Email: *research@nzta.govt.nz*
Website: *www.nzta.govt.nz*

Fairless, G.J.[1], Kirkcaldie, P.[2] 2008. Earthquake Performance of Long Span Arch Culverts. NZ Transport Agency Research Report 366. 150 pp.

1 Opus International Consultants, Hamilton
2 Opus International Consultants, Wellington

Keywords: arch, corrugated, culvert, design, earthquake, FLAC, large-span, modelling, New Zealand, numerical, performance, seismic, steel,

An important note for the reader

The NZ Transport Agency is a Crown entity established under the Land Transport Management Amendment Act 2008. The objective of the NZ Transport Agency is to undertake its functions in a way that contributes to an affordable, integrated, safe, responsive and sustainable land transport system. Each year, the NZ Transport Agency invests a portion of its funds on research that contributes to this objective.

This report is the final stage of a project commissioned by Land Transport New Zealand before 31 July2008 and is published by the NZ Transport Agency.

While this report is believed to be correct at the time of its preparation, the NZ Transport Agency, and its employees and agents involved in its preparation and publication, cannot accept any liability for its contents or for any consequences arising from its use. People using the contents of the document, whether directly or indirectly, should apply and rely on their own skill and judgement. They should not rely on its contents in isolation from other sources of advice and information. If necessary, they should seek appropriate legal or other expert advice in relation to their own circumstances, and to the use of this report.

The material contained in this report is the output of research and should not be construed in any way as policy adopted by the NZ Transport Agency but may be used in the formulation of future policy.

Acknowledgments

The author would like to acknowledge the contributions made to this project by the peer reviewers, Howard Chapman and Dr John Wood. They were involved at various stages in the project, reviewing and discussing the work and results as it progressed. Their inputs have been invaluable.

Contents

Executive summary

Large-span multi-plate corrugated metal arch culverts have proved to be an economical solution for many stream crossings in New Zealand and have also been used for a number of railway overpass structures, where they are especially economic in situations where the angle between the road alignment and the railway is nearer 45° than 90°. Few complete seismic design guides are available for these structures and no comprehensive study of the earthquake performance of large-span arch culverts has been reported.

One failure of a large span culvert in New Zealand has been caused by seismic shaking. The low failure rate is possibly caused by the low level of shaking that most of the culverts have experienced. In North America, such culverts are common and most have performed well in earthquakes, as long as the foundation conditions are uniform (not over a fault or a change in stiffness) and the surrounding soil does not liquefy.

Numerical modelling has been carried out in 2005–2007 to investigate the seismic performance of an 11.66 m span, 7.29 m rise high profile arch culvert. The finite difference code FLAC was used. Models were constructed in sequence, as they would be on site. The horizontal components of three earthquakes were used, scaled for Wellington conditions for 1:500 and 1:2500 year recurrence intervals. The effects of a number of parameters were tested by varying their values. These parameters were the soil shear strength, dilation angle and stiffness (measured as the shear wave velocity), the cover over the culvert, the presence and size of concrete stiffener beams, and whether or not slipping occurred between the soil and the culvert. The relationships between earthquake peak ground velocity, peak ground acceleration and the Arias Intensity, and between seismic deformation, structural bending moments and axial forces (also called thrusts) were examined.

Concrete rectangular and circular tunnels are often designed using a racking (for rectangular) or ovalling (for circular tunnels) method, where the shear across the entire section (racking or ovalling) is used in the design of the structural components. This shear is proportional to the peak ground velocity. Our models found that the peak ground velocity was not a very representative seismic design parameter for large span culverts, so the ovalling design method appears to be not very appropriate either. The peak ground acceleration was found to be more clearly related to the maximum bending moment and the maximum thrust.

Soil friction and cohesion were the parameters that most affected structural bending and thrusts. Soil stiffness was less important and soil dilation was a little less important than soil stiffness. However, footing thrusts increase far more with earthquake shaking for high-friction soil backfill than for low-friction soil.

Maximum structural seismic bending moments were usually controlled by the maximum construction bending moments, which were at the crown because of peaking. Stiffening

beams significantly reduce peaking, which results in lower bending moments in the crown than when stiffening beams are not used. Beams were associated with significantly less increase in seismic axial force in the culvert between the top and bottom of the beams, and thus between the upper and lower parts of the culvert. This latter effect is the current purpose of using stiffening beams in design.

Abstract

Dynamic numerical modelling has been carried out in 2005–2007 to investigate the seismic performance of an 11.66 m span, 7.29 m rise, high profile arch culvert. The horizontal components of three earthquakes were used, scaled for Wellington conditions for 1:500 and 1:2500 year recurrence intervals. The effects of a number of parameters were tested by varying their values. These parameters were the soil shear strength, dilation angle and stiffness (measured as the shear wave velocity), the cover over the culvert, the presence and size of concrete stiffening beams and whether or not slipping occurred between the soil and the culvert. Seismic deformation, structural bending moments and axial forces were examined, along with their relationship to earthquake peak ground velocity, peak ground acceleration and the Arias Intensity. It was found that the peak ground velocity and therefore the ovalling of the culvert were not useful in design. Soil shear strength (friction angle and whether it was cohesive or not) affect maximum seismic structural bending moments and thrusts more than soil stiffness. Maximum structural seismic bending moments were usually controlled by maximum construction bending moments.

1. Introduction

1.1 Purpose of the research

Large-span multi-plate corrugated metal arch culverts have proved to be an economical solution for many stream crossings in New Zealand and have been used for a number of railway overpass structures, where they are especially economic in situations where the angle between the road alignment and the railway is nearer 45° than 90°. As railway or road overpasses, these structures are required to maintain a clearance envelope from the railway or road passing through them.

Corrugated metal structures with spans greater than 1500 to 2000 mm (depending on shape) are denoted as Class 2 structures by AS/NZS 2041:1998. Figure 1.1 shows typical shapes of large-span multi-plate culverts and Figure 1.2 shows typical corrugation dimensions. Plate thickness for large-span culverts varies with span, cover and live load; typically, it is 3.0, 5.0, 7.0 or 8.0 mm. Culverts are constructed of galvanised steel or aluminium. Since 1998, at least 35 structures with spans greater than 3.0 m have been constructed in New Zealand:

- 6 Superspan structures (span greater than 6.0 m),
- 19 arch structures, and
- 21 pipe arch structures.

The Civil Defence and Emergency Management Act 2002 (New Zealand Government 2002) requires that utility operators including road controlling authorities manage the risks to their road networks to ensure that they can be brought back into service to the fullest extent possible after hazard events. Failures of some culverts in overseas earthquakes, the increasing use of such culverts as economic alternatives and the increasing span of culverts being used all raise concerns that these structures may be increasing the risk to the road and rail transportation networks. In the event of one of these structures suffering permanent deformation to the extent that the Ontrack (New Zealand Railways Corporation) clearance envelope around the railway track is intruded into, it is to be expected that Ontrack will require the structure to be rectified quickly or, if that is not possible, removed.

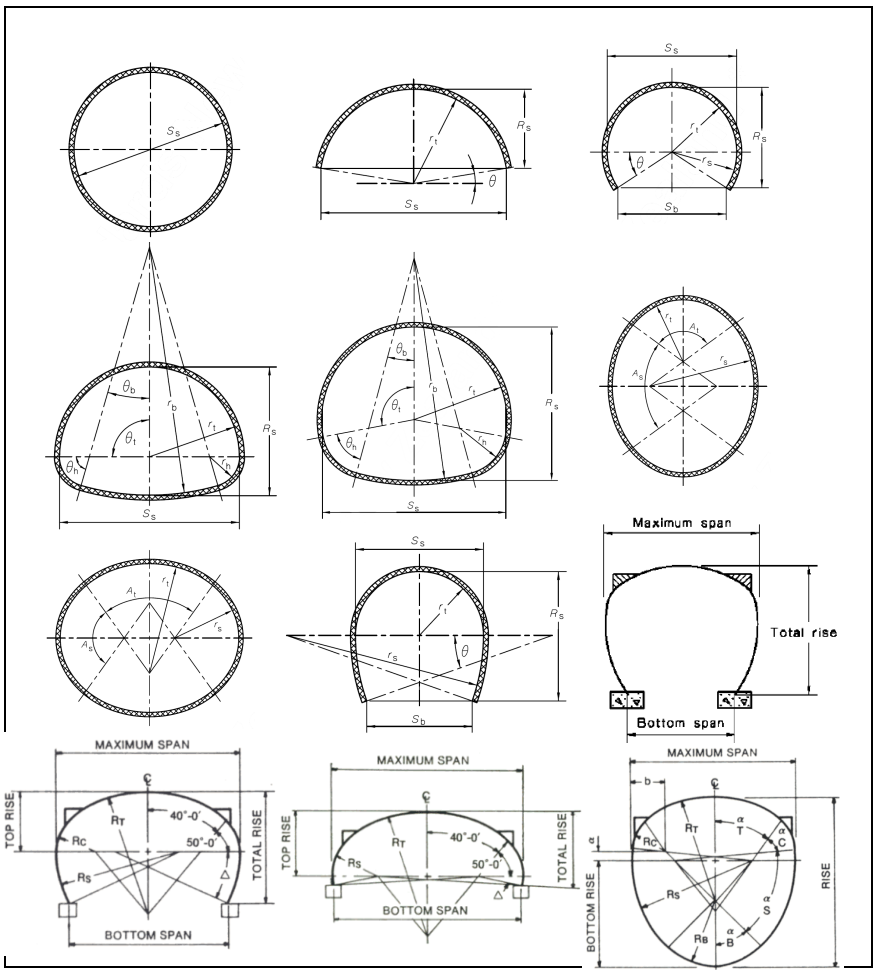

Figure 1.1 Superspan and large-span culvert shapes.
From top left to right: circular, arch (rise less than or equal to radius), horseshoe arch, pipe-arch, underpass, vertical ellipse; horizontal ellipse and elliptical arch (from AS/NZS2041:1998); pear arch (from AS3703:1989); high profile arch (a development of the pear arch); low profile arch, inverted pear shape (from CSP Pacific 2008).

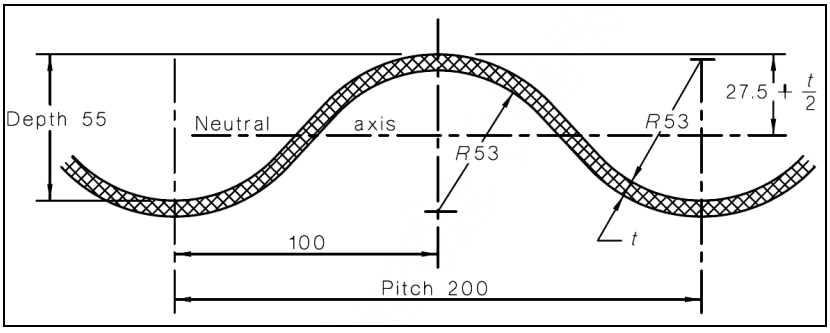

Figure 1.2 Typical corrugation details for large-span culverts (from AS/NZS 2041:1998).

Notes to Figure 1.2:
Units are millimetres.
Corrugations are designated as pitch by depth.

No report has been found of a comprehensive study of the earthquake performance of large-span arch culverts and few complete seismic design guides are available for these

structures[1]. Limited research in Canada indicates that these structures can be analysed using numerical modelling to study seismic effects. Currently, in the United States, the American Association of State Highway and Transportation Officials (AASHTO) load and resistance factor design (LRFD) Bridge Design Specifications for culverts and buried structures make no seismic provisions, except for a general requirement stating that 'earthquake loads should be considered only where buried structures cross active faults'[2]. The U.S. Transportation Research Board currently has a project (NCHRP 12-70) with the objective of 'develop[ing] analytical methods and recommended LRFD specifications for the seismic design of retaining walls, buried structures, slopes, and embankments'. The shortcomings of the current design methods were identified in the interim progress report, including

- the AASHTO 'no-analysis required' criterion proposed for bridge structures may not be applicable to large-span culvert structures;
- existing design and analysis procedures were developed typically for long, linear structures, whereas for most highway applications, the culvert or pipe is of limited length;
- existing design and analysis procedures were developed typically for the level ground condition, rather than a built-up embankment;
- the effect of soil overburden thickness (or embedment depth) is not well understood;
- the effect of the vertical components of ground shaking on culvert performance is not well understood;
- transient ground deformations cause three types of culvert deformations: axial, curvature and ovalling (for a circular cross-section) or racking (for rectangular cross section). Observations have suggested that smaller diameter pipes or highway culverts are more resistant to ovalling deformations than large size culverts, but large culverts have performed better than small diameter pipes under the effects of axial and curvature deformations; and
- simplified ovalling and racking analysis procedures developed for tunnel structures can be applied to large-span circular and rectangular culverts, respectively, but have not been adapted to non-circular and non-rectangular sections (for example, ellipse, arch, arch top three-sided, etc.).

Culverts are becoming larger as well. It is understood the suppliers are developing culverts with maximum spans twice the current maxima.

The purpose of this research project is to develop a methodology and a model to assess the performance of arch culverts in earthquakes. Ultimately, the research should be extended to assess the stability, safety and deformation characteristics of buried arch

[1] The Canadian Highway Bridge Design Code, CAN/CSA-S6-00, Section 7 – Buried Structures (Canadian Standards Association 2000) contains some guidelines on seismic design. Horizontal accelerations are said to increase moments; vertical accelerations to increase the thrust. AS3703.2:1989 contains no seismic consideration. Guidelines have been prepared by a working group of the French Association of Seismic Engineering and the French Tunnelling Association (2001), based on the work of Peck et al (1972). DR04421 CP (2004) includes seismic considerations, using ring theory.

[2] Extract from the NCHRP 12-70 Interim Report, early 2006, received by personal communication from David Beal, Officer in Charge at United States Transportation Research Board.

structures under different earthquake intensities to provide a basis to develop design criteria and requirements. In due course, this will lead to criteria that will be included in the Transit Bridge Manual and the joint Australian–New Zealand standard AS/NZS 2041 Buried Corrugated Metal Structures, for which input on earthquake design was sought by the standards committee from Transit New Zealand[3].

The research has been supported by a number of local authorities and the NZ Transport Agency (NZTA), who manage road networks.

1.2 Objectives

The objective of the research is to begin developing design criteria to ensure that long-span culverts are designed and constructed in a manner that provides for reliable performance in severe natural hazard events such as earthquakes.

1.3 Location of study

The research was carried out in 2005 to 2007 by Opus International Consultants Limited in their Hamilton and Wellington offices in New Zealand. The work relates to the seismic setting of New Zealand.

1.4 Steering group

Support for the project was received from a steering group consisting of the following people and organisations:

- Frank McGuire – formerly working for Transit New Zealand and currently a private consultant,
- Walter Rushbrook – Ontrack (New Zealand Railways),
- Ron Muir – The Hutt City Council,
- Ray Cannon – Tararua District Council, and
- Sue Walker – CSP Pacific.

This group represents several road controlling authorities, Ontrack (New Zealand Railways Corporation) – a party affected by these structures being used to bridge over its facilities – and CSP, the principal supplier in New Zealand of materials for construction of these structures.

[3] On 1 August 2008, Transit New Zealand and Land Transport New Zealand merged to establish the NZ Transport Agency.

1.5 Report outline

The project was carried out in several stages. This report discusses each of those stages as follows:

- observation of how large-span culverts in New Zealand have performed in past earthquakes (Chapter 2);
- literature search to review seismic design theory and practice applied to these structures, and research into their seismic performance (Chapter 3);
- design of the system to be modelled, including selection of the design characteristics of the culvert, soil properties and earthquake motions (Chapter 4);
- model development and calibration, in which the numerical model was developed and calibrated using known parameter values from previous studies or performance observations (Chapters 4 and 5); and
- numerical analysis and interpretation of results (Chapters 5 and 6).

The draft report was subjected to external peer review by:

- Howard Chapman, BSc (Hons, Civil Eng), MIPENZ, MICE, MIStructE, LifeMNZSEE; and
- Dr John Wood, BE (Hons), ME (Dist), PhD, MIPENZ, LifeMNZSEE.

Discussions were held with the peer reviewers at various stages in the work.

2. Observed performance of large-span culverts in New Zealand

It is difficult to determine from NZTA's Bridge Descriptive System (BDS) how many large-span culverts made from corrugated steel can be found on the road network. A number of searches of the database were carried out using different key words. Searches for 'arch' in the Type field or 'multiplate' in the material field returned 188 records. For most of the culverts and arches recorded in the BDS, it is not possible to obtain the span and rise from the database. The 'Drawings Comment' field contains 23 entries giving culvert type or size; of those, the largest appears to be a 7.5 m diameter pipe. The database lists 57 arch type culverts, one horseshoe arch, 78 pipes and 50 pipe arches. The 'fill depth' is given for 178 of the 188 records and ranges from 0.3 m to 22.0 m. 'Foundations' are given as driven steel piles for two arch culverts, 'other' for 35 culverts, and 'spread footings' for 106 culverts, of which 65 are shown as arches or pipe arches, and 41 as pipes.

We know of one failure (Sergeants Culvert on State Highway (SH) 52 near Wimbledon, listed in Table 2.1) that was probably the result of seismic shaking. The culvert invert and crown elevations were measured by Tararua District Council after the Weber earthquakes but no record of the as-built shape of the culvert could be found. Deformations included up to 75 mm of sag in the invert and up to 192 mm of sag in the crown relative to the invert (i.e. reduction of diameter). These values represent about 1.9% and 4.8% of the nominal diameter (3.980 m) respectively. No measurements of the horizontal diameter seem to be made at that time. The failure was near mid-span, caused by rolling in combination with the sag in the crown that opened the plate overlap joints there, resulting in a number of bolts pulling through the 3 mm thick plates (McCarten, pers. comm. 2007). It appears likely that structural failure followed settlement and some loss of support of the culvert sides.

As far as we have been able to ascertain, no other structural problems have been recorded with seismic shaking of large-span culverts in New Zealand. This may be a result of the low level of shaking they have experienced – see Table 2.1, where the maximum shaking at the 22 culverts listed was Modified Mercalli intensity (MM) VII (Waima overpass) although it may be MM VIII at Sergeants culvert (see Note 2 in Table 2.1). The shaking intensity was obtained by a search of the Geological and Nuclear Sciences Ltd (GNS) felt intensity database with shaking above MM VI captured. Culverts with a question mark were not included in the search – those culverts were discovered after the search had been done. Some of the data about the culverts came from NZTA's bridge database, but it is not fully maintained and other sources of data have been necessary.

The MM shown in Table 2.1 is a measure of the felt intensity and general damage caused by earthquake shaking. Pseudo-static seismic design uses peak ground accelerations (PGAs). Correlations between the two are approximate and are shown in Note c in Table 2.1.

Table 2.1 A selection of large-span culverts in New Zealand and the earthquakes they have survived, sorted by their north co-ordinate.

Name, location and designer	Details	mN[a] mE[b] NZMG[c]	Built	Earthquake shaking experienced ≥ MM VI[d]. Date, MM (magnitude)
Ngataki Stream Culvert ID 31483, BSN569 SH 1N RP 44/12.95	• 9 m span, • ≈4.5 m rise, • 15.2 m long, • skewed, • arch, • straight culvert with no road deck gradient. • 0.3 m cover with reinforced concrete slab added over the fill ca. 1998.	6718505 2515150	1975	?
Wairoro Stream Culvert ID 35233, BSN88 SH 12 RP 0/8.77 (Kaikohe)	• 7 m span, • 2.97 m rise, • cover 1.2 m, • 23 m long, • arch, • skewed.	6644750 2584510	1999	?
Merowharara Stream Culvert. ID 32238, BSN1001 SH 12 RP 89/11.10	• 5.25 x 2.25, • 4 m cover, • 11.1 m long, • pipe arch.	6615340 2562640	1984	?
Te Wharau Rail Overbridge SH 14 RP 44/4.30 ID 32301, BSN483 Opus Whangarei design	• 5.9 m span, • 5.4 m rise, • 30.2 m^2 area, • arch on spread footings, • 32.2 m long, • 1 m cover, • small skew	6591125 2591070	1980	?
Awaroa Coal Field haul road over Rotowaro Road. Opus Hamilton design	• 12.43 m span, • 9.32 m rise ellipse, • 3.0 m cover, • 7 mm plate, • 79 m on invert, • 1.5:1 end walls with 1.5 m vertical end at base, • no skew, • live load pressure 55 kPa (strain gauges fitted after construction and live load testing carried out).	6398325 2693390	2006	None
Whitehall Quarry haul road over Karapiro Stream. Opus Auckland/CSP design, Opus Hamilton headwalls	• 8.0 m span, • 3.64 m rise, • 2 m cover, • 1:1 ends, • no skew, • 30 m long on invert, • part circular arch.	6365220 2735870	2006	None
Sainsbury Road (over Ngaparierua Stream?), Pirongia	• circular 7 m diameter? • deep gully[f]	6354800 2702650	≈1985?	1997 May 25, VI (M7.9) 2000 Aug 15, VI (M7.6)

Table 2.1 (cont.) A selection of large-span culverts in New Zealand and the earthquakes they have survived, sorted by their north co-ordinate.

Name, location and designer	Details	mN[a] mE[b] NZMG[c]	Built	Earthquake shaking experienced ≥ MM VI[d]. Date, MM (magnitude)
Albert Park Drive over Mangaohoi Stream, Te Awamutu ID 35555 SH 3 RP 16/10.42	• 10 mm plate, • 8.16 span, • 4.61 rise, • pipe arch, • cover 1.0, • 27.4 m on bottom, • 2:1 ends, • skewed, • in stream bed	6352355 2714815	2000	2000 Aug 15, VI (M7.6)
Puketutu Rail Overpass SH 30 over NIMT RP 14/00 ID 33108, BSN140 Opus Hamilton design	• 7.2 span, • 5.3 rise, • arch, • 13 m long at top, • 30 m at base, • 1.2 m cover, • spread footings	6305230 2705075	1987	1997 May 25, VI (M7.9) 2000 Aug 15, VI (M7.6)
Tahora Rail Overpass SH 43 over railway RP 65/15.13 ID 33443	• 1.7 m cover, • 36.9 m^2 waterway area arch, • spread footings, • 39.6 m long	6239700 2666290	1980	1997 May 25, VI (M7.9) 2000 Aug 15, VI (M7.6)
McKenzie's Rail Culvert SH 2 over rail RP 577/12.31	• arch, • 1.8 m cover, • spread footings, • 32.9 m long	6229985 2862920	1975	1984 Mar 08, VI (M6.4) 1985 Jul 19, VI (M5.7) 1991 Jul 12, VI (M6.2) 1993 Aug 10, VI (M6.3) 1997 May 25, VI (M7.9) 1999 Oct 25, VI (M7.0) 2000 Aug 08, VI (M6.2) 2000 Aug 15, VI (M7.6) 2006 Jul 08, VI (M5.4)
Kelly Street Bridge, Inglewood over the Waiongana-Iti Stream. Opus Wellington design	• 8.7 m span, • 3.33 m rise, • 7 mm plate, • 1.4 m cover, • part circular arch with concrete inverted L footings, • vertical ends, • no skew?	6226700 2614000	2005	None
Ngaere Overbridge SH 3 over railway RP 279/4.18 BCHF design	• 1 m cover, • elliptical arch, 1 • 25.8 m long, • 6.29 m span, • 5.77 m bottom span, • 5.95 m rise	6202695 2621845	1998	2000 Aug 15, VI (M7.6)
Waiouru Rail Overpass SH 1N over NIMT RP 815/2.35	• pipe arch, • 1.2 m cover, • spread footings, • 107.3 m long, • Armco type 46EA13	6186003 2739961	1999	1999 Oct 25, VI (M7.0) 2000 Aug 08, VI (M6.2) 2000 Aug 15, VI (M7.6)
Vinegar Hill Rail Overpass SH 1N over NIMT RP 885/3.25 Payne Sewell design	• pipe arch, • 2 m cover, • spread footings, • 35.8 m long, • Armco type 42EA12	6139350 2731700	1999	1999 Oct 25, VI (M7.0) 2000 Aug 15, VI (M7.6)

Table 2.1(cont.) A selection of large-span culverts in New Zealand and the earthquakes they have survived, sorted by their north co-ordinate.

Name, location and designer	Details	mN[a] mE[b] NZMG[c]	Built	Earthquake shaking experienced ≥ MM VI[d]. Date, MM (magnitude)
Sergeants Culvert, replaced a bridge on SH 52 on Wainui River ≈4 km west of Wimbledon. Designed Opus Napier. Under construction during first Weber earthquake. Rebuilt 1991 after second Weber earthquake.	• 4 m diameter, • 4 m of cover, • 33 m long, • Failed in second Weber earthquake. Culvert settled and moved (rolled), and pulled bolts through 3 mm plate. Ends rose above water.	6079045 2804118	1990	Weber earthquakes Feb 1990, MM VII? May 1990, MM VIII?[e]
Wainui Road Underpass, Lower Hutt 4 lanes over 1 lane	• curved, • 9.95 m span, • 5.72 m rise high-profile arch, • 6.81 m radius crown and lower walls, • 1.68 m shoulders, • trafficked cover of 1.5 m	5995570 2670910	1979?	1992 May 27, VI (M6.8) 1995 Mar 22, VI (M6.4) 2005 Jan 20, VI (M5.6)
Elevation Rail Overpass, south of Picton SH 1S over SIMT RP 0/2.91 Connell Wagner design	• 3.2 m cover, • multiplate arch, • 60.3 m long	5988380 2592570	2005	none
Utawai Underpass, Dashwood Pass SH 1S over SIMT RP 43/00 Connell Wagner design	• Superspan arch, • spread footings, • 60.0 long, • 0.71 m cover	5956035 2597590	2002	2005 Nov 01, VI (M4.8)
Waima Rail Overpass, north of Waima (Ure) River SH 1S over SIMT RP 73/10.79 Opus Nelson design	• arch, • 33.2 m^2 area, • 1 m cover, • spread footings, • 114 m long	5923900 2602720	1984	1992 May 27, VII (M6.8) 1995 Mar 22, VI (M6.4) 1998 Feb 24, VI (M5.2) 1998 Jul 30, VI (M4.4) 1999 Jul 18, VI (M4.7) 2002 Dec 24, VI (M5.0) 2003 Jul 14, VI (M4.6) 2005 Jun 23, VI (M5.0)
Quartz Reef Culvert SH 8 RP 271/17.46	• circular, • 6.3 m diameter, • covering fill 3 m.	5568765 2212790	1983	?
Waianakarua Rail Overbridge SH 1S RP 601/15.11	• horseshoe arch, • 7.1 m span, • 5.4 m rise, • cover 1.5 m, • ≈82 m long?	5549325 2335990	2005	?

Notes to Table 2.1:

a mN = metres north

b mE = metres east

c NZMG = New Zealand Map Grid

d Approximate correlations between MM and peak ground acceleration (PGA) are as follows:
- MM VI ≈ 0.06 to 0.07 g;
- MM VII ≈ 0.10 to 0.15 g;
- MM VIII ≈ 0.25 to 0.30 g.

e Intensities for shaking at Sergeants Culvert were found with reference to Downes (1995) and are probably not as reliable as the others found by GNS in searching their database of felt intensities.

f Source: personal communication from Bryan Hudson (Opus Tauranga; formerly of the Waipa District Council) August 2006.

3. Literature search

3.1 Keywords and topics searched

Topics and keywords searched to find appropriate literature for review comprised the following:

- reports of earthquake performance of structures that included large-span culverts and shallow tunnels;
- load testing of large-span culverts;
- design methods, including design codes;
- proposals for research work on design methods and codes; and
- numerical modelling of large-span culverts and of construction stresses, load testing and performance, including seismic performance.

3.2 Outline of search results

The literature search results can be categorised for discussion into the following broad divisions:

- seismic performance of culverts, long-span culverts and other underground structures;
- load tests on large-span culverts and numerical analysis to try to match the findings;
- numerical analysis of construction stresses and construction failures, including development of soil constitutive models; and
- design methods, including design standards and comparisons of methods used.

3.3 Seismic performance of buried conduits

A number of reports have been written on the seismic performance of underground structures, but few cover the performance of buried flexible culverts, pipelines or large-span culverts.

Davis & Bardet (2000) reported investigations and analysis of 61 corrugated metal pipes (CMPs) that were shaken by the 1994 Northridge earthquake in California. Thirty-two of them were greater than 1.07 m in diameter and the largest pipe was 4.78 m. One 2.4 m diameter pipe collapsed (Davis & Bardet 1998a & b), eighteen suffered no damage, three were not inspected and the remaining ten suffered minor damage. Of these, five suffered deformations. One sustained transverse deformations of 140 mm. Eleven 19 mm diameter bolts were sheared in another, with 100 mm lateral separation and 64 mm of vertical shortening following. This pipe also suffered a reduction in diameter of 200 mm in one direction over an 18 m length. These latter two pipes also experienced some longitudinal buckling. A third pipe suffered mainly superficial damage caused by soil movement. The fourth pipe was deformed prior to the earthquake and was damaged by settlement of the embedding soils during the earthquake. The fifth pipe buckled because of severe corrosion at the invert.

Davis & Bardet's analysis showed that the collapse and deformations in the first two damaged pipes were caused by pore pressure build-up in the embedding soils and the resulting reduction in their stiffness. Deformation in the other damaged pipes was caused by permanent ground deformation, settlement of poorly compacted embedding soils and corrosion. Thus no reported failure was caused by inadequate structural capacity, other than that caused by corrosion. They comment that most pipes showed signs of either transient or permanent deflections. The transient deformations, mainly at pipe joints, were visible as marks in the pipe coating. Permanent deformations included impact damage between segments and cross-sectional shape distortion, although the lack of pre-earthquake measurements made it difficult to determine if the latter pre-existed or resulted from the earthquake.

Byrne et al. (1996) comment that Californian culverts have generally performed well during earthquakes. They comment on the one exception, the collapse of the 2.4 m diameter culvert reported by Davis & Bardet that was probably affected by liquefaction of the surrounding soil. Culverts in California were not designed specifically to resist seismic shaking. Byrne et al. conclude that, based on experience in California and their analysis (reported in the paper), if a structure is properly designed and constructed to resist static loads, it is likely to resist earthquake shaking in excess of 0.3 g horizontally and 0.2 g vertically. This is equivalent to about MM VIII shaking, which is probably the maximum intensity of shaking experienced by a large-span culvert in New Zealand (see Table 2.1).

Allmark (2001) discusses observed seismic damage to buried structures but does not specifically mention large-span culverts, perhaps because they have performed well in general. He indicates that damage to cut and cover structures and culverts is of three major types: inadequate lateral design strength, construction practice not reflecting design assumptions, and poor layout of construction or seismic joints.

Samata et al. (1997) reported on damage to some subway structures during the 1995 Hanshin–Awaji earthquake in Japan. They focus on concrete box culvert structures with middle columns that failed; this type of failure had not been seen before. They used equivalent linear finite element response analysis to examine the causes of failure. They found response was governed by ground displacement.

Han et al. (2003) analysed seismic performance of buried pipelines. They started from the premise that breakage of joints by seismic wave propagation was the main damage mode. They report the main damage modes, all of which are more related to pipelines rather than large-span culverts.

Pineda-Porras & Ordaz-Schroeder (2003) examined damage to large-diameter buried pipelines in Mexico City's primary water system. They developed an empirical relationship to estimate earthquake damage to water pipelines the city. Pipe diameters were not mentioned and the criterion is one of damage or no damage. They were interested in the likely value of repairs after an earthquake.

Youd & Beckman (1996, 1997 and 2003) reported the performance of CMP culverts up to 3.6 m in diameter during earthquakes. They reviewed reconnaissance reports from six earthquakes and conducted field investigations in areas shaken by three of those earthquakes. The earthquakes ranged from the 6.7 magnitude quake in Northridge, California, in 1994 to the magnitude 9.2 Alaska earthquake in 1964. They closely examined 32 culverts, some of which are the same ones reported by Davis & Bardet (1998b, 1999, 2000), including the 2.4 m diameter pipe that collapsed and the 3.6 m culvert with headwall damage.

Damage was reported for only ten culverts and the seven most severely damaged culverts were at sites disturbed by ground failure. They discuss the types of ground failures involved (generally liquefaction or slope instability) and the damage they caused to each of these seven culverts. Of the ten culverts damaged, one collapsed, six were buckled or bent, one was pulled apart at the joints, and two were slightly damaged by fracture of headwalls. No purely structural failures were reported. They comment that hundreds of CMPs were located in the strongly shaken areas, and no others were reported as damaged in published reports or by people they interviewed. During their investigation, they drove by or over many of these culverts and examined some of them; they saw no evidence of damage, either to the culverts or to the road surfaces over them. In the full report (Youd & Beckman 1996), they conclude that where foundation conditions were stable, many CMP culverts (up to 6 m in diameter) were undeformed and undamaged, even in areas where ground shaking was intense (up to about 0.5 g).

In the 1999 Turkey earthquakes, a significant length of motorway ran within a few kilometres of fault rupture. No large-span corrugated metal culverts are mentioned in Earthquake Engineering Research Institute (EERI) (2003), but the motorways were said to include underpasses that were simple-span box-type structures with features similar to culverts. Many were undamaged after undergoing MM VIII and MM IX shaking. One collapsed tunnel is mentioned.

3.4 Summary of seismic performance

It is concluded from the literature search on seismic performance that long-span culverts generally perform well where foundation conditions are stable. Observers in California have found that CMP culverts up to 6 m diameter were undeformed and undamaged in areas where ground shaking was intense (up to about 0.5 g).

Failures and deformation observed at a few installations have been attributed to ground failure by slope instability, loss of embedding or foundation soil stiffness caused by increased pore pressures (approaching or including liquefaction), permanent ground deformation (such as by fault movement under the foundation) or settlement of embedding soil. In addition, a small number of failures have occurred where the structure was severely corroded, especially at the footing of an arch. Often, observers have commented that it is unclear whether deformation observed after an earthquake was present before the shaking.

3.5 Load tests

A number of researchers have reported measurements of deformation and strains on large-span CMP culverts. Construction, static load, live load and compaction effects have been examined.

Early tests, such as Demmin (1966), were used to develop design methods and demonstrate that the factor of safety on the load was adequate. These tests loaded a 6.27 m span, 4.01 m rise pipe arch to more than twenty times the design load without failure, although signs of distress appeared. Later tests, such as Seed & Ou's 1987 investigation of an 11.7 m span, 4.8 m rise low profile arch, studied compaction effects and used the tests to calibrate a finite element study on how compaction stresses develop in the culvert. Seed & Ou used a hyperbolic soil constitutive model that does not provide for soil dilation or post-peak softening, which would probably not be suitable for dynamic modelling.

Seed & Ou (1988) also reported finite element modelling of an 11.80 m by 4.82 m arch that had undergone unacceptable structural deformations. This culvert was similar to the one they discussed in their 1987 work. They used a hysteretic loading and unloading soil model to simulate compaction stresses, and showed that the unsatisfactory structural behaviour resulted from poor backfill compaction procedures.

Webb et al. (1999) reported construction and live load testing of a 9.5 m span low-profile CMP arch for the purpose of improving the LRFD design specifications. Seed & Raines (1988) discussed failures of three long-span culverts caused by exceptional vehicle loads and performed finite element modelling (using the hyperbolic soil constitutive model mentioned above) of the tests. The culverts were all corrugated aluminium. These included:

- a pipe arch of 8.66 m by 5.44 m,
- a pipe arch of 8.23 by 5.23 m, and
- a 4.48 by 1.25 m low rise arch.

Field evidence showed that the loads barely exceeded each culvert's structural capacity, although the loads far exceeded the design loads. A new empirical procedure was used to develop equivalent line loads for use in the finite element studies.

Moore & Taleb (1999) carried out finite element analyses of a 9.5 m span low-profile arch culvert loaded to its design limit, with minimal cover, and compared the results to Webb et al.'s field measurements.

In unpublished work, Opus Hamilton (New Zealand) recently carried out live load tests on a 12.43 m span, 9.32 m rise horizontal ellipse steel CMP, with the purpose of proving that the owner could use traffic loads greater than the design loads. A coal mine haul road passes over this culvert with 3.0 m of cover. The design live load was a 325 tonne dump truck and the test load varied up to 375 tonnes. A linear elastic finite element model was

calibrated on the field measurements and predictions were made regarding the effect of the truck being loaded to 400 tonnes or more.

McCavour et al. (1998) reported an investigation of soil–metal structure interaction for two 12 m span low-rise arch culverts with 300 mm cover. The culverts were the largest built up to that time and were erected as test culverts, each with a different density backfill and with a different type of crown reinforcement. Strain and deflections were measured in response to static axle loads at six locations on the culverts. Finite element models were developed in a non-linear soil–structure interaction program specifically developed for long-span soil–metal culverts. They reported that a definitive relationship was found between soil stiffness and metal structure stiffness.

In summary, the review revealed a number of static load tests and finite element simulations, but no reports of measurements using dynamic loads.

3.6 Numerical modelling

A number of numerical modelling studies have been reported. Generally, they were considering either the seismic performance of buried flexible pipelines of relatively small diameter or the performance of deeper structures such as tunnels. The performance at pipeline bends was of interest to some authors (for example, Ogawa & Koike 2001, Kan et al. 2005) and the performance of the pipeline in general to others (Babu & Rao 2003). The dynamic load on flexible buried cylinders investigated by Duns & Butterfield (1971) was from pressure waves on the ground surface, such as from a nuclear blast. Generally, these studies are considering plane stress models, where the pipeline or tunnel is long compared to its diameter. Thus the thrusts and moments discussed are within the plane of the model.

Byrne et al. (1996) carried out finite element analyses of a 10.5 m span, 5.2 m rise concrete arch, including horizontal and vertical seismic loading. They found significant increases in thrust and moment in the arch when the PGA was greater than 0.3 g. Their results indicated that for horizontal shaking, the surrounding soil was much stiffer than the arch and the loads are taken by the soil rather than the arch. Under vertical shaking, the arch was stiffer than the surrounding soil and attracted significant load. They suggest factoring the soil unit weight by an amount proportional to the vertical acceleration, which was implemented in the Canadian and draft Australian and New Zealand standards (see below). Byrne et al. comment that in California, where large-span culverts are not designed for seismic loads, they have performed well in shaking greater than 0.3 g PGA.

3.7 Seismic design methods

3.7.1 Abdel-Sayed et al. (1994): summary

As noted in Section 1.1, no comprehensive studies have been done on the effects of loads imposed by earthquakes on soil–steel bridges (their term for a large-span culvert). Abdel-Sayed et al. (1994) also say this then conclude that it seems reasonable that the response of a soil–steel bridge to seismic loads should not be very different from the response of an equivalent embankment without a conduit through it. Thus they recommend that the same considerations be given to large-span culverts. The most important requirement they identify is that the backfill soil and the engineered materials used in the bedding zones do not liquefy during the earthquake.

Abdel-Sayed et al. discuss three broad design methods for large-span culverts. They give no indication that any of them give specific consideration to seismic loads, unless they are hidden in the live load. The methods they discuss are:

- the Ontario Highway Bridge Design Code (Ministry of Transportation of Ontario 1992);
- AASHTO (1989) specifications method; and
- Duncan (1979) method.

Thrusts and bending moments considered are always circumferential (in the plane of the cross-section); longitudinal thrusts and moments are ignored.

The Canadian code (discussed below) refers to the Ontario code. The Ontario code requires consideration of only the ultimate limit state under one combination of dead and live loads. Thrust alone is considered for the conduit wall; bending moments are neglected.

The AASHTO method (1989) neglects bending moments, and considers only dead and live loads. Three possible modes of failure are considered:

- failure by crushing,
- failure by buckling, and
- failure of longitudinal seams.

Conduit wall thrust is calculated by ring compression theory. No specific allowance for seismic loads appears to be made. Abdel-Sayed et al. say that the AASHTO requirements for the design of soil–steel bridges are not explicit enough and require interpretation.

The Duncan method was derived for pipe structures made of corrugated aluminium sheets and is also applicable to the design of soil-steel bridges. The method disregards the failure of the conduit wall by buckling and controls the design through the formation of plastic hinges when the depth of cover is shallow, and through yielding by axial forces when it is deep (Abdel-Sayed et al., 1994). The structure is designed for two conditions: construction with the fill at crown level (no live load considered), and the completed structure. Moments and thrusts are calculated considering both live and dead loads in this case. This design method is likely to be conservative because the formation of one plastic

hinge will not cause failure, and even after several plastic hinges have formed in the conduit wall, the whole structure does not become unstable because the soil support restrains deformation. In addition, thrust and moment capacities are calculated using the yield stress, whereas steel hardens after yielding.

3.7.2 Canadian method

The Canadian Highway Bridge Design Code CAN/CSA-S6-00 (1992) gives seismic load requirements in section 7.5.5. The code provides for two types of large-span culvert: box structures, which are essentially a low-rise arch with vertical sides below the arch; and soil–metal structures, which include the other shapes shown in Equation 3.1. The commentary discusses the reasons for the seismic load requirements. Dynamic analyses are said to show that the horizontal component of earthquake shaking imposes significant additional moments in box structures. This cannot be incorporated easily into the design formulae, so they suggest that an additional seismic moment be included as:

$$M_E = M_D A_V \qquad \text{[Equation 3.1]}$$

where:

- M_D is the moment caused by dead load, and
- A_V is the vertical acceleration ratio, which is equal to two-thirds of the horizontal acceleration ratio (proportion of gravitational acceleration).

M_E is factored by κ (kappa) and (1- κ), and added to the factored crown and haunch bending moments respectively. κ is the crown moment coefficient and is given by an empirical relationship with the span: κ = 0.70-0.0328*span.

For soil–metal structures, thrust alone is the basis of design and the Canadian code commentary says that horizontal shaking has little effect on thrust. Thus they recommend the additional thrust caused by earthquake loading should be:

$$T_E = T_D A_V \qquad \text{[Equation 3.2]}$$

where T_D is the maximum thrust in the conduit wall per unit length caused by unfactored dead load. For the seismic load case, T_E is then added to the factored dead load thrust.

3.7.3 AASHTO developments

McGrath et al. (2002) reported a review and evaluation of the state of the art in design and construction of large-span reinforced concrete and metal culverts, investigated culvert behaviour through full-scale field tests and extensive computer modelling, and developed recommended specifications for design and construction. They found that current practice produced safe, reliable structures but considered that much of the success resulted from experience. Current design procedures were said to be not specific and they left many important structural details unspecified. In particular, procedures for metal culverts are largely empirical and do not address several key aspects of design, such as the role of stiffeners or the evaluation of moments that develop during construction or in shallowly buried structures subject to live load. The focus of their work was to develop a simplified procedure that would accurately model most culvert installations and be suitable for incorporation into AASHTO specifications, and to develop a comprehensive procedure that could be used for unusual installation or design conditions. They did not mention seismic loading at all in their report or design recommendations. Byrne et al. (1996), discussed in Section 3.3 above, observed that no specific seismic design of large-span culverts has been developed in California.

As discussed in Section 1.1 above, work is underway in the US to improve the AASHTO design standards for bridges including buried large-span culverts. The preliminary report for project NCHRP 12-70 has identified work requirements to do this (Beale, pers. comm.).

3.7.4 Australian and New Zealand standards

The Australian standard AS3703:1989 contains no reference to seismic design. The horizontal ellipse at Awaroa coal field (see Table 2.1) was designed to this standard.

AS/NZS2041:1998 says buried corrugated metal structures in backfills are not sensitive to earthquake effects. Seismic loads are only considered in situations when the backfill is prone to liquefaction; in that case, an 'arching factor' should be set to 1.0.

DR04421 (2004), the draft revised Australian/New Zealand standard for buried corrugated metal structures, takes a risk approach to setting seismic loads (Section E2.6). Criteria are given for determining whether seismic loads need to be considered. These criteria are:

- high importance, or
- lower importance with long design life in seismic areas, or
- if seismic design is required by another standard, or
- in special situations.

The code states that the calculation of earthquake action is for vertical loads resulting in wall compression and does not take account of lateral wall loads expected during an earthquake. The vertical stiffness of the structure is said to cause an increase in wall compression caused by the vertical component of shaking but the stiffness of the backfill limits the lateral loads applied to the structure. Factors are used in the formulation to

represent the relative stiffness of the metal structure wall with respect to the adjacent soil. Different factors apply to the upper and lower parts of the structure.

The commentary in Appendix E of the draft standard indicates that the geotechnical design of the foundations and backfill, including seepage compatibility with the surrounding soil, is most important. End stiffening is recommended in all seismic designs and typical details are given.

DR04421 uses the work of Byrne et al. (1996) (see Section 3.3) and the Canadian Highway Bridge Design Code (2000) in setting the seismic design requirements. Using the nomenclature of the Canadian code, A_V is two-thirds of the horizontal acceleration, which is derived using the seismic hazard analysis from AS/NZS1170.5 (2005). Where required, the extra pseudo-static seismic load is included in wall compression, connection and footing design.

3.7.5 The racking or deformation design method

Flexible buried structures are assumed to undergo the same deformations as the soil during seismic shaking. Rather than trying to estimate the loads on the structure from seismic forces, another way would be to consider the loads imposed on the culvert by deformation during the seismic shaking. It is postulated that rectangular structures will undergo a racking deformation under rising shear waves, while circular and elliptical structures will undergo ovalling deformation (Figure 3.1). This method has been postulated mainly for tunnels (which are long relative to their width or diameter) (e.g. Wood 2007, Wang 1993, Hendron & Fernandez 1983) and does not appear to have yet been developed for short, shallowly buried large-span culverts.

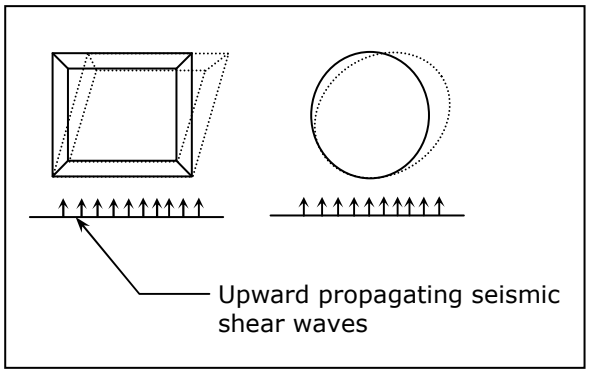

Figure 3.1 Diagrammatic representation of racking and ovalling with earthquake shaking. Rectangular sections become trapezoidal and circular sections become elliptical.

3.7.6 The racking method as described by Wang (1993)

Wang presents three design sequences, with variations within each. Others have presented some or all of the work earlier (e.g. Hendron & Fernandez 1983, Peck et al. 1972, St John & Zahrah 1987, Owen & Scholl 1981):

- **Free-field axial and curvature deformations (in terms of strain) in the soil** assuming upward propagation of shear waves, with maxima determined relative to a hypothetical tunnel centreline direction. This provides an upper-bound assessment of tunnel response and is applicable to a tunnel structure that is flexible relative to its surrounding medium.
- **Shear forces, bending moments and axial forces in the lining** calculated assuming a circular opening with full-slip or no-slip interaction between the soil and the lining. This is for when the tunnel structure is longitudinally stiff relative to the surrounding soils and thus resists deformations imposed by the ground. The tunnel–ground system is simulated as an elastic beam on an elastic foundation, with waves propagating upwards in an infinite, homogeneous, isotropic medium. Using examples, it is shown that these strains are not critical to the design of horizontally aligned tunnels.
- **Ovalling of circular openings caused by shear deformations propagating through the ground.** The tunnel lining conforms to free-field shear deformations. The results are cycles of additional alternating compressive and tensile stress in the lining, superimposed on the existing static state of stress in the lining. Vertically propagating shear waves are probably the most critical and predominant mode of seismic deformation in most situations. Cases include full-slip and no-slip between soil and lining, and different relative stiffnesses of the lining compared to the soil. Closed form solutions and design charts based on them are presented.

The ovalling effects are over- or under-estimated depending on the relative stiffness between the ground and lining, mainly because of the uncertainty in the lining–soil interaction conditions. Wang says that in most practical situations, the flexibility ratio is likely to be large enough that the tunnel-ground interaction can be ignored. Thus the distortions of the lining can be reasonably assumed to be the same as those of the perforated ground. The flexibility ratio is discussed further below.

Based on his work, Wang recommends that designers use the more conservative full-slip assumption for the lining–soil interface to calculate bending moments in the lining. The effects of site amplification need not be considered in that case. The same case is recommended for calculating the maximum lining distortion, although the lining distortion has relatively low sensitivity to the lining–soil interaction. The effects of stress amplification need not be considered using the full-slip interaction case.

In contrast, the full-slip condition is said to significantly under-estimate the lining thrust. Thus it is recommended that the no-slip equations be used, and factored by 1.15 to account for dynamic stress amplification caused by the opening in the ground.

All of Wang's discussion and recommendations were based on the assumption that the lining is a monolithic and continuous circular ring with intact, elastic properties. Many of the structures we are considering are not continuous; they are on spread footings and have no 'floor'. In addition, they are short.

3.7.7 Free-field shear distortion in the deformation design method

Arriving at the free-field shear distortion is one difficulty with the ovalling method. The seismic ground motion parameters used in the formulation are the shear wave velocity C_S (which is a soil property) and the maximum soil particle velocity V_S as the shear wave passes through the soil. These are used to calculate the maximum free-field shear strain in the soil, γ_{max}, as:

$$\gamma_{max} = \frac{V_S}{C_S}. \qquad \text{[Equation 3.3]}$$

The New Zealand loadings code, AS/NZS 1170:2005, makes no reference to the soil particle velocity. This code provides guidance on the design response spectrum (or spectra) to be used for a project, but gives no relationship between any of the spectral properties given and the maximum soil particle velocity. The American Lifelines Alliance (2005) provides the following equation for peak ground velocity (PGV) in cm/s:

$$PGV = \frac{\left(\left(\frac{386.4}{2\pi}\right) * SA_1\right)}{1.65} * F_V * 2.54 = 94.6 * SA_1 * F_V \qquad \text{[Equation 3.4]}$$

where:

- SA_1 is the spectral acceleration in g at 1 second period for 5% damping at rock sites
- F_v (the ground coefficient) is a scaling factor depending on the site and ground class, as per Table 3.1.

A lookup table is provided, as shown in Table 3.2, which is referred to for each possible source fault for earthquakes at the project site. American Lifelines Alliance (2005) provides extensive discussion of how to obtain and use PGVs.

3.7.8 Shear stresses in the lining or culvert

Wang's closed form solutions include use of 'flexibility' and 'compressibility' ratios to calculate tunnel lining stresses. These ratios were postulated and modified by various authors considering tunnelling (for example: Burns & Richard 1964, Höeg 1968, Peck et al. 1972, Einstein & Schwartz 1979, Wood 2007). They are functions of the elastic moduli of soil and lining, Poisson's ratios of soil and lining, and the moment of inertia and area (or thickness) of lining.

Table 3.1 Ground coefficients for scaling peak ground velocity (from American Lifelines Alliance 2005).

Ground class[a]	Subsurface profile name	Shear wave velocity m/s	Ground coefficient *Fv*				
			PGV ≤ 10 cm/s	PGV = 20 cm/s	PGV = 30 cm/s	PGV = 40 cm/s	PGV ≥50 cm/s
A	Hard rock	>1520	0.8	0.8	0.8	0.8	0.8
B	Rock	760–1520	1.0	1.0	1.0	1.0	1.0
C	Very dense soil and soft rock	360–760	1.7	1.6	1.5	1.4	1.3
D	Stiff soil	180–360	2.4	2.0	1.8	1.6	1.5
E	Soft soil[b]	<180	3.5	3.2	2.8	2.4	2.4
F	Very soft soil[c]		Note d	Note d	Note d	Note d	Note d

Notes to Table 3.1:

a The ground classes shown in the left-hand column are the US ground classes and do not match those in AS/NZS 1170.5 (2005). For example, classes A and B above are combined into class A in AS/NZS 1170.5.

b Includes any profile with more than 3 m of soil having the following characteristics:
- plasticity index (PI) >10;
- moisture content w ≥40%, and
- undrained shear strength Su <25 kPa.

c Includes soil profile having one or more of the following characteristics:
- soils vulnerable to potential failure or collapse under seismic loading such as liquefiable soils, quick and highly sensitive clays, collapsible weakly cemented soils,
- peats or highly organic clays (H >3 m of peat or highly organic clay where H = thickness of soil);
- very high plasticity clays (H >7.5 m with PI >75); or
- very thick soft or medium stiff clays (H >36 m).

d Site-specific geotechnical investigation and dynamic site response analyses are recommended to develop appropriate values.

Table 3.2 PGV to PGA ratios for source earthquakes (from American Lifelines Alliance 2005).

Soil classification	Ratio of PGV (cm/s) to PGA* (g) Source-to-site distance (km)		
Moment magnitude	**0–20 km**	**20–50 km**	**50–100 km**
Rock: A, B			
6.5	66	76	86
7.5	97	109	97
8.5	127	140	152
Firm soil: C, D			
6.5	94	102	109
7.5	140	127	155
8.5	180	188	193
Soft soil: E, F			
6.5	140	132	142
7.5	208	165	201
8.5	269	244	251

* Peak ground acceleration

The flexibility ratio relates the cross-sectional flexibility of the structural cylinder to the flexibility of a solid soil cylinder. The compressibility ratio is the cross-sectional compressibility of the steel cylinder relative to a solid soil cylinder. Höeg (1968) also proposed a compressibility ratio where the soil–cylinder interface has a compressible layer. Compressibility relates the support load to the relative support stiffness of the soil.

The various authors were considering different situations when deriving their ratios, but all were considering plane strain conditions where the tunnel is assumed to be long in proportion to its diameter. The cross-sectional moment of inertia and end area of the tunnel lining were considered per metre length of tunnel. For short large-span culverts, the ratios will not be strictly correct as plane stress conditions are more appropriate.

Burns & Richard's (1964) solution is applicable to elastically lined cylindrical openings under plane strain conditions in a linearly elastic ground mass. The lateral free-field ground stresses are restricted to a fixed function of the vertical stresses and Poisson's ratio. Höeg (1968) relaxed this constraint on the lateral stresses. This is the 'unperforated ground' or 'external loading' case, where the load is applied after the lining is installed. Peck et al. also developed this case. It assumes that the confining stresses are uniform all around the lining.

Einstein & Schwartz (1979) mention that finite element studies have shown that variations of stress with depth are important at depths of less than one tunnel diameter below the surface. They explore the 'excavation unloading' or 'perforated ground' condition that occurs with tunnelling.

The assumption of plane strain is appropriate for locations far from the ends or the tunnel face. Conditions are more complicated near the ends and tunnel face.

Hendron & Fernandez (1983) point out that the compressibility ratio has little effect on the dynamic behaviour of the liner. This is because the predominant earthquake motions are produced by shear waves, which primarily change the shape of the soil elements without changing the average principal stress.

Hendron & Fernandez (1983) also point out that the dynamic response of a lining in the soil has two parts: the distortions imposed by strains in the ground as the seismic waves pass, and the dynamic amplification of forces associated with a stress wave impinging on the opening.

DR04421 (2004) includes a flexibility ratio in the factor K_5 for calculating relative wall stiffness. K_5 includes the ratio of the culvert wall stiffness to the soil stiffness (Young's modulus) divided by the cube of the radius of curvature of the wall. The moment of inertia of the lining is per metre length of culvert. K_5 is used in determining the design capacity in compression of the wall of the metal structure. K_5 is related to either the square root or the fourth root (depending on the case) of the inverse of the Einstein & Schwartz (1979) flexibility ratio. The ratio EI/R^3 is related to the critical uniform pressure causing elastic buckling of a circular arch (Timoshenko & Gere 1961).

The 'flexibility number' n_f is found in DR04421. It is used in calculating the moment in the culvert wall caused by filling to the crown and to final cover depth in order to check for plastic hinge formation during construction, as per the Duncan method (see Section 3.7.1). N_f includes the ratio of soil stiffness to culvert wall stiffness times the cube of the effective horizontal dimension (span). This also is related to the inverse of the Einstein & Schwartz flexibility ratio.

The flexibility ratio equations in DR04421 do not include the relative Poisson's ratios of the soil and culvert material.

4. Modelling carried out

4.1 Scope

The approach of the modelling reported here was to examine a large-span arch culvert of the type used for overpasses under seismic shaking. The culvert modelled was the maximum span arch currently available. It is understood that culverts perhaps twice this span are under development by a supplier.

The purpose was to investigate the effect of a number of variables and modelling conditions on the forces and moments in the culvert. In addition, variables related to the deformation design method would be examined. Currently, seismic design of large-span culverts, when carried out, is by pseudo-statically derived forces.

The key issues to be considered included the effect of:

- small cover depth over the culvert,
- intensity of earthquake shaking,
- slip or non-slip condition of the backfill on the culvert wall,
- stiffening beams above the spring line,
- culvert deformation relative to the intensity of shaking, and
- culvert forces and moments relative to deformation.

4.2 Cases tested

A number of variables affect the seismic performance of large-span culverts. Some of them are shown in Table 4.1, which also indicates which were tested.

Table 4.1 Variables affecting culvert design and seismic performance.

Variables	Comments
Geometry of opening in the soil (culvert shape), including the radii of the plate bends	Not considered in this report. Only a high profile arch of 11.66 m span (10.00 m bottom span) was modelled.
Culvert size and length; hence span and rise, and the ratio between them	Not considered in this report. One size was considered.
Fill cover over the culvert.	Low cover depth may provide insufficient depth of cover to develop soil arching. Cover from 1 to 3 m was modelled.
Soil–structure interaction (slip or no-slip)	Both conditions modelled. Wang (1993) suggests that bending moments and lining distortion are found assuming no slip and that lining thrust is found using full slip. But he was probably assuming concrete lining.
Relative stiffness of soil and structure (flexibility ratio) and extensional stiffness of soil relative to the liner (compressibility ratio).	Perforated & non-perforated ground versions available. DR04421 (2004) gives flexibility factors for the upper and lower parts of structure. Three soil stiffnesses (measured as the shear wave velocity) were tested, but the culvert structural properties were not changed.
On-ground v. trench construction?	Not considered in this report. Culvert was constructed as if in an embankment of uniform height – thus the effect of road ramps up and over the culvert was not modelled.
Soil properties strength and volumetric behaviour (cohesion, friction angle, dilation angle)	Several values of each tested.
Earthquake properties, and relative effect of vertical and horizontal shaking.	Three records used, scaled to Wellington with R= 1.0 or 1.8 (a return period of 500 years or 2500 years). PGAs and PGVs were recorded. Vertical shaking was not modelled.
Site properties – depth of soil and amplification (ignore liquefaction and loss of strength, fault rupture under the culvert, change in foundation soil under the culvert).	Foundation depth was uniform but the elastic and plastic properties and stiffness of the soil were varied.
Skew relative to the alignment of embankment	Not considered in this report.
The presence of headwalls	Concrete headwalls will act as stiffeners at the ends of the culvert. Skewed culverts may also have ring beams on the battered or tapered ends. The culverts will be stiff and resistant to distortion at the ends. End effects will be important in relatively short culverts. Two-dimensional modelling is appropriate for the part of the culverts not near the ends.
The presence of stiffening beams	Are they beneficial in seismic shaking? When can they be omitted? Tested without stiffening beams and with beams at one location on each side, in three sizes.

4.3 Software used

FLAC (Fast Lagrangian Analysis of Continua) was used for the modelling. FLAC is a two-dimensional explicit finite difference program for engineering mechanics computations (Itasca 2005a). The program simulates the behaviour of structures built of soil, rock or other materials that may undergo plastic flow when their yield limits are reached. Materials are represented by elements or zones which form a grid that is adjusted by the user to fit the shape of the object to be modelled. Each element behaves according to a prescribed linear or nonlinear stress/strain law in response to the applied forces or boundary restraints. The material can yield and flow, and the grid can deform (in large-strain mode) and move with the material that is represented. The explicit Lagrangian calculation scheme and the mixed-discretisation zoning technique used in FLAC ensure that plastic collapse and flow are modelled very accurately. The drawbacks of the explicit formulation (i.e. the small timestep limitation and the question of required damping) are overcome to some extent by automatic inertia scaling and automatic damping, neither of which influence the mode of failure.

FLAC was chosen because it models soil well and because it includes appropriate structural elements that can have an interface with the surrounding soil. Beam and lining elements are available to model the corrugated steel, and the interface with the soil can have realistic physical properties, including the ability for separation and slippage between the soil and the lining elements.

One useful feature of FLAC is that it contains a programming language (known as FISH) that allows the user to alter the value of almost any variable, and to calculate and store values for additional variables at any time, including during simulation of earthquake shaking.

During shaking, the values of more than 200 variables were saved every few hundred steps, equivalent to about every 0.017 seconds. Each of these histories is then able to be plotted against step number or against any other history (one of which was dynamic time). Calculations were carried out after completion of shaking using the values,.

4.4 Model details

A high profile arch (see Figure 1.1 and Figure 4.1) of 11.66 m maximum span, with 10.00 m span at the footings and 7.29 m rise was modelled (CSP Pacific 'Superspan' model 45A10.15). The element mesh extended some 50 m wide (about five times the span) each side of the culvert and a similar distance below the culvert (Figure 4.2) to minimise edge effects on the model. The minimum element size near the culvert was about 1.0 m wide and 0.6 m high, and the maximum element size was about 1.4 m square at the extremities.

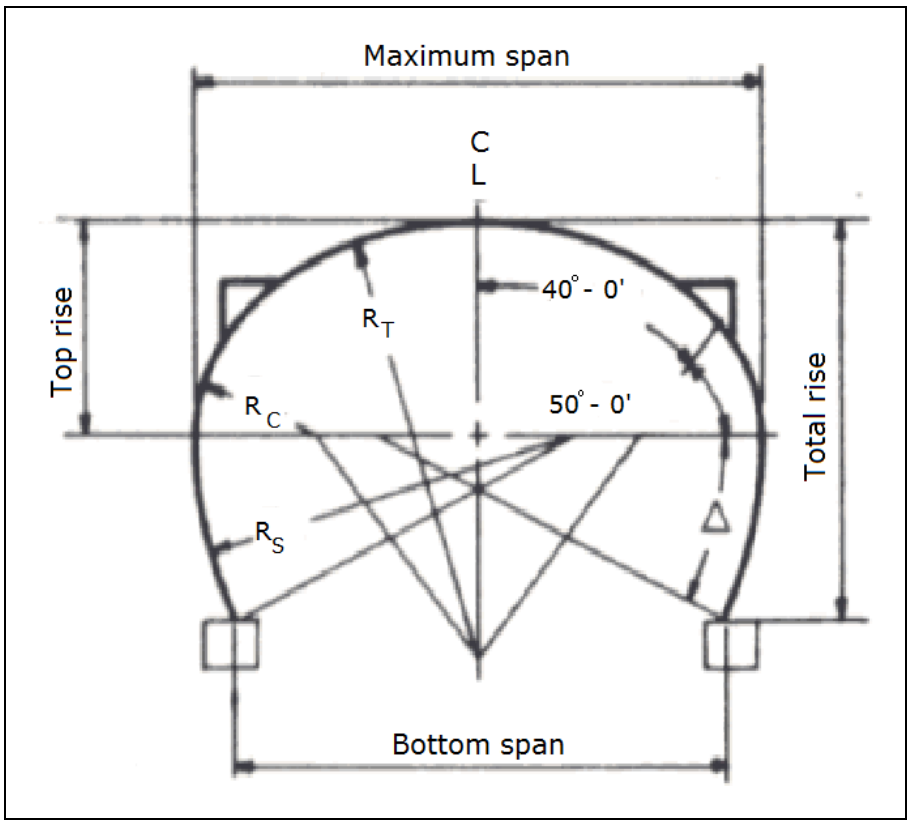

Figure 4.1 'Superspan' arch modelled: R_S=7.57 m, R_T=7.57 m, R_C=2.69 m, Δ=27°07", maximum span 11.66 m, bottom span 10.00 m, total rise 7.29 m, top rise 3.84 m (from CSP Pacific Limited 2008).

FLAC's liner elements were used for the structural members. Thirty-six were used, with each structural element initially defined to be the same length as the soil element beside it (Figure 4.3). The structural node numbers are shown in Figure 4.3.

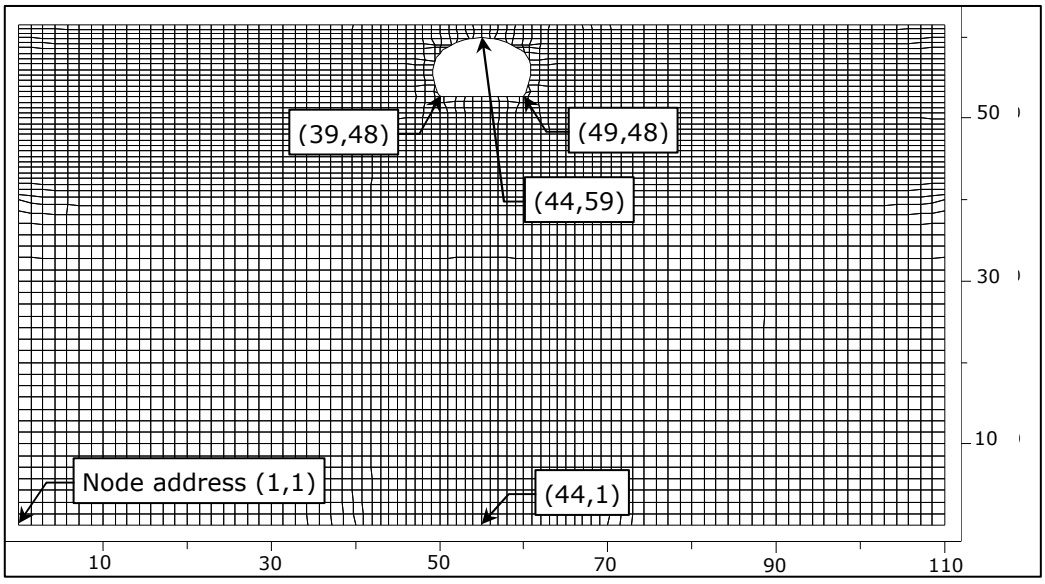

Figure 4.2 Finite difference mesh layout used in FLAC.

Interfaces were installed between the structural elements and the soil as the structural elements were defined. An interface allows for slip and separation to occur between the elements attached to the opposite sides of the interface. They can also be 'glued' to prevent any movement.

Concrete footings 1.1 m wide and 0.6 m deep were used (one zone deep and two zones wide; see Figure 4.3). This was thought to be a typical footing size in good soil. Tests were carried out with and without concrete stiffening beams on the upper shoulders and for three sizes of stiffening beam: 0.87, 1.57 and 1.87 m high (Figure 4.3). The interfaces between the concrete elements and liner elements were 'glued' to represent the steel hook bars usually used to fasten stiffening beams to the steel culvert.

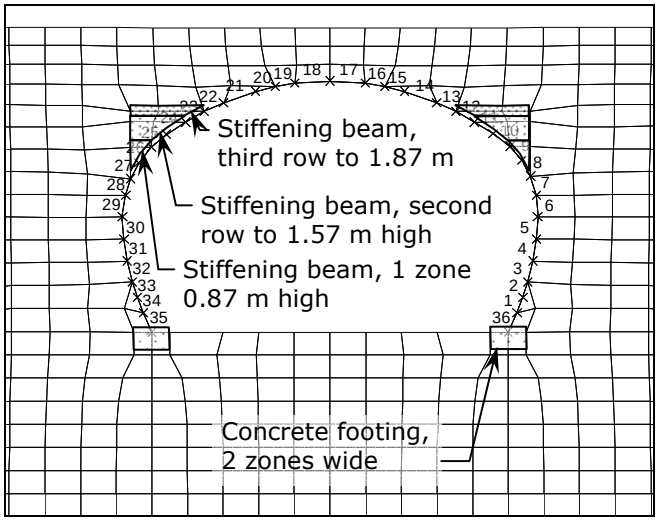

Figure 4.3 Structural liner element numbers used in the FLAC modelling.

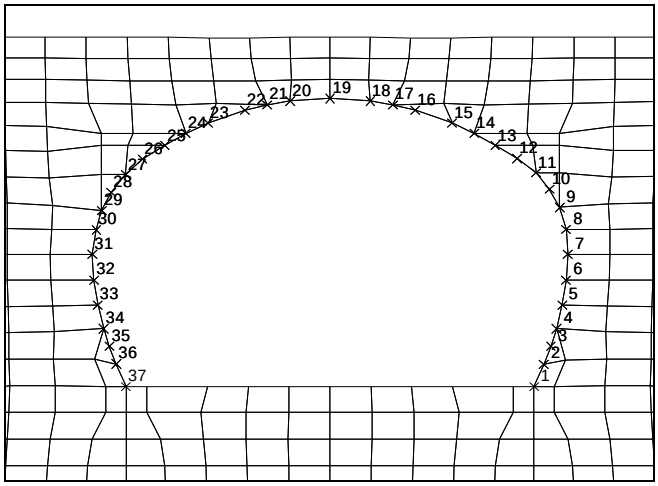

Figure 4.4 Structural liner node numbers used in FLAC modelling.

4.5 Boundary conditions

'Free field' boundaries were applied at the lateral (vertical) boundaries of the models to minimise wave reflections from them. In the FLAC formulation, the lateral boundaries of the main grid are attached to the free-field grid by viscous dashpots[4] to simulate a quiet boundary; the unbalanced forces from the free-field grid are applied to the main grid boundary. Plane waves propagating upward suffer no distortion at the boundary because the free-field grid supplies conditions that are identical to those in the infinite model. The free-field grid consists of a one-dimensional column of unit width, simulating the behaviour of the extended medium.

A quiet or absorbing boundary was applied along the base of the models. These quiet or absorbing boundaries are formulated as dashpots attached independently to the boundary in normal and shear directions. Normal and shear tractions, proportional to soil mass density, P- and S-wave velocity, and soil particle normal and shear velocity, are applied at every timestep in the same way that boundary loads are applied.

The boundaries have no x- or y-fixity. It is thus important that the earthquake records used are baseline corrected to have zero residual displacement and velocity at the end of shaking.

4.6 Material properties

4.6.1 General

The philosophy used in the modelling was to adopt a 'base model' and then to change parameter values and observe the effects. The base model property values are shown in the following sections.

4.6.2 Soil

The soil was modelled as silty and clayey gravel with a Mohr-Coulomb bilinear elastic plastic failure criterion. The properties shown in Table 4.2 were used. Where multiple values are shown, the effects of the changes were tested. For convenience, soil properties were varied independently, although in reality, soils with high friction angles tend to be denser with higher shear wave velocities.

[4] A dashpot is a damper that resists motion via viscous friction, for example by forcing a viscous liquid through a small hole. The resulting force is proportional to the velocity, but acts in the opposite direction, slowing the motion and absorbing energy. Everyday examples of dashpots include shock absorbers in cars and mountain bikes.

Table 4.2 Soil properties modelled.

Property	Base model values	Tested values
Density, ρ	2000 kg/m^3	–
Cohesion	1.0 Pa	5 kPa, 10 kPa
Friction angle, ϕ	35°	30°, 40°
Tension limit	0 Pa	–
Dilation angle, ψ	5°	0°, 10°
Shear wave velocity C_S	201 m/s	300 m/s for foundation + 150 or 201 m/s for backfill; 300 m/s for all soil.
Poisson' s ratio ν,	0.3	
Bulk modulus K	175 MPa	150 m/s soil: K =75 MPa, G =45 MPa, ν =0.25.
Shear modulus G.	80.8 MPa	300 m/s soil: K =390 MPa, G =180 MPa, ν =0.3

The elastic moduli appear to be relatively high. They are small-strain values, calculated from the shear wave velocity, the density and Poisson's ratio, using

$$G = C_S^2 \rho \qquad \text{[Equation 4.1]}$$

and

$$K = \frac{2G(1+\nu)}{3(1-2\nu)}. \qquad \text{[Equation 4.2]}$$

The maximum frequency response in numerical modelling, whether using finite difference or finite elements, is governed by $C_s/10\Delta L$, where C_s is the shear wave velocity and ΔL is the maximum element size. With a maximum element size of about 1.4 m and a shear wave velocity in the soil of 200 m/s, this equates to a maximum of around 14 Hz.

4.6.3 Structural liner (culvert) elements

All structural elements were liner elements. The properties used are shown in Table 4.3. No tests were carried out on the effect of varying any structural element properties, other than the shape factor, which does not affect the results significantly (see Note c in Table 4.3).

Properties for the corrugated section, which were not used in the modelling but were used in deriving the bending stresses, are the section modulus and the corrugation dimensions. The standard corrugation height for a class 2 structure is 62 mm from crest to crest (see Figure 1.2). The section modulus, which is the second moment of area for a 1 m long section divided by the distance to the extreme fibre is given by:

$$Z = \frac{I}{2(\textit{total corrugation height})} \qquad \text{[Equation 4.3]}$$

or

$$Z = 104.84 * 10^{-6}\ \text{m}^3. \qquad \text{[Equation 4.4]}$$

The radius of gyration of the corrugations is 19.8 mm, according to Table 5.5 of AS/NZS 2041:1998.

FLAC's liner elements can be used in reinforced concrete linings. The tensile residual yield stress and compressive yield stress are applicable to those sections. The values set earlier in the project were not exceeded so they were left for the remainder of the FLAC runs.

The tensile yield stress used was probably a little higher than it actually is for grade 250 steel.

Table 4.3 Structural element (liner) properties.

Property	Base model values	Tested values
Radius	Crown 7.29, shoulder 2.69, sides 7.57 m	
Number of liner elements	36	
Cover	1.5 m	1.0, 2.0, 3.0 m
Poisson's ratio	ν=0.3	
Young's modulus[a]	E =219.8 GPa	
Steel thickness	7 mm	
Structural area[b]	8.290x10^{-3} m^2/m	
Second moment of area, I	3.250x10^{-6} m^4/m	
Spacing	1.0 m (equal to unit thickness of model)	
Shape factor[c]	0.4	0.833
Tensile yield stress	320 MPa	
Tensile residual yield stress	320 MPa	
Compressive yield stress	250 MPa	
The following properties are derived for the culvert:		
Ultimate compressive wall stress (equation 5.9(3) in AS/NZS2041:1998)[d]	107.7 MPa	
Elastic section modulus[e] Z_e Moment at first yield (f_y = 250 MPa)	104.84 x10^{-6} m^3/m 26.2 kNm/m	
Plastic section modulus Z_P Plastic Moment[f] (f_y = 250 MPa)	165.6 x10^{-6} m^3/m 41.4 kNm/m	
Buckling stress[g] • 150 m/s soil, 1.5 m cover • 201 m/s soil, 1.5 m cover • 201 m/s soil, 2.0 m cover • 201 m/s soil, 3.0 m cover • 300 m/s soil, 1.5 m cover	 134 MPa 186 MPa 239 MPa 250 MPa 250 MPa	

Notes to Table 4.3:

a The structural element logic is a plane stress formulation, so the value specified for Young's modulus (200 GPa) is divided by $(1 - \nu^2)$ to correspond to the plane strain mode.

b The structural area and second moment of area are AS/NZS 2041:1998 values for 7 mm plate and are per metre length of culvert.

c The FLAC manual gives typical values for the shape factor but is not clear what it represents. For a square section, the shape factor is 5/6; for an I-beam, it is the web area divided by the total area. Michael Coulthard of Itasca, Australia, said the default (5/6) should be sufficient in most cases (personal communication Novermber2006).

d A yield stress of 250 MPa is assumed. AS3703 (1989) also provides for this calculation, assuming a yield stress of 230 MPa. Using AS3703, the ultimate compressive wall stress is 58.8 MPa. Using the AS/NZS2041 (1998) formula (250 MPa yield stress) with (2*top radius) replacing the span and correcting for arc angle being less than 180 degrees, the value is 80.8 MPa.

e The elastic section modulus is calculated as I/y. The distance to the extreme fibre, y, is 31 mm, half the corrugation height.

f Plastic moment is approximate and calculated using the method of Beer & Johnston (1982) assuming the corrugation each side of the neutral axis is approximately arcuate.

g Buckling stress was calculated using the method of Abdel-Sayed et al. (1994), for a radius of 7.57 m (the top and lower side radii) and a span of 11.66 m. It is an average through the section and has been converted to a bending moment using the elastic section modulus. The maximum buckling moment is the plastic moment. When cover is 1.5 m at the crown, it is about 3 m at the stiffening beam locations.

The maximum elastic bending moment is given by the yield stress multiplied by the section modulus, or 26.2 kNm per metre length of culvert. The plastic moment is more difficult to determine; using the method of Beer & Johnston (1982), with no soil outside, it is about 41 kNm/m, which is 1.58 times the moment at first yield.

The ultimate compressive wall stress shown in Table 4.3 was calculated using the set of three equations given in AS/NZS2041 (1998). The equations are based on the results of field tests in the late 1960s on circular culverts up to 1.5 m diameter. Similar equations are given in AS3703.2 (1989). Which equation to use from the set of three given is determined based on the ratio of span to the radius of gyration of the corrugations in AS/NZS2041 and on the ratio of top radius to the radius of gyration in AS3703.2. The equations are shown and discussed further in Appendix A, along with discussion of the buckling stress calculations using the method of Abdel-Sayed et al. (1994).

Based on the discussion in Appendix A, the buckling stress and the ultimate compressive wall stress are describing the same phenomenon. As stated in Appendix A, the ultimate compressive wall stress takes the application of non-extensional bending moment into account as well as compressive thrust in the culvert walls. We note that several possible values are possible for the ultimate compressive wall stress, depending on whether one uses AS/NZS2041 (1998), AS3703.2 (1989), DR02241 (2004) or the AASHTO (1989) method.

As a result, no failure limit was given for the culvert elements in the modelling because of uncertainty of what it should be. It would vary with cover depth, as shown above, as well as location in the culvert (based on radius of curvature). For the purposes of the modelling, steel culvert behaviour was assumed to remain elastic.

For the 201 m/s soil culvert, the buckling stress reaches the yield stress through the entire section at a cover depth of 2.11 m, which is located about 3.0 m from the centre of the crown when it has 1.5 m of cover. The stiffening beams in the model began at some 4.4 m depth. The stiffening beams would affect the buckling stress in the culvert if they were ‘glued’ to the steel, effectively raising the stiffness of the structural section. As constructed, they are attached by a single row of hook bolts, as well as by adhesion between the concrete and steel, so little effect is likely on the buckling moment with the compression side on the inside of the culvert. The stiffening beams may, however, increase the buckling moment by shedding load off the culvert into the soil and thus reduce the effective span of the culvert crown, which appears to be the thinking in the design standards.

4.6.4 Stiffening beams

Longitudinal stiffening beams are added to transfer transverse compression in the wall of the structure to the fill (DR04421 2004), where the bearing load on the soil is assumed to take half the ring compression in the metal structure.

As shown in Figure 4.3, models with and without concrete stiffening beams were tested. Three sizes of beam were trialled: one zone high (0.87 m), two zones high (1.57 m) and three zones high (1.87 m). When stiffening beams were used, the interface between the beam and the lining was glued, so no slip or separation was allowed. No interface was used between the concrete and the soil. The concrete zones had the same properties as the concrete zones forming the footings:

- density =2300 kg/m^3,
- bulk modulus =14.4 GPa,
- shear modulus =10.8 GPa,
- cohesion =1.5 MPa,
- friction angle =30°,
- dilation angle =5°, and
- tension limit =860 kPa.

The reinforced concrete elastic moduli are based on a value for Young's modulus, E, of 25.9 GPa (from $E=4730*\sqrt{f'_c}$ (Park & Paulay 1975) where f'_c is the concrete compressive strength of 30 MPa) and Poisson's ratio of 0.2. The cohesion is given approximately by $0.05*f'c$ (Park & Paulay, Fig. 2.10).

The base model contained a two-zone stiffening beam (1.57 m high).

4.6.5 Material damping

Trial analyses were carried out using various values of soil and structural damping. It was found that damping nearly always increased the high frequency 'ringing' within the model, so all subsequent runs were carried out with no soil or structural damping applied. When stress in a soil element exceeded the Mohr-Coulomb failure criterion, plastic flow occurred until the stress reduced to below the failure limit. This flow absorbed energy, so adding damping was unnecessary. This effect has also been observed in other non-linear numerical modelling carried out by Graham Fairless.

A vibrating structure in or on the surface of a modelled region creates a disturbance both in the plane of analysis and in the out-of-plane direction. The energy radiated in-plane is reasonably well absorbed by the quiet boundary condition. However, in a three-dimensional system, energy would also be radiated in the out-of-plane direction. To represent this effect approximately, dashpots are connected from all gridpoints in the main grid to corresponding gridpoints in the free field (although the force is not applied to the free-field grid). This mechanism is termed three-dimensional (3D) radiation damping. The 3D damper acts on the difference between the actual particle velocity under the

structure and the free field velocity around the model region (Itasca 2005b). Three-dimensional damping was applied to the models.

4.6.6 Interfaces

Interfaces were used between culvert and soil. Their properties are shown in Table 4.4. The interface failure criterion is the Coulomb shear-strength criterion, given by:

$$F_{Smax} = c*L + \tan\varphi*F_N \qquad \text{[Equation 4.5]}$$

where:

- F_{Smax} is the maximum shear force
- c is the cohesion
- L is the length
- F_N is the normal force.

If the shear force, F_S, exceeds F_{Smax}, Equation 4.5 is set to F_{Smax} until the force reduces. During sliding, shear displacement can cause an increase in the effective normal stress on the interface. In addition, the interface may dilate at the onset of slip (non-elastic sliding). Dilation is governed in the Coulomb model by a specified dilation angle, ψ, and is a function of the direction of shearing.

The interfaces were defined so as to allow slip and separation of the soil from the steel culvert. In this situation, the friction, cohesion and tensile strength are important but the elastic stiffness is not. Approximate elastic stiffnesses were set up in the first run, which used soft soil with a shear wave velocity of 91 m/s. They were chosen to be about ten times the apparent stiffness of the stiffest neighbouring soil zone in the normal direction. Subsequent runs with stiffer soils used the same values, which were thus a little low for those soils. However, because slippage and separation were the effects being modelled, these values should have had little effect on the solutions obtained and in fact should have improved solution numerical efficiency.

The only variable that was tested for the structural elements was whether slippage was allowed between them and the soil. A test was done with all structural elements 'glued' to the soil, where no slippage or separation was allowed. This is set in the interface properties. As part of this test, the culvert was constructed with all interfaces glued.

Table 4.4 Soil–culvert interface properties modelled.

Property	Base values	Values tested
Friction	20°	
Cohesion	0	
Shear stiffness[a]	155 MPa/m	
Normal stiffness[1]	155 MPa/m	
s-b ratio[b]	100 Pa (default value)	
Tensile bond stress	0 Pa	
Glued	No Yes at the concrete stiffening beams	Yes or no Always glued at stiffening beams

Notes to Table 4.4:

a Interface shear and normal stiffnesses were set as about 10 times the apparent stiffness of the stiffest neighbouring zone, which is given by $max[(K + 1.33G)/\Delta z_{min}]$, where Δz_{min} is the width of the narrowest neighbouring zone that is normal to the interface. K and G are the bulk and shear moduli of the soil.

b S-b indicates the shear bond strength. The shear bond strength is set to s-b ratio times the normal bond strength, using the s-b ratio property keyword. The default shear bond strength is 100 times the tensile bond strength. This ratio had no effect because the tensile bond strength was zero.

4.7 Construction of the model

The construction sequence of the model was as follows:

1. Define the grid to full height. Define the culvert opening shape. Set the elements above the concrete footings to the 'Null model' (i.e. make them invisible, with no strength or density).
2. Equilibrate gravity stresses in the foundations.
3. Install the concrete footings and the culvert. Equilibrate under gravity in a number of steps, increasing the density of the steel by 1000 kg/m^3 at a time. Ramping up gravity in this way reduces elastic bouncing of the culvert as it comes to stress equilibrium.
4. Install the fill, one row of elements at a time, completely across the model. Install the interface between the culvert and soil. Bring each layer to stress equilibrium before adding another.
5. Where used, stiffening beams were installed when the layers of fill containing them were installed.

Construction of the model was carried out in small-strain mode, whereby the soil element co-ordinates were not updated during stepping to equilibrium in FLAC. Attempts to use the large-strain mode during construction made it very difficult to put the interfaces around the culvert because it deformed too much during construction. Large-strain mode was used for the earthquake modelling.

Trials were carried out whereby compaction stresses were added to the surface of each layer. The result was that the structural bending moments were greater than the buckling moment, so simulation of compaction stress was not carried out.

4.8 Earthquake inputs

4.8.1 Method of input

The earthquake record was input as a shear stress in the bottom row of zones. The shear stress is calculated at $2\rho C_S V_S$, where V_S is the ground motion velocity history. The factor of 2 is to account for the absorbent boundary on one side of the elements. The value ρC_S was calculated using the properties of the middle soil element at the base of the model – construction and consolidation resulted in small density variations in the soil.

4.8.2 Ground motions

Ground motion velocity histories were supplied, integrated from recorded accelerations, by the processing agency. They were then baseline corrected to zero residual displacement and ramped using a long-period sine wave to zero residual velocity.

As outlined in Section 4.6.1 above, the maximum frequency that could be modelled was 14 Hz in the Superspan arch model with 200 m/s shear wave velocity soil. To reduce high frequency 'ringing' in the models, all earthquake time histories were first filtered at 10 Hz using a low-pass Butterworth filter.

Horizontal components for three earthquakes were chosen to match New Zealand seismic conditions. The records were scaled to improve the match, up to about a 1.5 second period, of their 5% damped response spectrum to the Class C Site spectrum in AS/NZS1170.5 (2005). While no particular site was being modelled, earthquakes and scaling factors to represent sites in Wellington (Z =0.4) were used to test the effect of strong shaking on the structures. The scaling factors were calculated by GNS, using a procedure similar to that outlined in the commentary of NZS 1170.5 section C5.5.2, and received from Graeme McVerry (pers. com. 2007). Factors were used to represent the 500-year return period (R =1.0) and 2500-year return period (R =1.8) earthquakes.

Because the earthquake shaking (scaled to match the Class C Site spectrum) was applied in the bottom row of the model, by the time the shear waves reached the base of the culvert, some 52 m higher, the response spectrum had been slightly modified by the intervening soil. Pseudo-response spectra are shown in Figure 4.5 to Figure 4.12 for the base model. Generally, low period intensity is attenuated while intensity is amplified above a period of approximately 0.4 seconds as the waves travel up through the model. From the base of the culvert to the crown and ground surface, the shaking is amplified below about 0.7 s period.

Table 4.5 shows the earthquake records used in the modelling, along with their peak ground accelerations, their peak ground velocities and the calculated Arias Intensity at the footings. Arias Intensity is included because it is examined as an earthquake parameter that may be useful in design. The Arias Intensity, I_A, is defined (Arias 1970) as the sum of the squared acceleration values in the recorded accelerogram:

$$I_A = \frac{\pi}{2g}\int_0^{\infty}[a(t)]^2 dt \qquad \text{[Equation 4.6]}$$

where g is the acceleration caused by gravity. In this work, the acceleration was normalised by dividing by g within the integral. Thus the units are s^3/m.

Table 4.5 Earthquake records used in the modelling.

Earthquake	**El Centro Imperial Valley Irrigation District (USA) 1940 May 19 @ 0436 UT (distance 12 km, depth 10 km, Mw 7.0)**		**Michoacan (Mexico) 1985 Sep 19 @ 1317 UT (distance 121 km, depth 15 km, Ms 8.10)**		**Tabas (Iran) 1978 Sep 16 @ 1535UT (distance 52 km, depth 5 km, Mw 7.23) with forward directivity pulse present[a]**	
Component	S00E	N90W	N90E	S00E	N16W	N74E
For R=1 (500-year return period)						
Scale factor	1.52	1.1	2.85	1.9	0.55	0.56
PGA (g)[b]	0.65	0.40	0.61	0.50	0.56	0.56
PGV (m/s)	0.76	0.78	0.65	0.71	0.59	0.88
Arias Intensity (s^3/m)	0.943	0.371	1.036	0.727	0.575	0.655
For R=1.8 (2500-year return period)						
Scale factor		1.98		3.42		1.01
PGA (g)		0.59		0.75		1.12
PGV (m/s)		1.36		1.24		1.50
Arias Intensity (s^3/m)		1.072		2.345		1.944

Notes to Table 4.5:

a 'Forward directivity' is a near-fault effect where a rupture occurs along the fault from the epicentre towards the recording site. Constructive interference occurs between body shear waves when the fault's slip direction is aligned with the rupture direction, which is towards the recording site. At high period ranges, forward directivity effects at near-fault locations result in high amplitude velocity pulses. At high frequencies, the accelerogram at the far end of the fault is short and intense, compared to the lower-amplitude, longer-duration accelerogram near the origin of rupture (Erdik & Durukal 2004).

b PGA, PGV and Arias Intensity values are averages of those recorded at the culvert footings during model shaking.

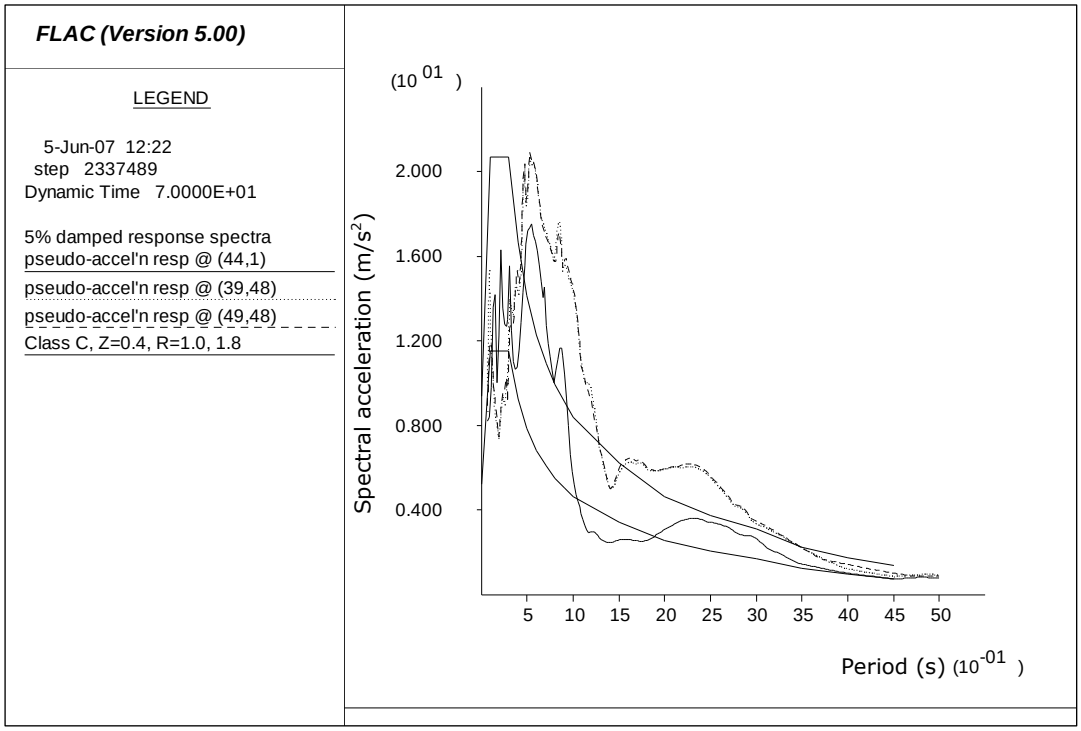

Figure 4.5 Five percent damped response spectra for the El Centro Imperial Valley Irrigation District 1940 May 19, S00E component, for R=1.0.

Note: (44,1) is the input at the base of the model; (39,48) and (49,48) are the nodes at culvert footings (see Figure 4.2).

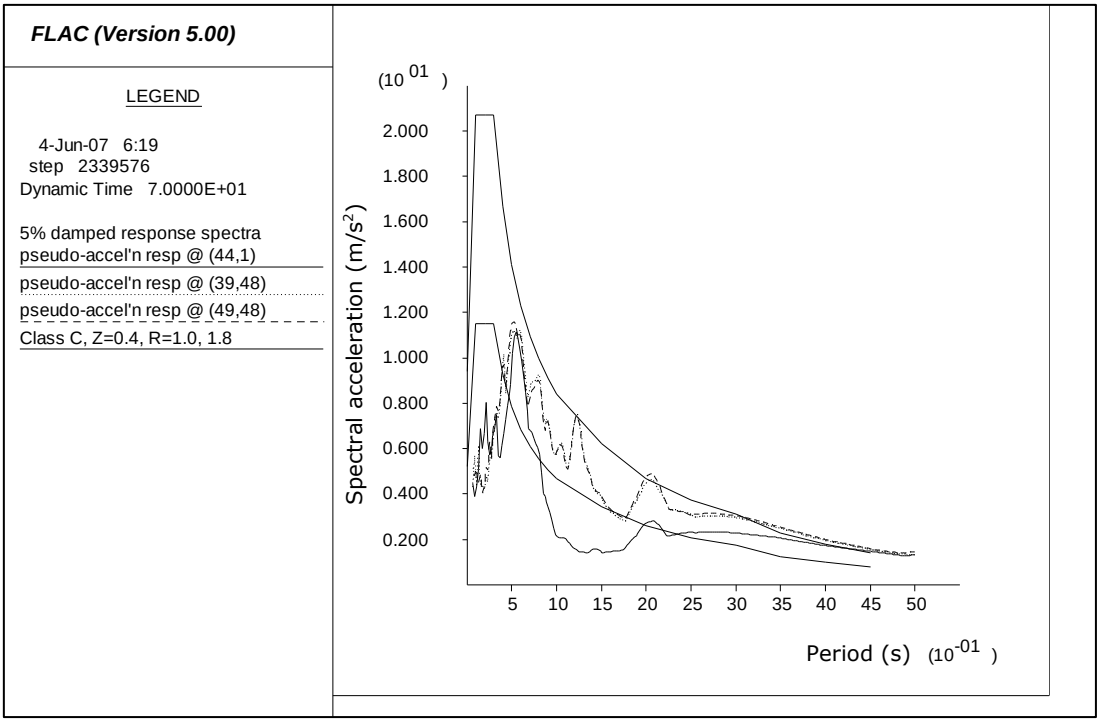

Figure 4.6 Five percent damped response spectra for the El Centro Imperial Valley Irrigation District earthquake recording of 19 May 1940, N90W component, for R =1.0.

Note: (44,1) is the input at the base of the model; (39,48) and (49,48) are nodes at the culvert's left and right footings (see Figure 4.2).

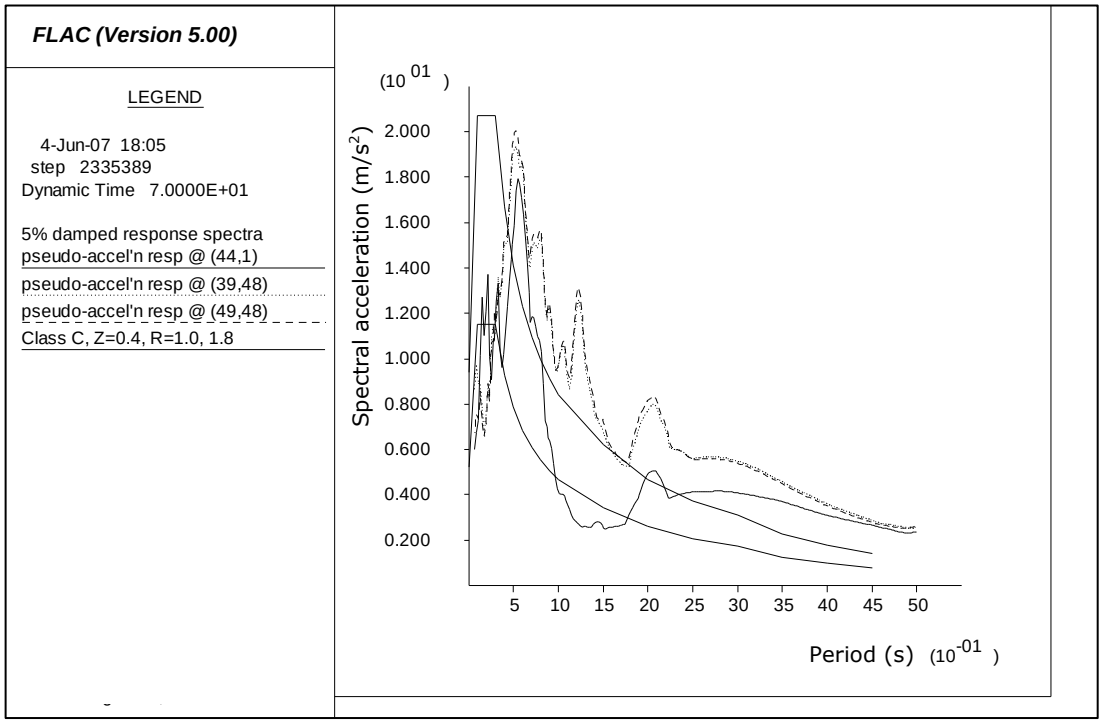

Figure 4.7 Five percent damped response spectra for the El Centro Imperial Valley Irrigation District earthquake recording of 19 May 1940, N90W component, for R =1.8.

Note: (44,1) is the input at the base of the model; (39,48) and (49,48) are nodes at the culvert's left and right footings.

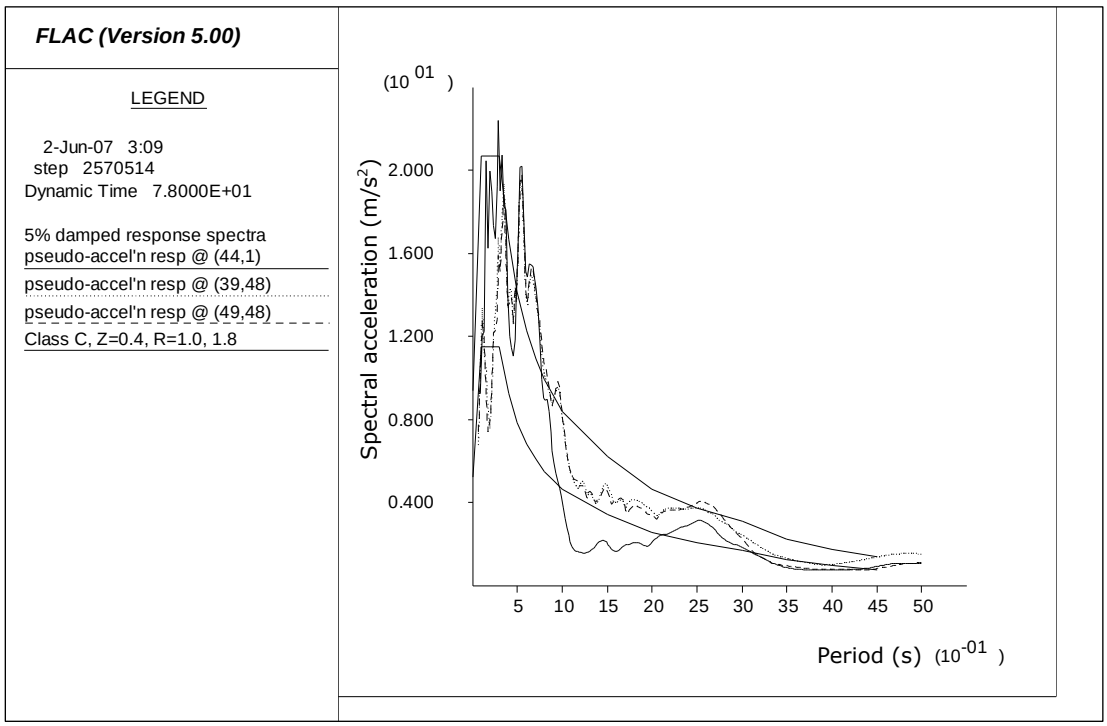

Figure 4.8 Five percent damped response spectra for the Michoacan earthquake of 19 September 1985, N90E component for R =1.0.

Note: (44,1) is the input at the base of the model; (39,48) and (49,48) are the nodes at culvert footings.

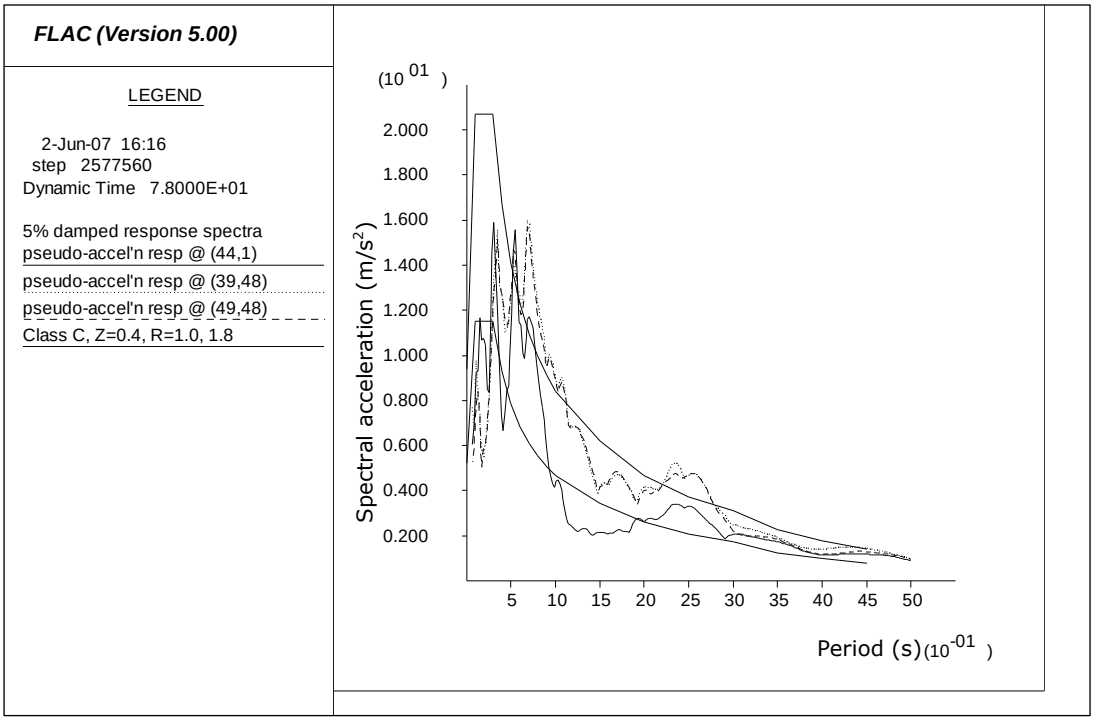

Figure 4.9 Five percent damped response spectra for the Michoacan earthquake of 19 September 1985, S00E component for R =1.0.

Note: (44,1) is the input at the base of the model; (39,48) and (49,48) are the nodes at culvert footings.

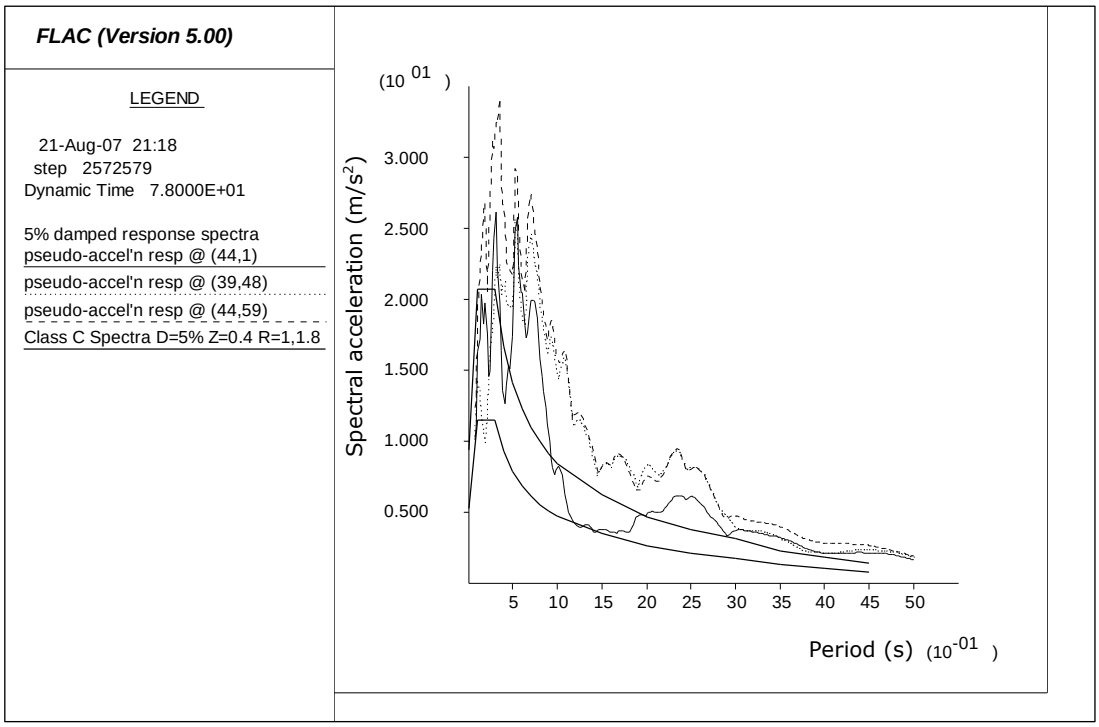

Figure 4.10 Five percent damped response spectra for the Michoacan earthquake of 19 September 1985, S00E component for R =1.8.

Note: Nodes (44,59) and (44,62) are nodes at culvert crown and ground surface (1.5 m cover).

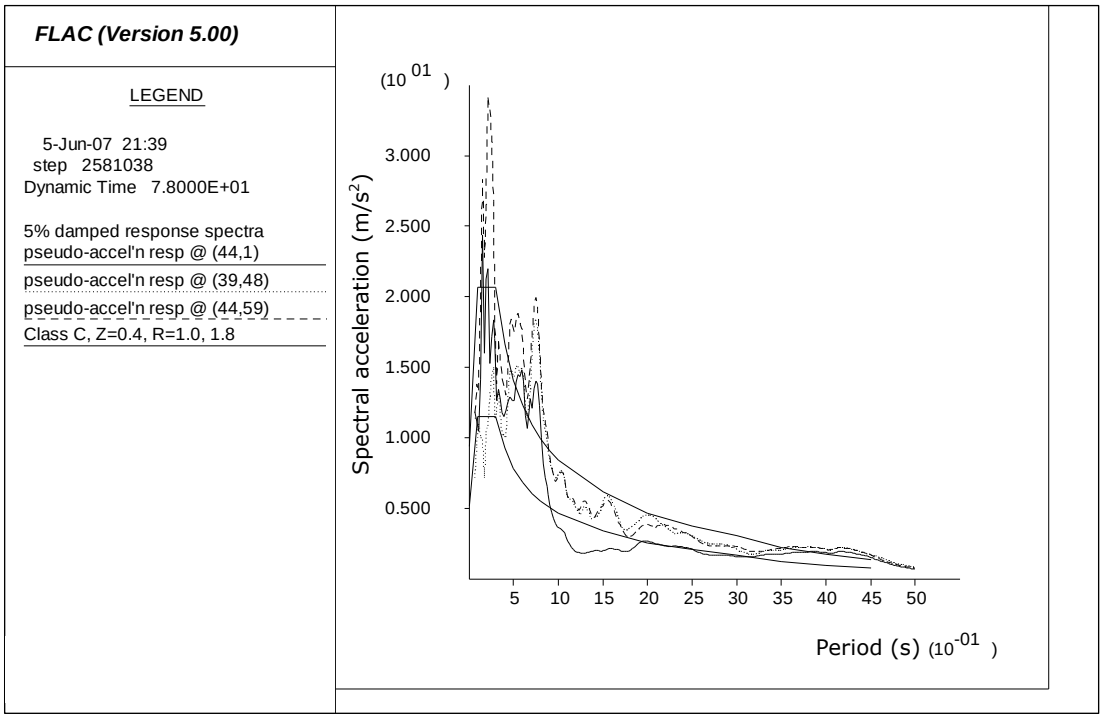

Figure 4.11 Five percent damped response spectra for the Tabas earthquake on 16 September 1978, N16W component, for R =1.0.

Note: (44,1) is the input at the base of the model; (39,48) is the node at the culvert's left footing; (44,59) is the crown of the culvert.

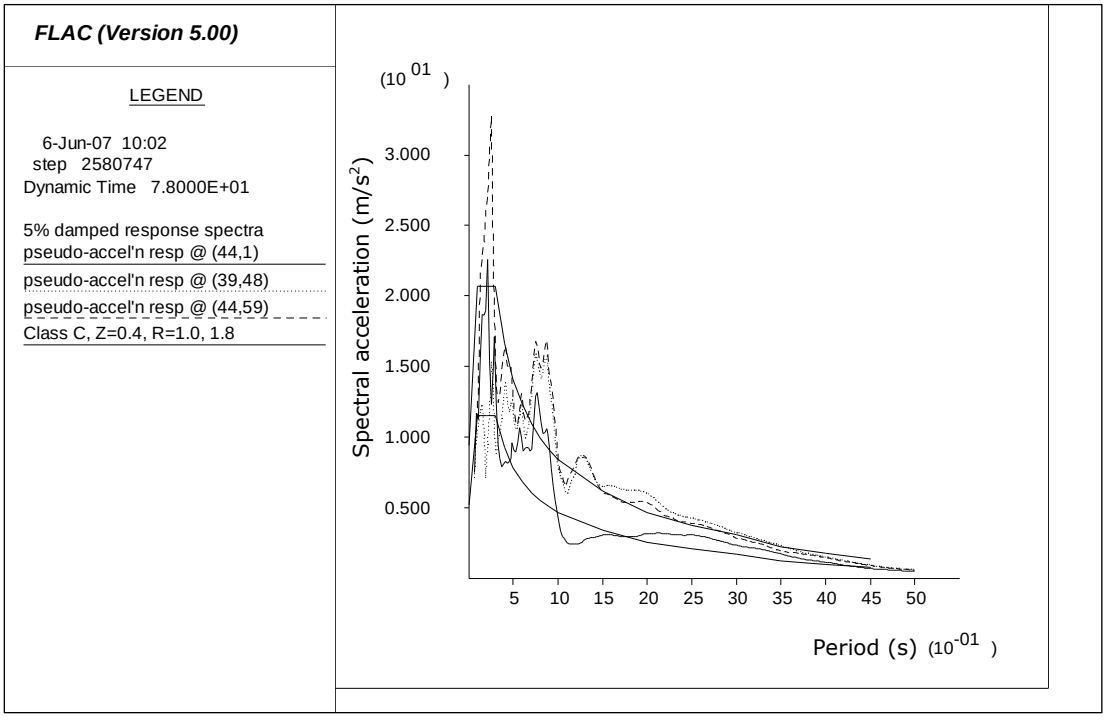

Figure 4.12 Five percent damped response spectra for the Tabas earthquake of 16 September 1978, N74E component, for R =1.0.

Note: (44,1) is the input at the base of the model; (39,48) is the node at the culvert's left footing; (44,59) is the crown of the culvert.

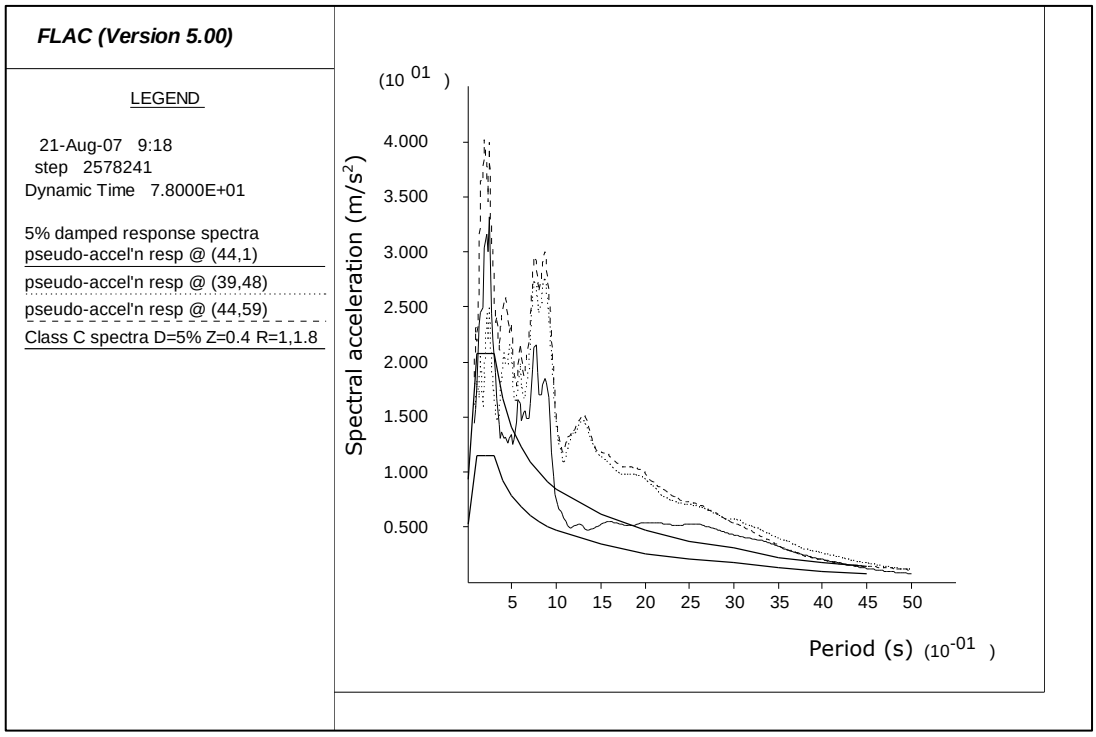

Figure 4.13 Five percent damped response spectra for the Tabas earthquake of 16 September 1978, N74E component, for R =1.8.

Note: (44,1) is the input at the base of the model; (39,48) is the node at culvert left footing; (44,59) is the crown of the culvert.

4.9 History recordings

In FLAC, a history is a recording of the value of a variable at a regular interval during execution of the modelling. During the modelling reported here, histories were recorded for displacements, velocities and accelerations at a number of critical grid points and structural nodes, as well as the axial forces and moments in each structural element.

5. Results

5.1 Overview

5.1.1 Scope

In this chapter, the results of the modelling are presented. Because we are most interested in the structural performance and deformation of the culvert, the results presented will concentrate on those responses. In general, the maximum forces and moments are reported, because they are likely to indicate the structural condition after an earthquake.

The maximum bending moment reported sometimes exceeds the first-yield and buckling moments shown in Table 4.3. We note that these maxima are transitory and generally occur at one location at a time, and it takes more than one plastic hinge to cause structural collapse of the culvert. FLAC calculates bending moments. The bending stresses shown in the following have been calculated using the elastic section modulus. Stresses less than 250 MPa indicate elastic bending. The plastic moment is reached at an indicated stress of 390 MPa using this section modulus.

Post-shaking forces and moments are not reported. We note, however, that values of both parameters are always greater after shaking than the values before shaking. It is expected that those increases will relax slightly over time with particle rearrangement of the soil against the steel culvert reducing the shear stress between them, but consideration of how much and the rate of reduction is beyond the scope of this work.

Maximum average transient racking (left and right movement of the crown compared to the footings) and the post-earthquake racking are reported. In addition, post-earthquake closure is reported at three heights in the culvert, because this deformation is likely to indicate whether remedial work is necessary before the culvert can continue to be used, even if it has not failed structurally. Seismic deformations were calculated by subtracting the deformations present before shaking started, i.e. the construction deformations.

The results of the tests on a particular set of variables are presented individually. The individual sections are:

- soil properties,
- culvert cover,
- interface condition, and
- the earthquake and its intensity of shaking.

Bending moments reported are per metre length of culvert, into the plane of the model. Axial force in the liner elements (the steel culvert), also called thrust, is also per metre of length of culvert.

5.1.2 Definitions of terms

A number of phrases and terms are used in this chapter as follows.

- **'Axial'** (abbreviated as Ax.) in the context of force (or thrust) means within the circumference of the culvert, which is within the plane of the model. Forces and moments are calculated per unit length of culvert in the out-of-paper direction (for an example, see Figure 4.4). The model represents one metre of culvert. Moments are thus calculated about horizontal longitudinal axes that coincide with each structural node.
- **'Closure Nd 8–30 mid-height'** indicates post-earthquake closure or a reduction in span across the culvert between structural nodes 8 and 30, which are at mid-height, one element above the widest part of the culvert (see Figure 4.4).
- **'Closure Nd 14–24 shoulder'** indicates post-earthquake closure across the culvert between structural nodes 14 and 24, which are at the top of where the three-zone stiffening beams would be located (Figure 4.4).
- **'Closure Nd 37–1 at base'** is post-earthquake closure or narrowing at the footings, which are nodes 37 and 1 (Figure 4.4).
- **'Max. rise in floor relative to ftgs'** is the maximum rise, after shaking, in the floor of the culvert (i.e. the soil) relative to the footings. This is illustrated in Section 5.2.2.
- **'Av. racking nd 19'** is the average horizontal displacement of node 19 compared to the footings (nodes 37 and 1). Node 19 is at the centre of the crown. Racking is a measure of overall culvert shear strain. Average racking is used because the footings usually move towards each other. Movement to the left is negative. Figures showing racking often contain three parts: 'residual ave. racking' (defined below), and up and down bars resembling error bars. These bars represent the maximum average transient (i.e. during shaking) horizontal movement (racking) of node 19 relative to nodes 37 and 1. The down bar represents leftward movement and the up bar represents rightward movement. The total average racking of node 19 is the sum of the left and right movements, and represents the total range of the culvert shear strain experienced in the earthquake.
- **'Residual av. racking nd 19'** is the post-earthquake average horizontal displacement of node 19 relative to the footing (nodes 37 and 1).

Footing reaction forces are the maximum transient axial force or thrust in structural elements 35 and 36 (see Figure 4.3). They are circumferential, in the direction of the relevant structural element. The stress is derived by dividing the thrust by the area of the liner element.

As stated in Section 4.6.3, the bending stresses have been calculated using the elastic section modulus. Stresses between 250 and 390 MPa indicate partial yielding of the section; 390 MPa is the indicated (but false) stress at the plastic moment. Bending stresses shown are maxima during shaking.

Where values are considered at the footings (for example, the earthquake properties, peak ground acceleration, peak ground velocity and Arias Intensity), they are averaged between the values at the left and right footings. For non-structural parameters, the

footings were taken as the finite difference mesh node connected to the structural nodes 1 and 37 (see Figure 4.2 on page 37 for the mesh node numbers and Figure 4.3 on page 38 for the structural node numbers).

5.2 Soil properties

5.2.1 Parameters tested

As shown in Table 4.2, the values of soil stiffness (shear wave velocity), friction angle, cohesion and dilation angle were changed to examine the effect, using the base model (Superspan high profile arch with 1.57 m stiffening beams and 1.5 m cover). Each of these variables was tested with just one earthquake record, the Imperial Valley recording of El Centro 19 May 1940, S00E component scaled times 1.52 for R =1.0.

5.2.2 Soil stiffness (shear wave velocity)

All trials were with the base model:

- 1.5 m cover;
- 1.57 m (two zone) high stiffening beams,
- soil with friction angle of 35°,
- cohesion of 1 Pa,
- dilation angle of 5°,
- El Centro 1940 S00E component with scale factor 1.52 (for R =1.0), and
- slip and separation allowed between soil and culvert but not between soil and stiffening beams.

Figure 5.1 shows the effect of soil stiffness, measured as the shear wave velocity, on the culvert deformation during construction. A little less 'peaking' (narrowing laterally at mid-height and rising of the crown, node 19, relative to the footings) is seen with the stiffest soil (shear wave velocity of 300 m/s) but little changes otherwise.

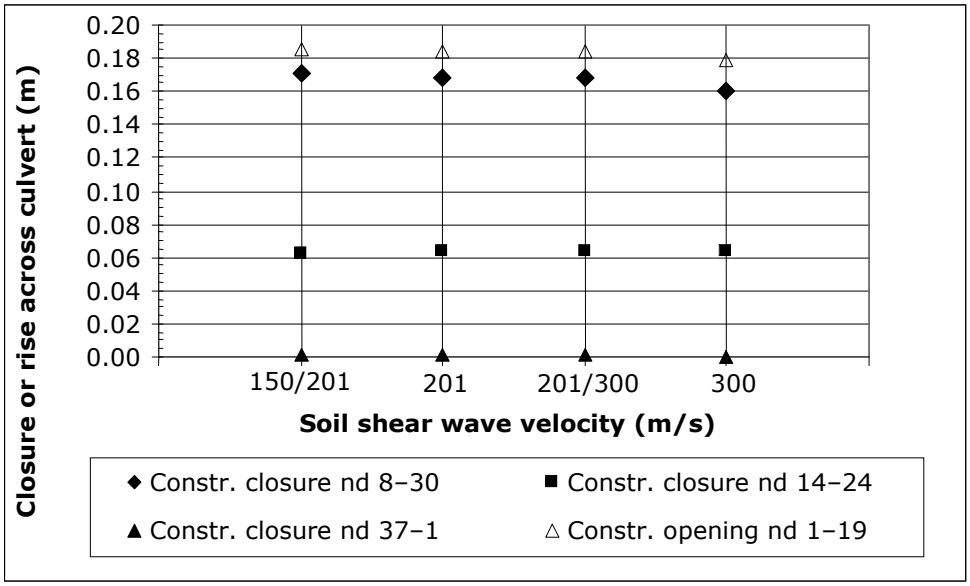

Figure 5.1 Deformations of the culvert at completion of construction.

Note: 150/201 means 150 m/s backfill and 201 m/s foundation soil. A single figure, such as 201 m/s, means backfill and foundation soils were the same.

Figure 5.2 shows the effect of soil stiffness on deformation caused by seismic shaking (construction deformations have been subtracted). Closure (span reduction) is greatest for the softest backfill, with narrowing at the footings (closure between nodes 37 and 1) nearly tripling between the 300 m/s and 150 m/s culvert backfill cases. Closure across the spring line (nodes 8 to 30) is small but increases almost five times with the softer soil. At the shoulder, above the stiffening beams (nodes 14 to 24), closure is nearly three times as great with the 150 m/s backfill compared to the 300 m/s backfill. Closure is reduced significantly in all cases when the foundation stiffness increases but the culvert backfill does not (compare the 201 and 201/300 shear wave velocity points).

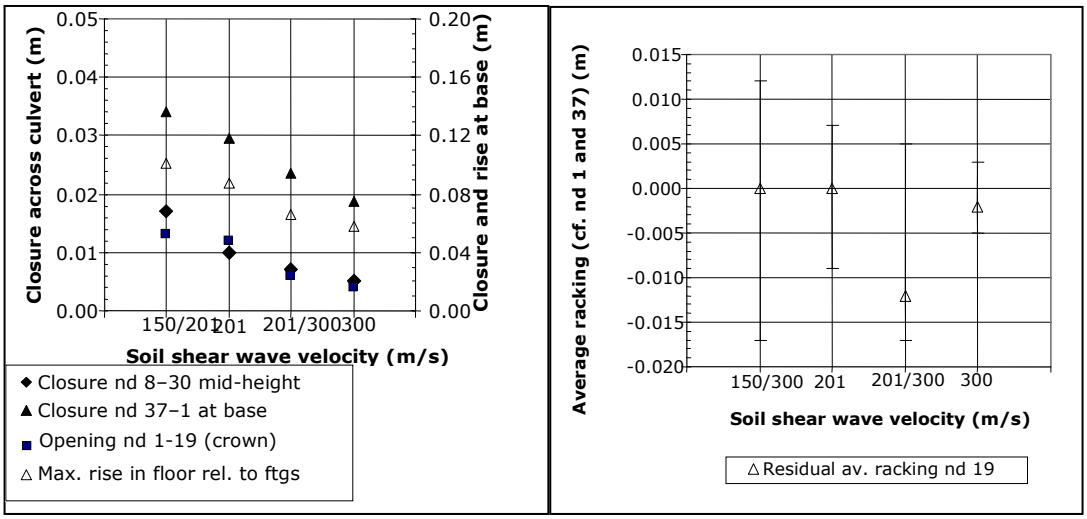

Figure 5.2 Effect of soil shear wave velocity on culvert deformation.

Notes:
- 150/300 means 150 m/s culvert backfill and 300 m/s foundation soil. Similarly, 201/300 means 201m/s backfill and 300 m/s foundation soil.
- Down error bar indicates maximum left racking; up error bar indicates maximum right racking.

Overall culvert shear strains are measured as the average racking of the culvert crown relative to the footings. In the 150 m/s soil, the maximum left to right racking (-17 to +12 mm, a total of 29 mm) is more than three times the amount in the 300 m/s soil (8 mm) (Figure 5.2).

When closure occurs between the footings, the soil between the footings is pushed upwards as passive failures occur inside each concrete footing beam (Figure 5.3). The post-earthquake (maximum) rise in the floor relative to the culvert base is shown in Figure 5.2; between the soft and stiff soil cases, the rise in the floor is reduced by two-thirds. This ratio is similar to the change in closure between the footings.

Typical bending moment and axial force distributions are shown in Figure 5.4 to Figure 5.7. Construction values and post-earthquake values are shown for two depths of cover. In both cases, the main change in the axial force with seismic shaking is over the crown between the stiffening beams, where the model with the greatest cover had the largest increase. The purpose of the stiffening beams is to unload axial forces into the soil on the vertical face of the beam; these distributions indicate that they are effective in doing that because the forces below the beams are not significantly increased by seismic shaking. The amount of the reduction, however, is less than the 50% assumed in design (Section 8 of DR04421 (2004)).

Bending moments in both cases increase just above the stiffening beams, indicating that the crown is bending downwards between the beams. With greater cover (2.5 m, shown in Figure 5.4 and Figure 5.5), bending in the crown remains relatively unchanged before and after the earthquake. With minimum cover (1.5 m), the crown's bending moments increase with earthquake shaking (Figure 5.6 and Figure 5.7). In both cases, the moments below the beams decrease and possibly change direction, and the moments increase below that towards the footing. This increase probably reflects the passive failure in the soil inside the footings. Bending moments inside the beams remain nearly unchanged after seismic shaking compared to the construction values.

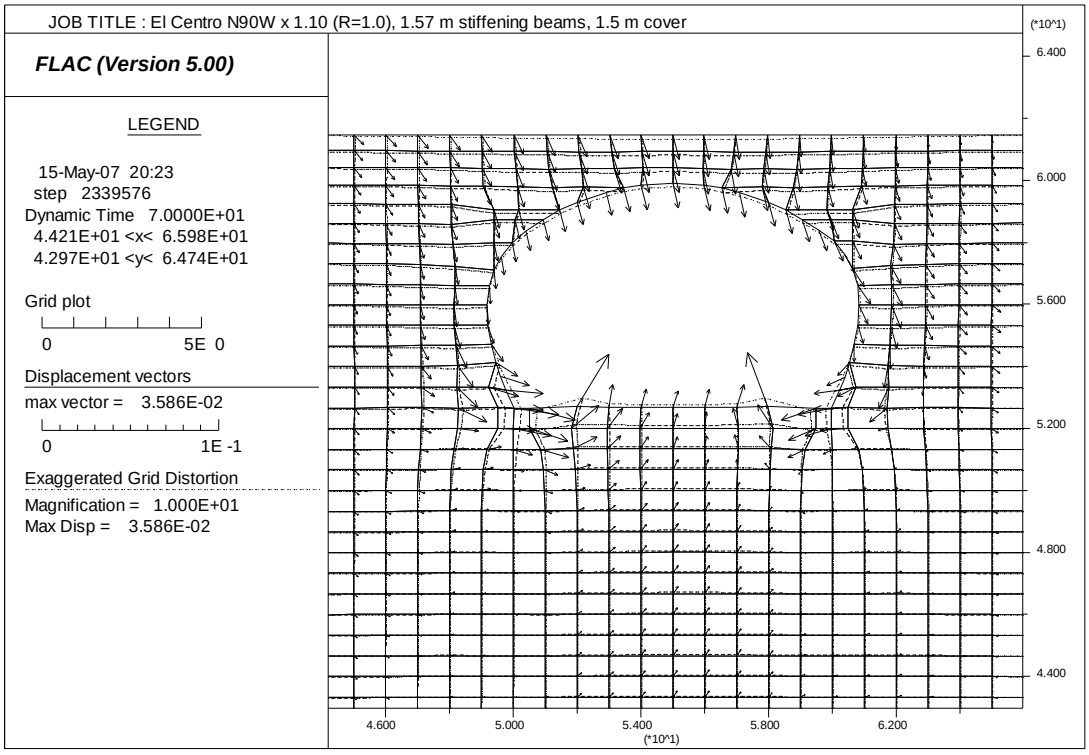

Figure 5.3 Typical displacement vectors and magnified deformed grid.

The axial force (also known as thrust) in elements 35 and 36 is the footing axial reaction force. The construction thrust decreases as the soil stiffness increases (Figure 5.8); a similar trend is seen for the dynamic forces. With the culvert backfilled with 201 m/s soil on 300 m/s foundation soil, the seismic reactions are greater than when the foundation soil is softer; this may be caused by attenuation of the earthquake as the waves travel up through the foundations. In Figure 5.9, the Arias Intensity of the input at the base of the culvert varies with soil stiffness. Differential attenuation of the seismic energy happens within the soil at different frequencies, depending on soil stiffness. We note that the maximum stresses are up to about a half of the ultimate compressive stress (107.7 MPa/m; see Table 4.3).

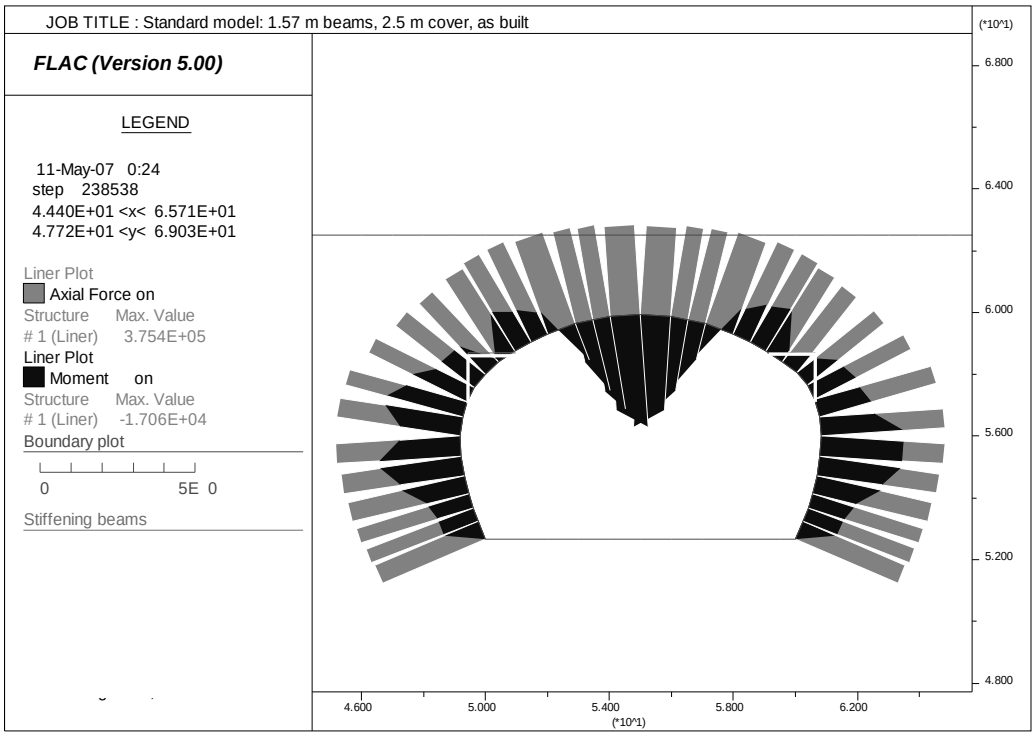

Figure 5.4 Axial force and bending moment distributions around the culvert for the model with 1.57 m beams and 2.5 m cover after construction.

Note: Moments are plotted on the compression side. Forces are in N/m and moments in Nm/m.

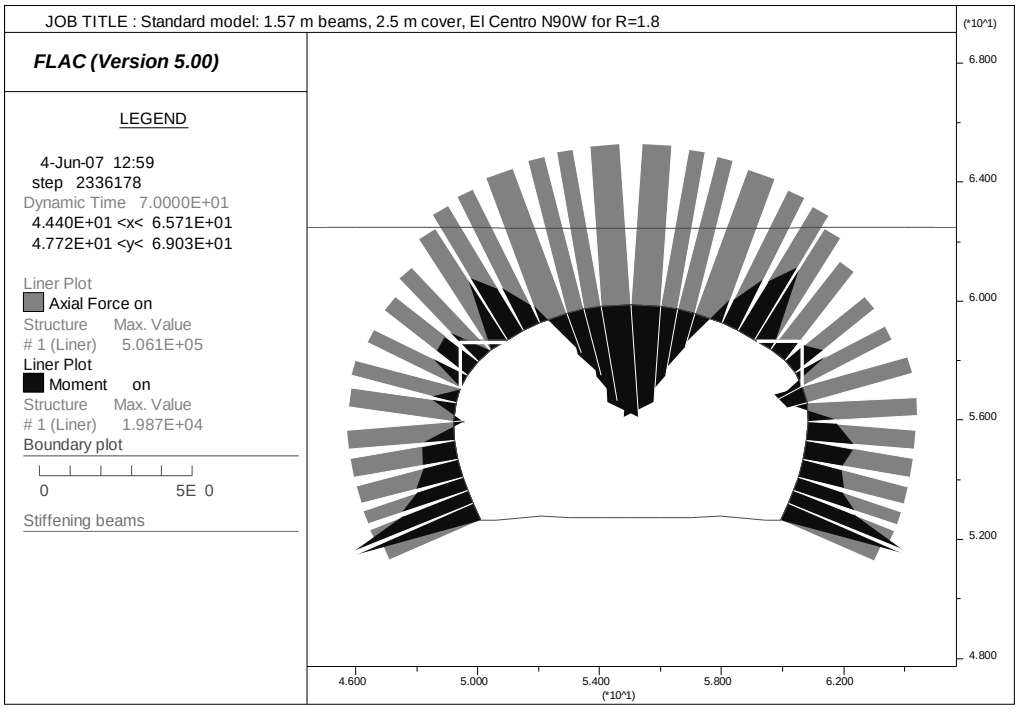

Figure 5.5 Axial force and bending moment distributions around the culvert for the model with 1.57 m beams and 2.5 m cover after shaking for an R =1.8 earthquake.

Note: The scale is the same as in Figure 5.4 (construction forces and moments are included). Forces are in N/m and moments in Nm/m.

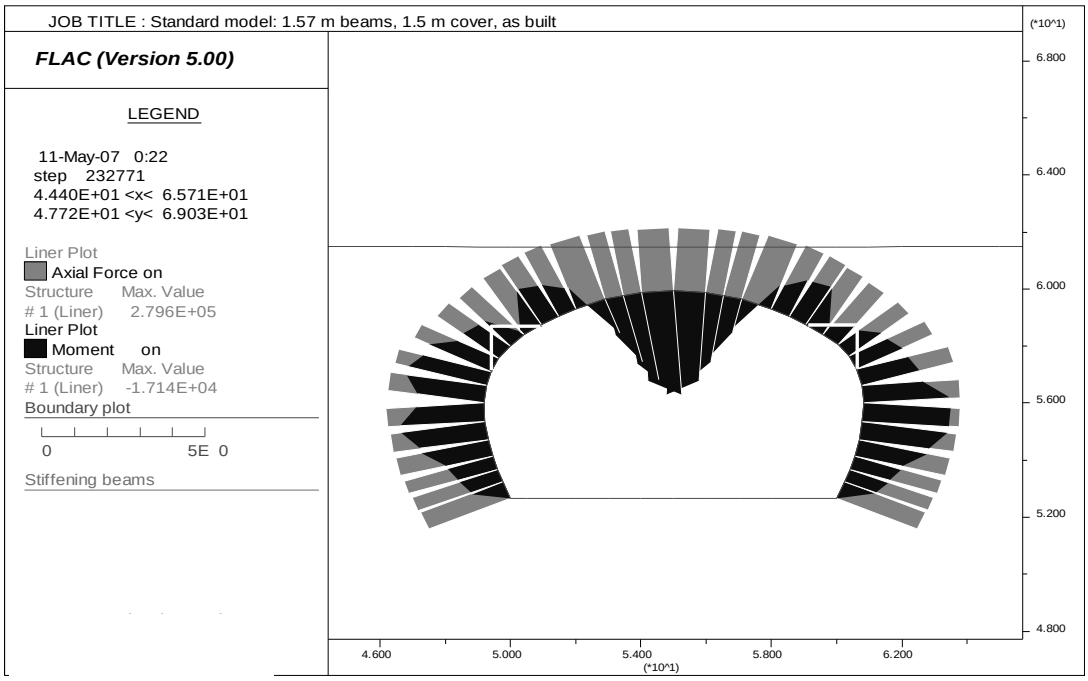

Figure 5.6 Axial force and bending moment distributions around the culvert for the model with 1.57 m beams and 1.5 m cover after construction.

Note: The scale is the same as in Figure 5.4. Forces are in N/m and moments in Nm/m.

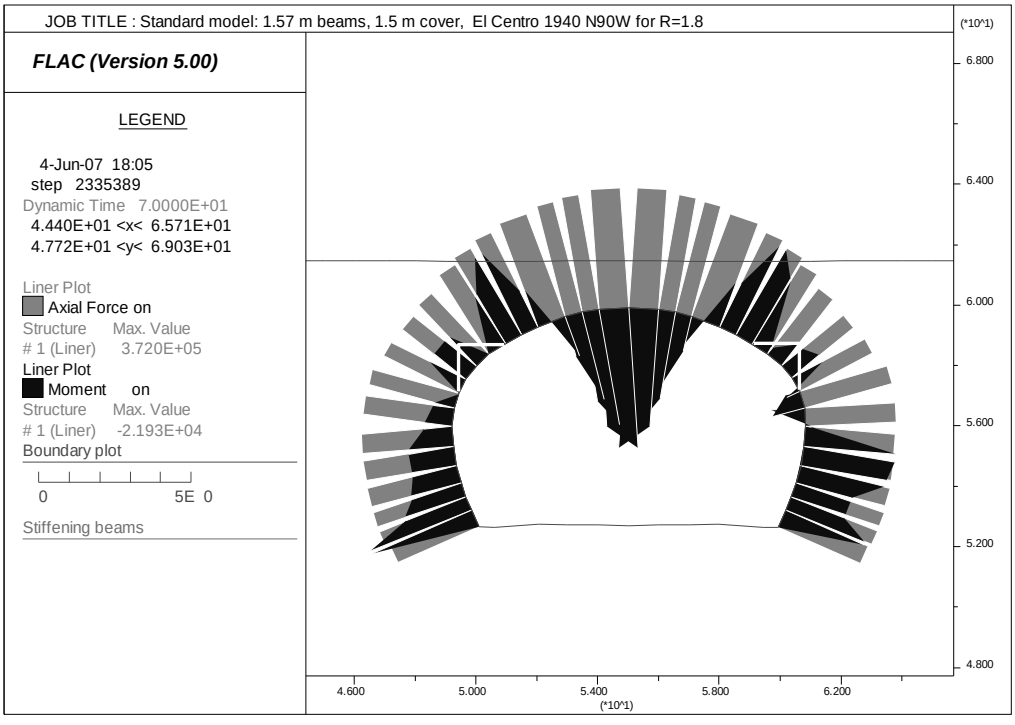

Figure 5.7 Axial force and bending moment distributions around the culvert for the model with 1.57 m beams and 1.5 m cover after shaking for an R =1.8 earthquake.

Note: The scale is the same as in Figure 5.4 (construction forces and moments are included). Forces are in N/m and moments in Nm/m.

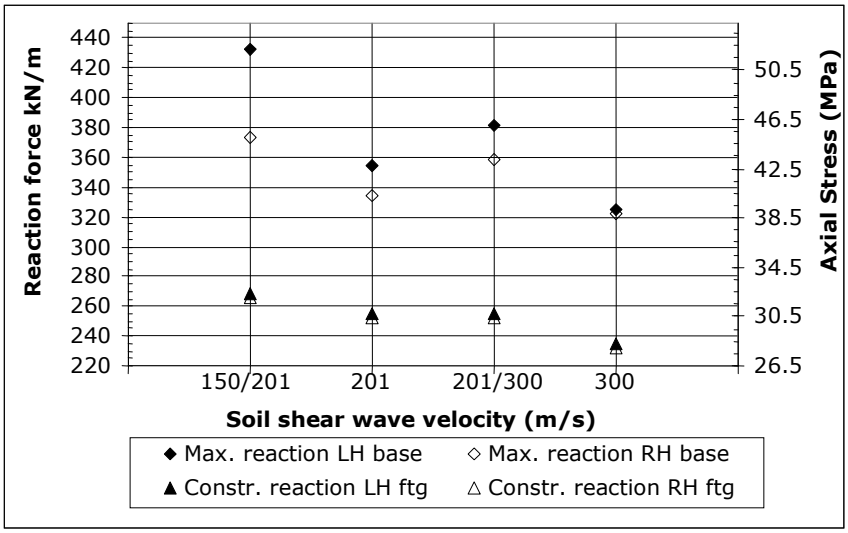

Figure 5.8 Footing thrust forces and stresses at left hand (LH) and right hand (RH) footings.

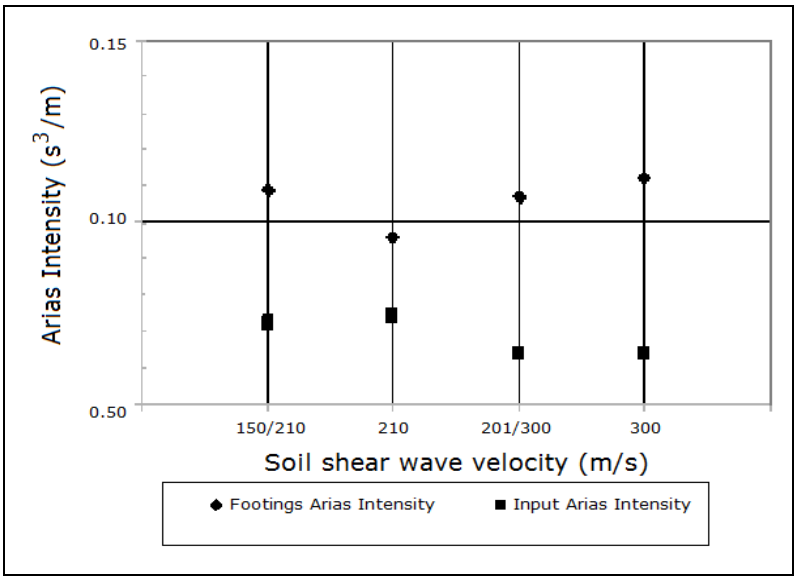

Figure 5.9 Arias Intensity at the input (base of model) and at the culvert footings.

The maximum axial and bending stresses, over all structural elements during the earthquake, are shown in Figure 5.10 and Figure 5.11, along with the greatest dynamic increments in those stresses. The dynamic increments are the maximum transient increase during the earthquake above the value in place before the earthquake started. The axial stresses change little during the earthquake in all soil types. The maximum bending moment increments, however, are greatest in the soft soil (about one quarter more in the 150 m/s soil compared to the 300 m/s soil) and the maximum increase in bending moment during shaking is nearly double in the softer soil compared to the 300 m/s soil. In most cases, maximum bending and axial stresses during shaking occurred at or near the crown (element 17 or 18; see Figure 4.3). The maximum dynamic increment in bending stress occurred in the elements below the spring line while the

maximum dynamic increase in axial force was near the crown. A higher dynamic bending increment below the spring line with the softer soil reflects the doubling of the closure between the footings with the softer soil compared to the stiffer backfill (Figure 5.2).

The maximum axial or thrust stresses shown in Figure 5.10 are all less than half the ultimate compressive wall stress of 107.7 MPa (see Table 4.3). The maximum bending stresses, are greater than the buckling moment for the 150 and 201 m/s soil models but still less than the yield stress.

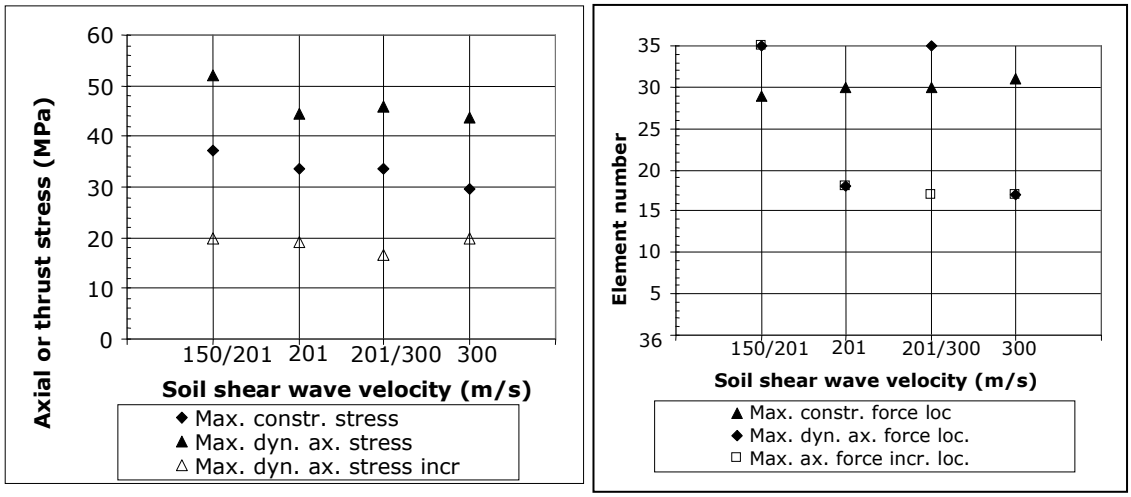

Figure 5.10 Maximum axial stresses and their locations.

Notes to Figure 5.10:
- Elements 35 and 36 are the footings
- 'Incr' means increment.

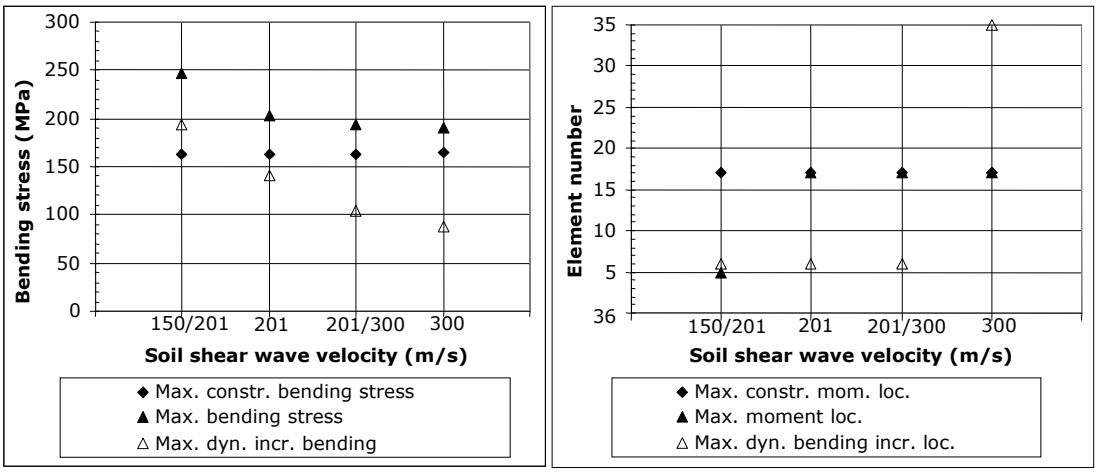

Figure 5.11 Maximum bending stresses and their locations. Elastic behaviour is assumed.

Note: Elements 35 and 36 are the footings

5.2.3 Friction angle

The effect of soil friction on culvert deformation is shown in Figure 5.12. It has almost no effect on the closure of the culvert around the stiffening beams, but has a strong effect on the closure at the footings and thus in the passive rise of the floor. The closure at the footings with 30° soil is more than five times the amount with 40° soil; the closure with 35° soil is intermediate. The overall shear deformation of the culvert, shown in Figure 5.12 as the average racking of node 19 compared to the footings at nodes 1 and 37, is essentially unaffected by the friction angle of the soil.

The axial reactions at the footings are shown in Figure 5.13. Forces – and hence stresses – are greatest for the 40° soil, about 3–4% greater than backfill with a friction angle of 35°, and 7–8% greater than when the backfill has a friction angle of 30°. The maximum stress in the 40° soil is about 40% of the ultimate compressive wall stress (Table 4.3). The dynamic increments of reaction for the 40° soil are almost double those for the 30° soil.

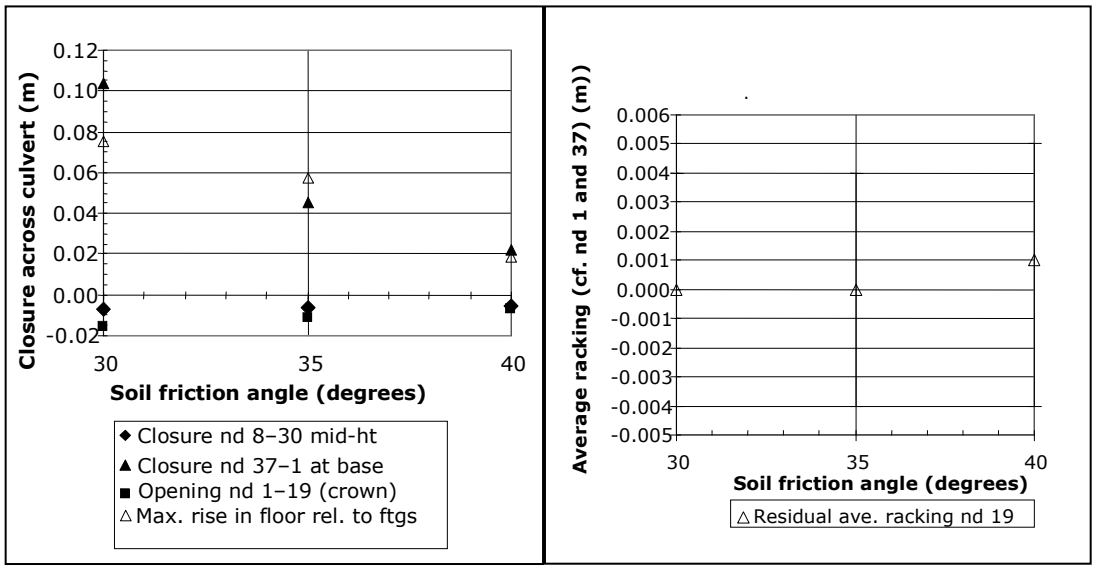

Figure 5.12 The effect of soil friction angle on culvert deformation.

Note: Down error bar is maximum left racking; up error bar is maximum right racking.

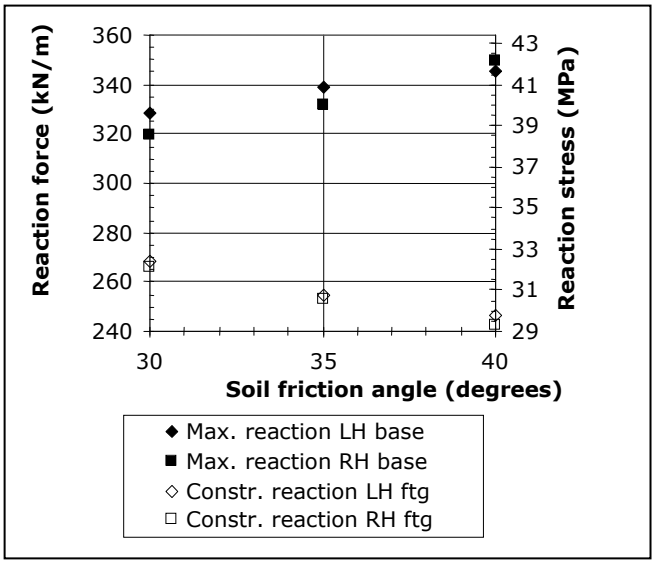

Figure 5.13 Axial reaction forces and stresses compared to soil backfill friction angle.

The maximum bending and axial stresses in the culvert elements are shown in Figure 5.14 and Figure 5.15. The maximum axial stress is relatively insensitive to the soil friction angle. The maximum dynamic increment of axial stress has some sensitivity to backfill friction angle but the differences are minor. The bending stresses are more strongly affected by the soil strength when the friction angle is less than about 35°, with an increase of about 50% between 35° and 30° soil. The reduction in bending stress between 35° and 40° soil is small. With weaker (30°) soil, the maximum bending and axial stresses are located near the crown. With the 35 and 40° soil, the maximum axial force is near the footings; the maximum moment is near the footings for the 40° soil only. The greatest dynamic increase in axial force follows the location of the maximum dynamic force and the maximum increase in bending is always below the spring line (the widest point) or near the footings.

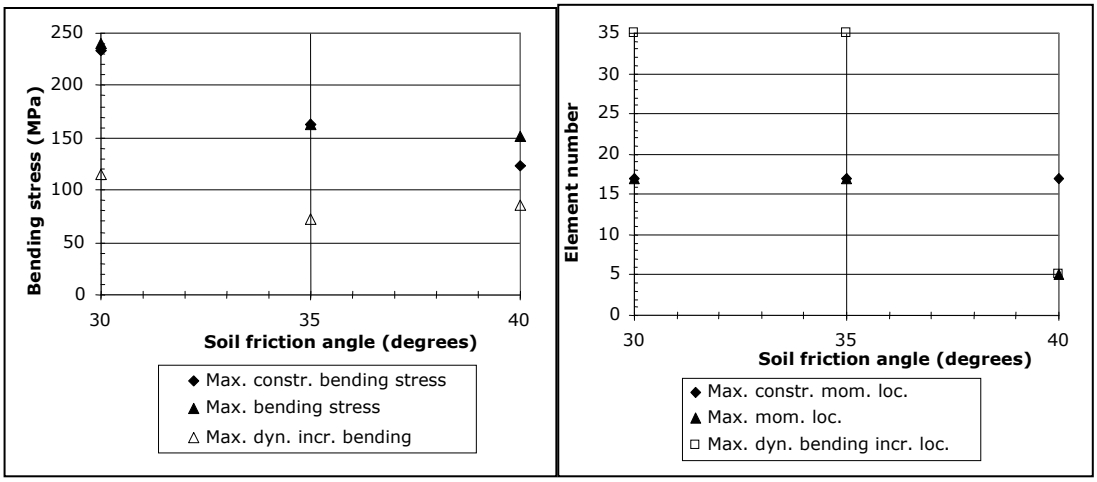

Figure 5.14 Maximum bending stresses compared to soil friction angle (left) and the locations of the maxima (right).

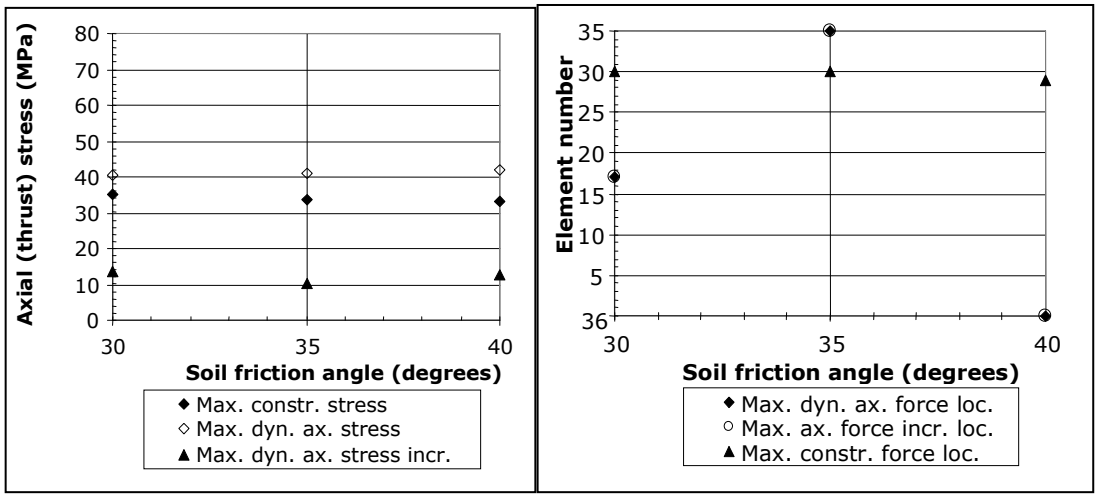

Figure 5.15 Maximum axial stresses compared to backfill soil friction angle and the locations of the maxima.

Note: Elements 35 and 36 are the footings.

5.2.4 Cohesion

The effect of backfill soil cohesion on culvert deformation is shown in Figure 5.16. As for backfill soil friction angle, backfill cohesion has no significant effect on closure (span reduction) near the spring line (nodes 8 to 30) or above the stiffening beam locations (node 14 to 24). However, the stiffer soil (cohesion of 10 kPa) has about one-quarter of the closure at the footings (node 37 to node 1) of the non-cohesive soil. The culvert in intermediate soil has about half the closure of the culvert at stiffer soil. The shear deformation of the culvert (residual racking at node 19 and the maximum left and right racking, shown in Figure 5.16) does not appear to be affected by the soil cohesion.

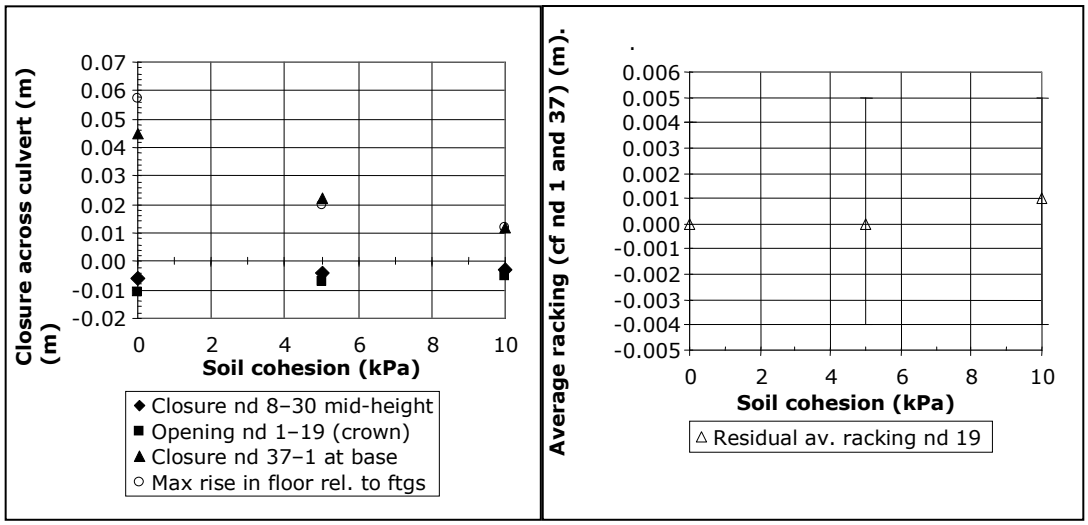

Figure 5.16 The effect of backfill soil cohesion on culvert deformation – closure (left) and racking of node 19 in the crown (right).

Note: Down error bar is maximum left racking; up error bar is maximum right racking.

Axial reaction forces at the footings are shown in Figure 5.17. The reaction force is only slightly sensitive to the soil cohesion, although reaction reduces by about 3% between the 5 kPa and 10 kPa soil models.

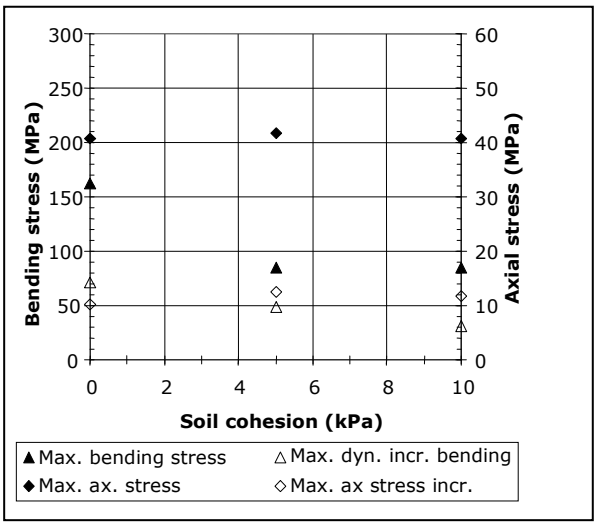

Figure 5.17 Axial forces and stresses at the footings.

Backfill soil cohesion has almost no effect on the maximum axial stress in the culvert (Figure 5.18) or on its location at the footings. Where the backfill soil has no cohesion, the maximum bending stress is nearly double the value when the soil has significant cohesion. The maximum dynamic increment of bending stress decreases with backfill cohesion, by about one-third between each interval, from 0 to 5 and from 5 to 10 kPa cohesion. With no cohesion, the maximum bending moment is near the crown (element 17); with significant cohesion, it is at the base of the stiffening beam (element 29) for 5 kPa cohesion and below the springline for 10 kPa. The maximum dynamic increment in bending moment is always near the footings.

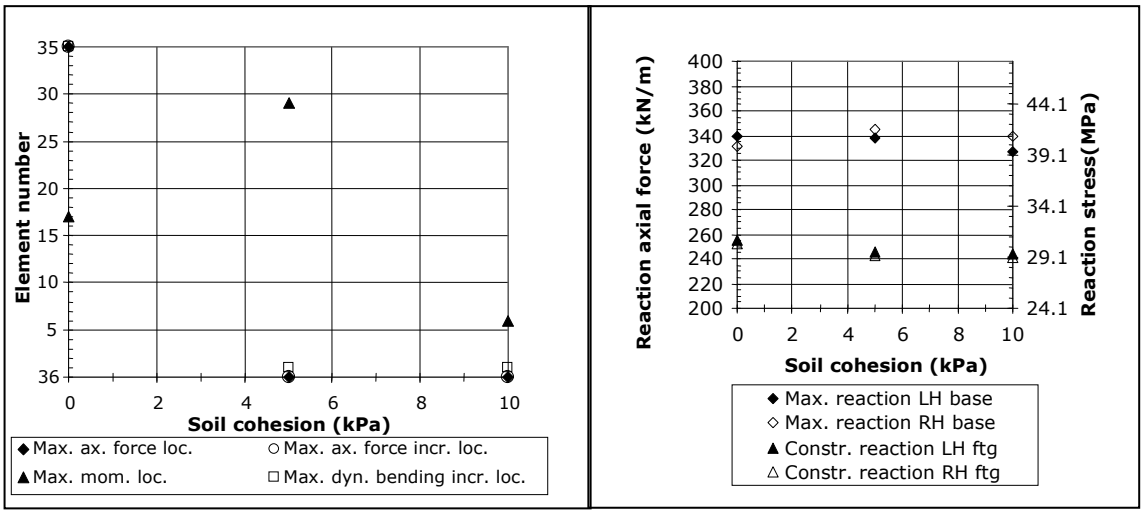

Figure 5.18 Maximum stresses per metre of culvert, as affected by backfill soil cohesion (left) and their locations (right).

Note: Elements 35 and 36 are the footings.

5.2.5 Dilation angle

Soil dilation is a variable often ignored in numerical modelling. For example, the soil constitutive model used by Duncan & Seed (1986) and Seed & Duncan (1986) was a hysteretic K_0 model which could not model dilation, but gave acceptable results at low strains (Seed & Ou 1987).

Shear dilatancy (or simply dilatancy) is the change in volume that occurs with shear distortion of a material. Dilatancy is characterised by a dilation angle, ψ, which is related to the ratio of plastic volume change to plastic shear strain (Itasca 2005a). During seismic shaking, elements of soil behave plastically from time to time (absorbing energy and thus damping the passing seismic waves) so the effect of soil dilatancy on culvert deformation and stresses during earthquake shaking should be tested.

The effect of backfill dilatancy on culvert deformation is shown in Figure 5.19and Figure 5.20. Only minor differences appear in construction deformations when dilation is considered. When no dilation is allowed, 'peaking' deformations (rise of the crown relative to the footings plus narrowing of the widest span) are about one-third greater during construction than when dilation is modelled.

The dynamic deformations were zero at the beginning of shaking. Between 0° and 10° dilation, closure reduces by 60% across the spring line (Node 8 to 30), although this closure is insignificant (less than 10 mm or 0.1% of the span). No effect on closure appeared above the stiffening beams (node 14 to 24). At the footings, more dilatant soil leads to an almost linear reduction in closure from some 57 mm with 0° dilation angle to 37 mm with 10° dilation angle. The heave in the floor relative to the footings increases about two-thirds from the non-dilatant to the 5° case but no further with increased dilatancy. Racking of node 19 relative to the footings is small and the changes with soil dilation are not significant. Thus soil dilatancy affects the nature of the passive failure that is part of closure at the footings and causes heave of the floor relative to the footings, but has little effect on deformation otherwise.

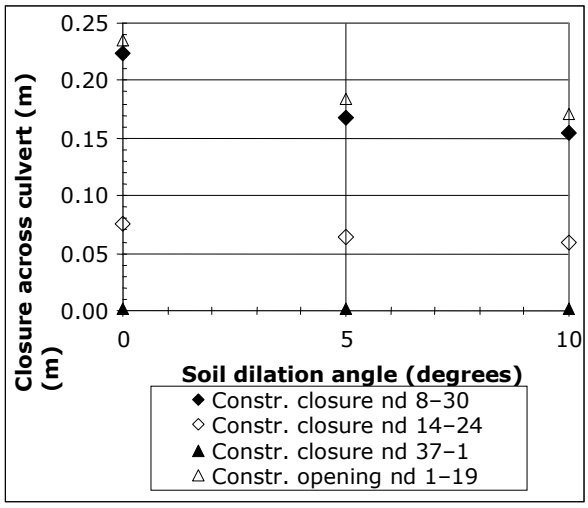

Figure 5.19 Construction deformations as affected by soil dilation angle.

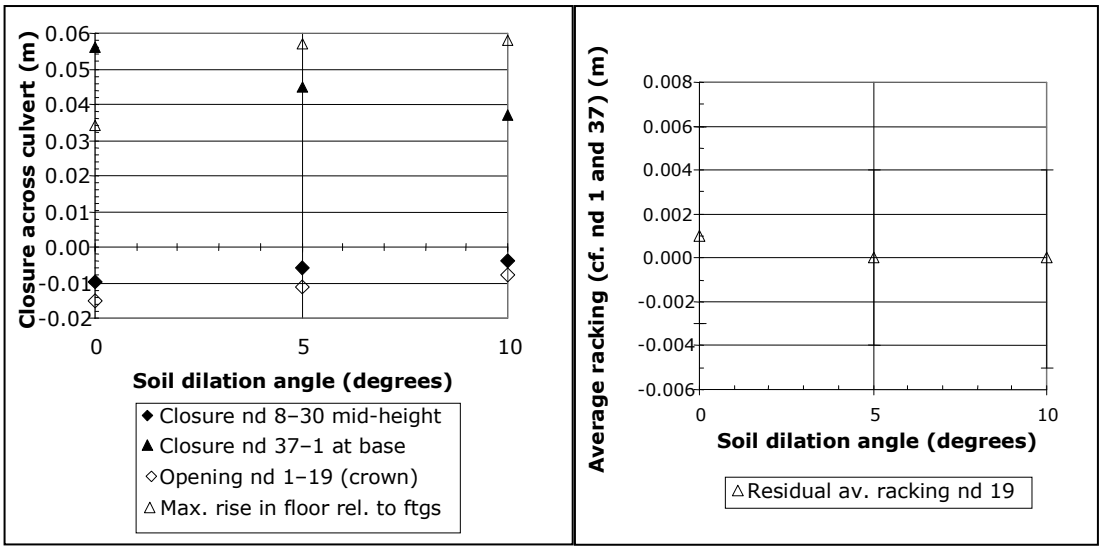

Figure 5.20 The effect of soil dilation on culvert deformation.

Note: Down error bar is maximum left racking; up error bar is maximum right racking.

The axial forces at the footings reduce slightly (about 1.5%) as soil dilation increases from 0 to 5° (Figure 5.21) and a further reduction of about half this amount as the dilation angle increases to 10°. The same pattern is seen in the construction footing forces (Figure 5.21).

The maximum bending stresses versus soil dilation angle are shown in Figure 5.22. Construction and dynamic maximum bending stress forces are the same for all values of dilation angle and are located in the crown. They reduce by 17% as the dilation angle increases from 0 to 10°. The maximum dynamic increment of bending reduces by 14% as the dilation angle increases from 0 to 10° and remains located at the footings. This effect originates from construction.

Figure 5.23 shows the effect of soil dilation on thrusts. Construction forces reduce slightly as soil dilatancy increases. The maximum dynamic increment in thrust also decreases by a few percent for each increase in dilation angle. The maximum dynamic thrust is in the footings while the maximum construction forces are around the springline, where the plate curvature is greatest. The maximum dynamic increases for both bending and thrust are in the footings when the soil is dilatant; the maximum thrust increase when the soil is non-dilatant is in the crown.

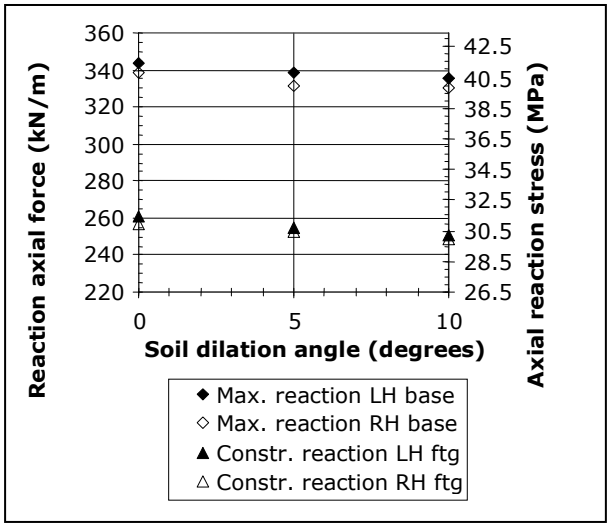

Figure 5.21 The effect on axial reaction forces and stresses at the footings from backfill soil dilation angle.

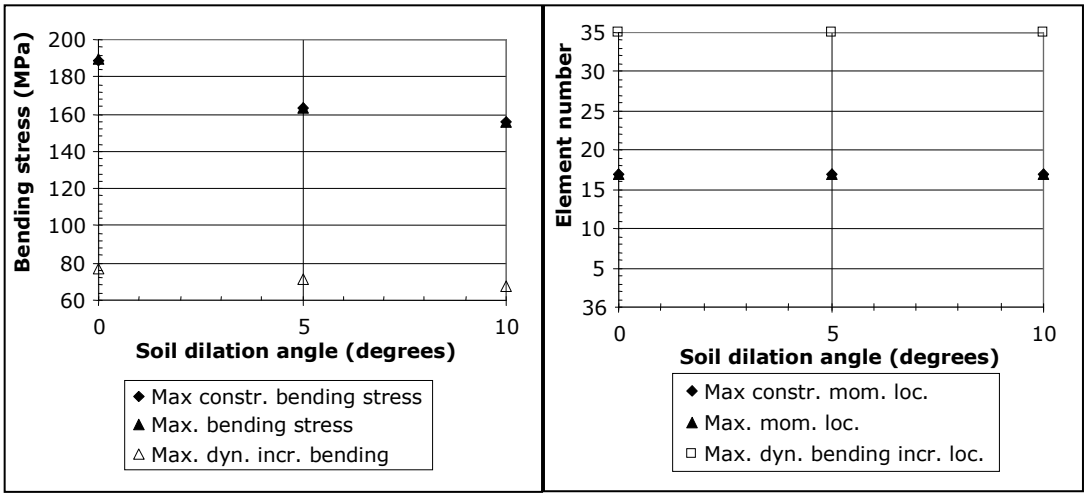

Figure 5.22 Bending stresses and how they are affected by backfill dilation angle.

Note: Elements 35 and 36 are the footings.

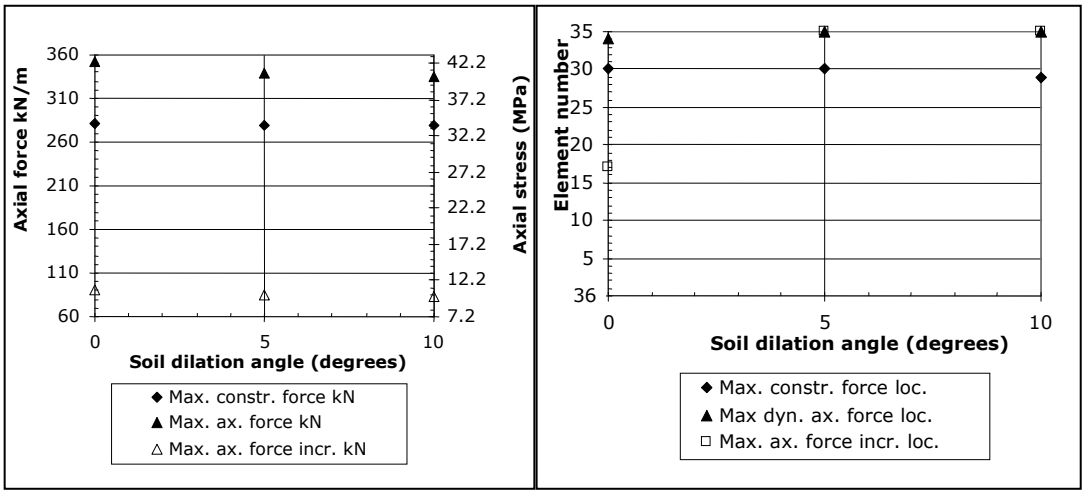

Figure 5.23 Soil dilation angle and how it affects the maximum thrusts.

Note: Elements 35 and 36 are the footings.

5.3 Cover

The effect of culvert cover was tested using 1, 1.5, 2, and 3 m of cover with no stiffening beams, and 1.5, 2 and 2.5 m cover with 1.57 m stiffening beams. The tests with no beams used the El Centro Imperial Valley Irrigation District S00E component scaled by a factor of 1.52 for R =1.0. The tests with beams used the N90W component of this earthquake, scaled for R =1.8. The results are shown in Figure 5.24 to Figure 5.28.

Construction deformations are essentially unchanged by the depth of cover (Figure 5.24). Two-zone stiffening beams reduce construction deformations by about 40%. With seismic shaking (Figure 5.25), closure of the culvert across the spring line reduces as the cover increases, from 16 mm with minimal cover of 1 m, to about 3 mm with 2 m of cover; the culvert spreads with greater cover. Stiffening beams make no significant difference on closure of the culvert during an earthquake. The change between 2.5 and 3 m of cover probably reflects the phenomenon discussed at the end of this section. Closure between the footings, and the rise in the floor that accompanies it, appear to be directly related to culvert cover within the range tested. Stiffening beams result in an increase of about one-third in this deformation.

In Figures 5.24–5.29, filled (solid) marks indicate that the model used 1.57 stiffener beams, while unfilled (hollow) marks indicate the absence of beams.

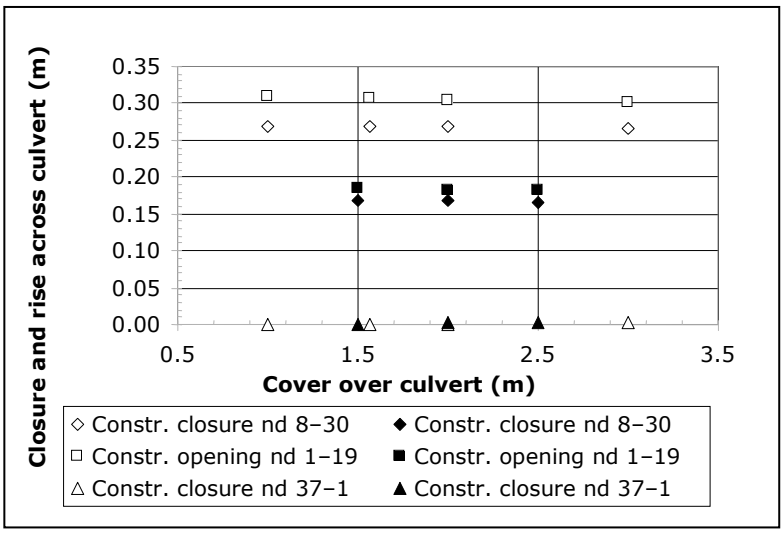

Figure 5.24 Construction deformations related to the cover depth.

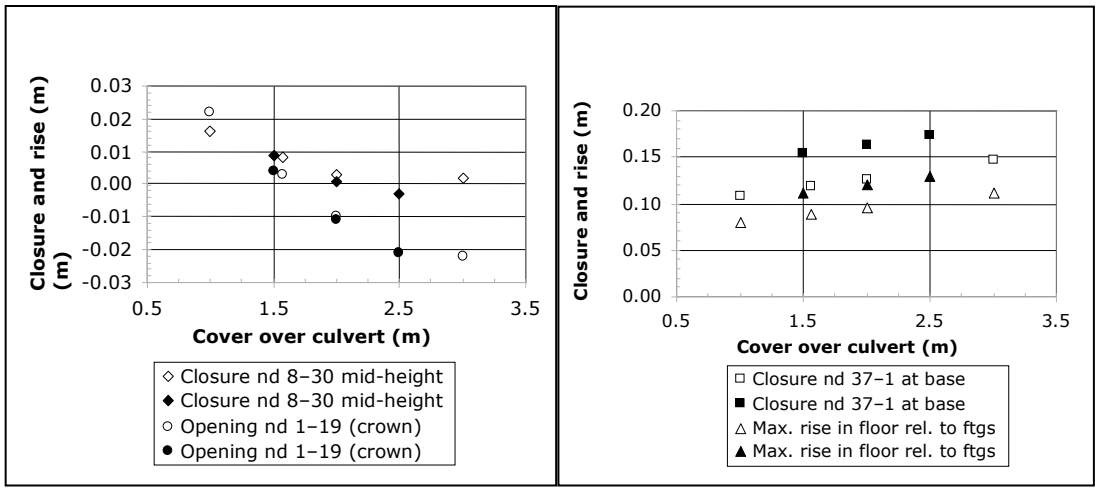

Figure 5.25 Culvert deformation as affected by cover depth.

Transient racking of the culvert relative to the footings (Figure 5.26) increases linearly with cover within the range tested, from some 15 mm with 1 m cover to 21 mm with 3 m of cover. Stiffening beams cause a small decrease in racking deformations.

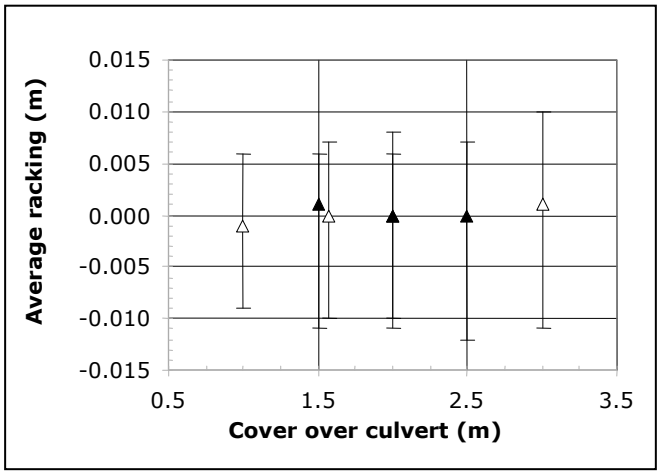

Figure 5.26 Culvert racking deformation of node 19 in the crown, as affected by cover depth.

Note: The triangles are the permanent deformation. Deformations are averaged relative to nodes 1 and 37 (the footings).

Figure 5.27shows the relationship between the reaction forces and culvert cover. It appears to be linear within the range of the test. Construction reactions are about 10% greater with stiffening beams, but dynamic reactions are almost the same with or without beams in place. The maximum stress is about half the ultimate wall compressive stress (Table 4.3).

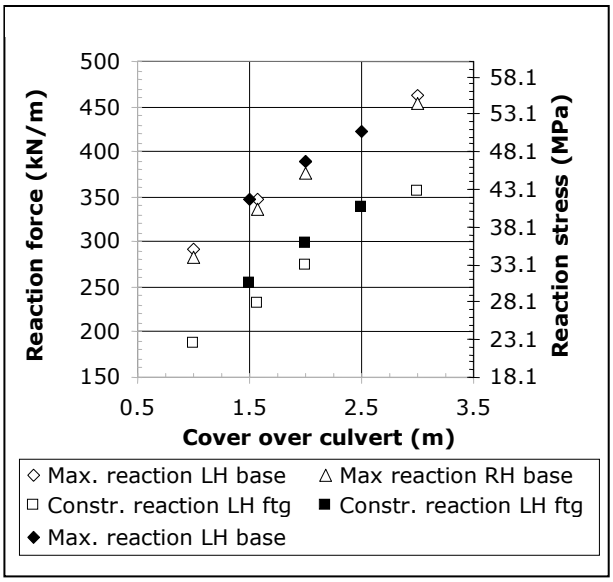

Figure 5.27 Footing axial reaction forces and stresses.

The maximum construction bending stresses are almost unaffected by depth of cover (Figure 5.28) for cases with or without stiffening beams. In all cases, maximum construction bending stresses are located in the crown. The stiffeners, however, cause a decrease in maximum construction bending stresses of about one-third.

Without stiffeners, the maximum dynamic bending stress decreases significantly (more than 20%) as cover increases from 1 to 2 m, with a small decrease (about 2%) from there to 3 m cover. With stiffeners, the effect is similar and the maxima bear a similar relationship to the construction moments, as they do when stiffeners are not used. The maximum dynamic bending increments are similar, with and without stiffeners, for cover greater than about 1.5 m. With only 1 m of cover, the maximum dynamic bending increment is about two-thirds of when more realistic cover depths are used. In all cases, the maximum dynamic increments are located either near the spring line or near the footings. The maximum dynamic moments are located in the crown when no stiffeners are present, and move to the footings when stiffeners are present and cover is 2 and 2.5 m.

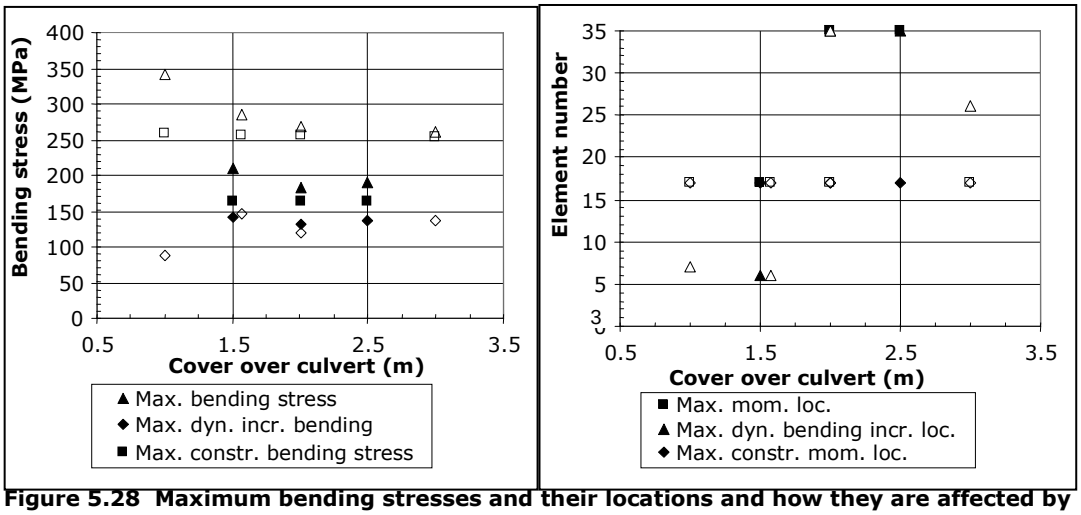

Figure 5.28 Maximum bending stresses and their locations and how they are affected by cover depth on a culvert.

Note: Elements 35 and 36 are the footings.

Maximum axial (thrust) stresses show the opposite effect, with a linear increase (nearly 50%) to 2 m cover and about half as much again over the next metre to 3 m cover. With stiffening beams present, the increases with cover are similar and the amounts are slightly greater (up to about 5%). The maximum dynamic increases in thrust also increase with cover, almost linearly to about 2 m, but the rate of increase seems to reduce as cover increases further. With no stiffeners, no increase is seen from 2 to 3 m cover, while with stiffeners, a further increase appears to 2.5 m, but the rate is less than from 1.5 to 2 m. With stiffeners, the increase is greater above 1.5 m cover than without them.

Maximum construction thrusts are always around the widest part of the culvert with stiffening beams (i.e. just below the beams) and within the area covered by the beams when beams are absent (above the widest part of the culvert). The maximum dynamic thrust and the maximum dynamic increment of thrust are in or near the crown with or without stiffeners, apart from the case with 1 m cover, when it is at the footings.

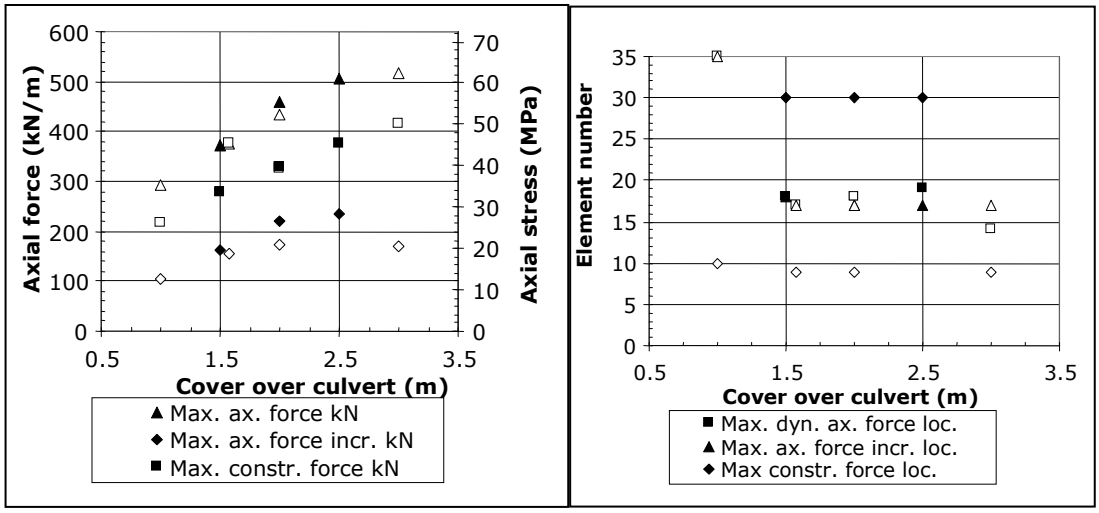

Figure 5.29 Maximum axial forces and their locations and how they are affected by cover depth on a culvert.

An unusual effect was observed in the models with 3 m of cover. The density was reduced in four places located symmetrically on each side of the culvert, as shown in Figure 5.30. Horizontal stress also reduced slightly at those locations, but no other property seems to have been affected significantly enough to show up, including vertical and shear stresses. An attempt was made to run a model with 1.57 m high stiffening beams and 3 m of cover, and the same effect was observed. In this case, however, the geometry of the surface elements changed so much the run stopped after about 17 seconds of dynamic time. This appears to be the result of a focusing of the upward travelling shear waves by the culvert opening and is expected to be a real phenomenon related to the geometry of the system.

Figure 5.30 also shows the formation of an arch of increased density, from the shoulder of the culvert away to the side. The change in density is less than 20 kg/m^3; areas shaded lightly had a density ranging from 2000–2010 kg/m^3, while darker areas indicate a density of 1990–2000 kg/m^3. Figures 5.31–5.33 show that the density arch diminishes as the cover decreases. It appears likely that a culvert with 2 m cover should perform better than one with 1.5 m because the arch is more complete. These figures show culverts without stiffening beams.

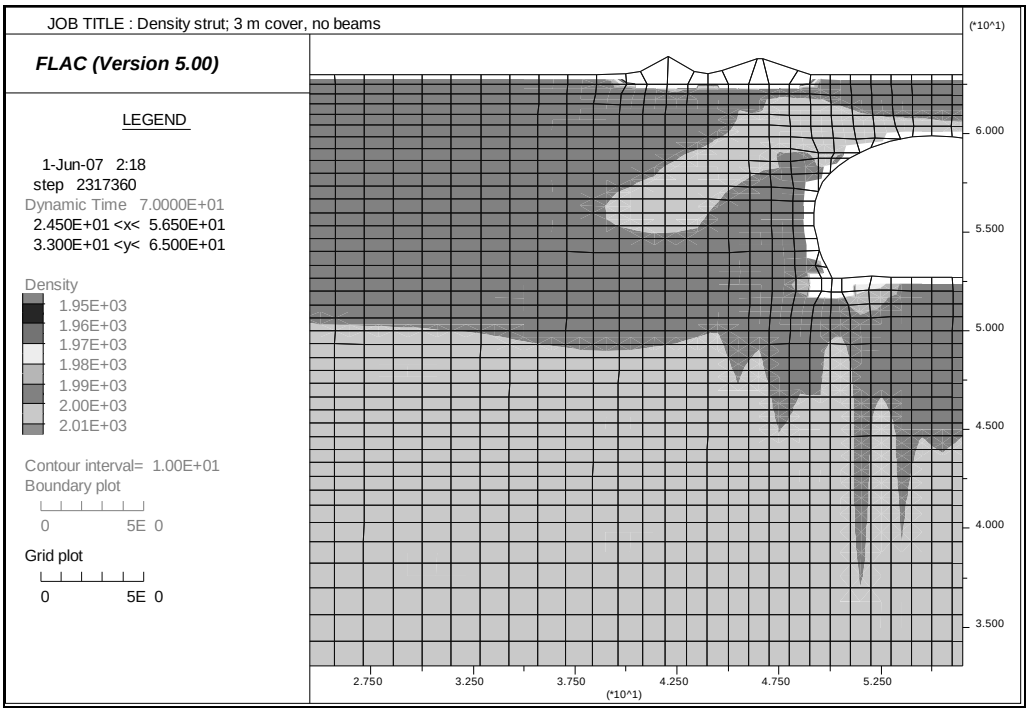

Figure 5.30 Density contours showing the surface disturbance (reduced density) with 3 m of cover, after earthquake shaking (dynamic time =70 seconds).

Notes: The effect is symmetric on the other side and only appears with 3 m of cover. Note the increased density (lighter shade) forming a soil arch.

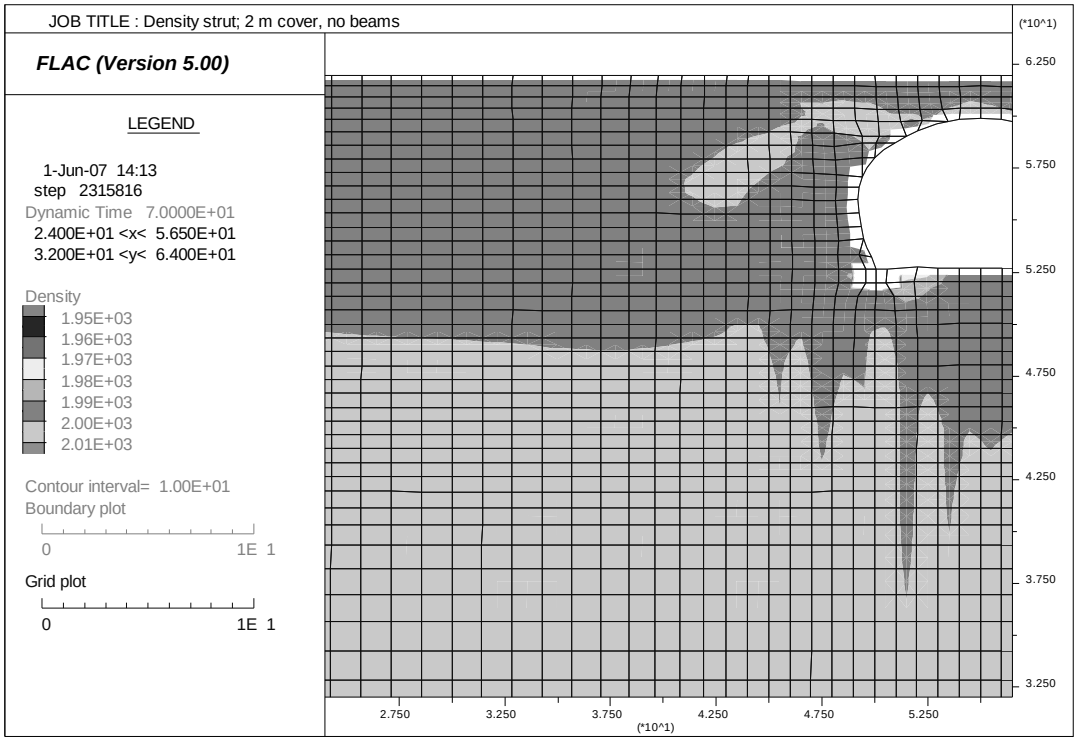

Figure 5.31 Density contours for model with 2 m cover and no beams, after shaking.

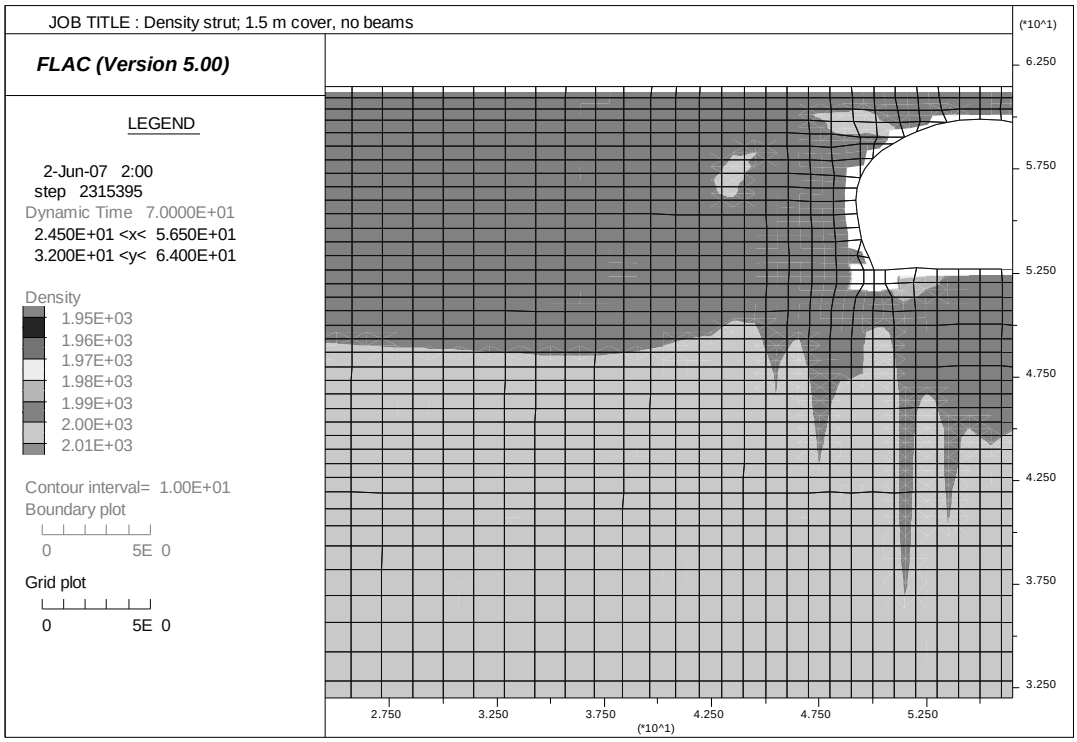

Figure 5.32 Density contours for model with 1.5 m cover and no beams, after shaking.

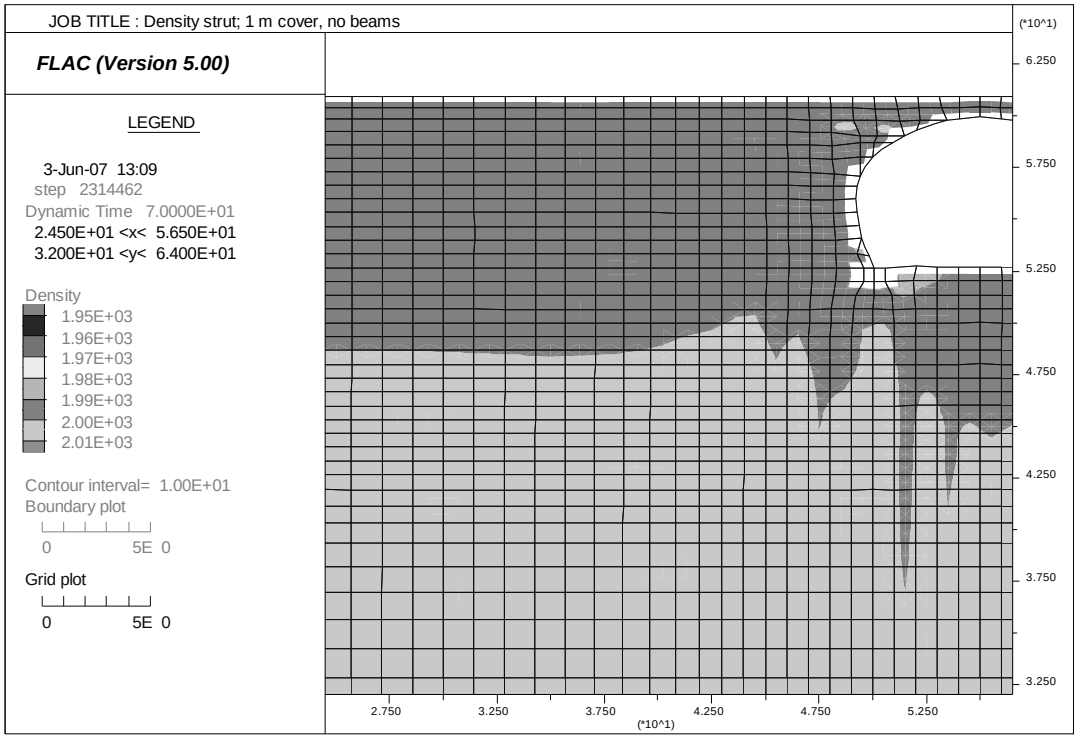

Figure 5.33 Density contours for culvert with 1 m cover and no beams, after shaking.

Figures 5.34–5.36 show the effect on the density arch of adding stiffening beams. These figures show results for the base model, which has stiffening beams 1.57 m high. The arch is incomplete in all cases. A short segment of increased density appears on top of the stiffening beam and another in the same area as the arch seen on the models with no

beams. It seems likely that the incomplete arch will take less load off the culvert than a complete one, so stiffening beams may result in more load being taken by the steel culvert.

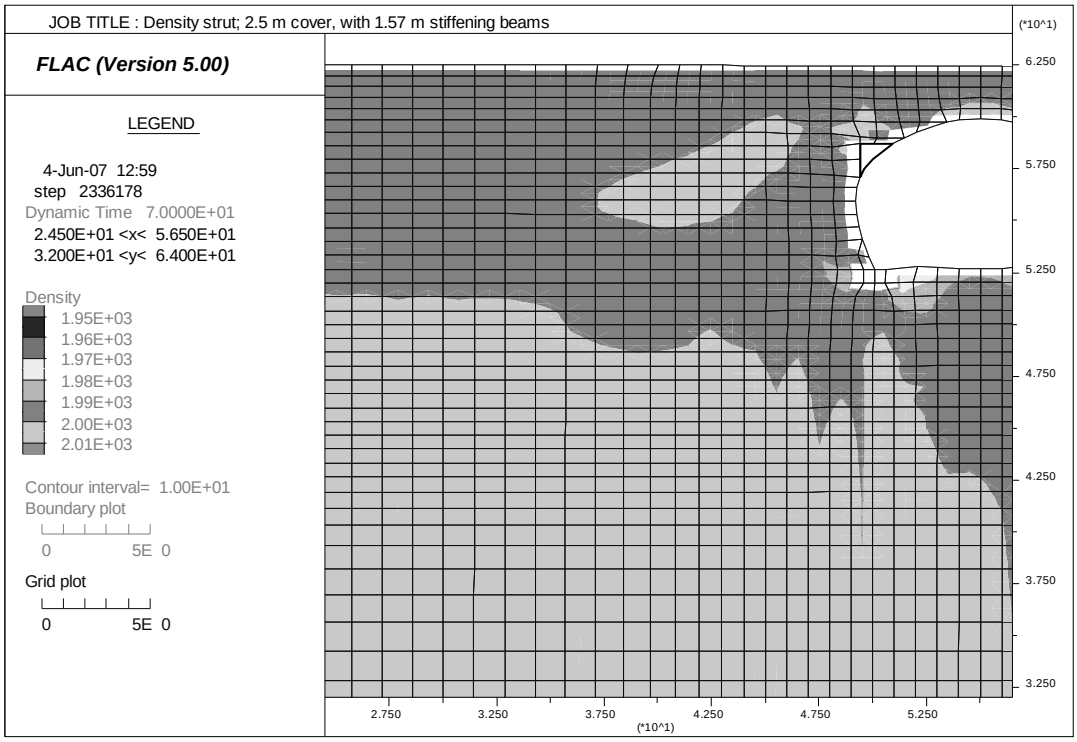

Figure 5.34 Density contours for culvert with 2.5 m cover and 1.57 m stiffening beams, after shaking (dynamic time =70 seconds).

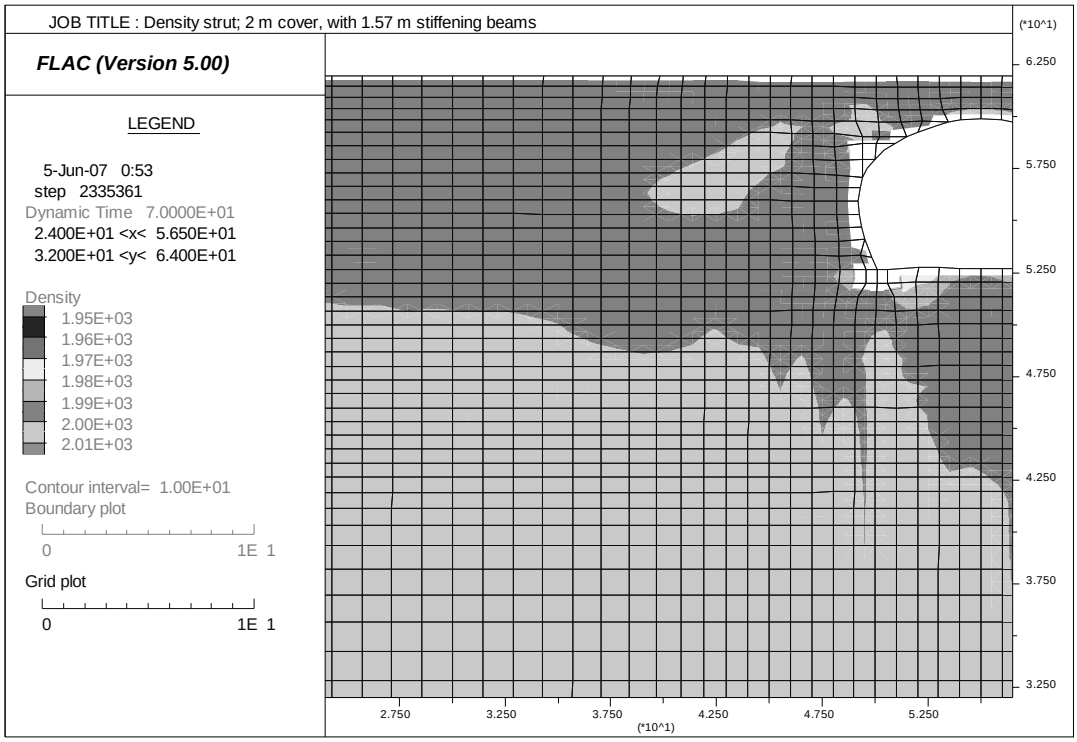

Figure 5.35 Density contours for culvert with 2 m cover and 1.57 m high stiffening beams, after shaking.

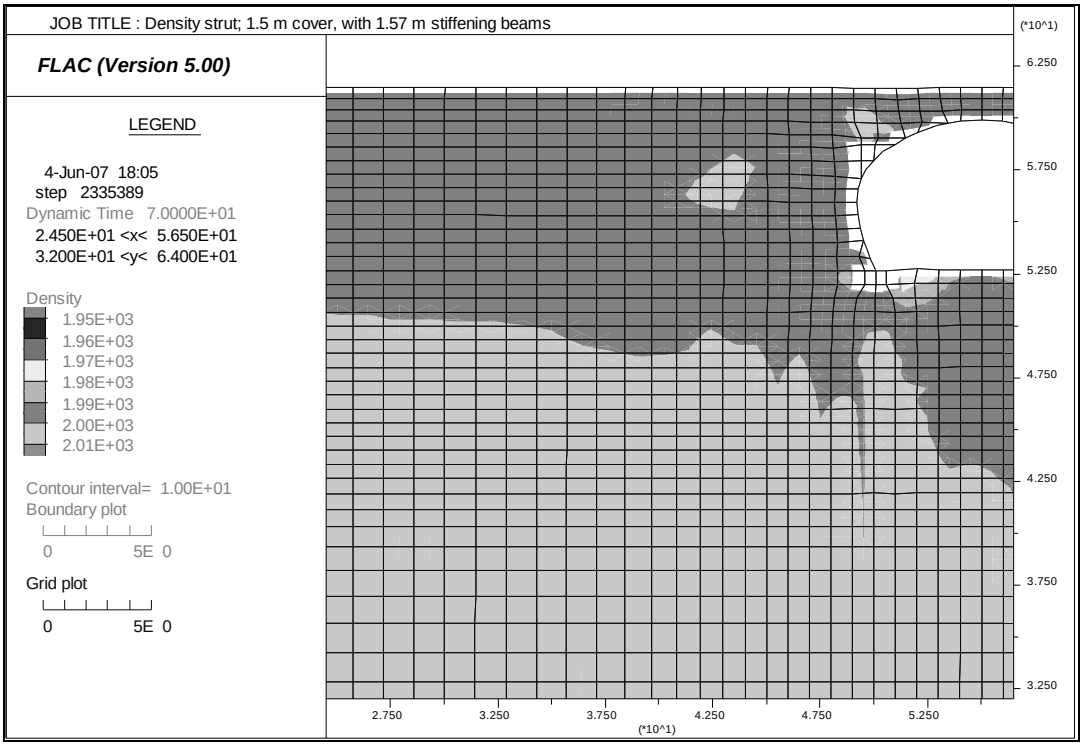

Figure 5.36 Density contours for culvert with 1.5 m cover and 1.57 m high stiffening beams, after shaking.

5.4 Stiffening beam height

Tests were carried out with no stiffening beams, and with beams one, two and three zones (0.87, 1.57 and 1.87 m) high (see Figure 4.3). The locations of the stiffening beams are shown in Table 5.1. The beams had elastic moduli, friction angle, dilation angle and cohesion properties representative of concrete and were glued to the structural elements they were beside. The soil and the stiffening beams had no interface between them. The base model was used for these tests:

- 1.5 m cover,
- soil with 201 m/s shear wave velocity,
- a friction angle of 35°,
- a dilation angle of 5°,
- cohesion 1 Pa, and
- El Centro 1940 earthquake S00E component scaled to R =1.0.

As noted earlier, the addition of a stiffening beam reduces the peaking construction deformations by about one-third (Figure 5.37). This reduced peaking should also cause a reduction in the bending moment at the crown; this is discussed below. A small further reduction in deformation is seen as the beam increases from 0.87 to 1.57 m high but almost no further effect is seen as it increases further to 1.87 m high.

Table 5.1 Locations of stiffening beams.

Beam height (m)	Structural elements beside stiffening beams		Structural nodes beside stiffening beams	
	Left-hand side	Right-hand side	Left-hand side	Right-hand side
0.87 (1 zone)	27, 26	8, 9	29, 28, 27	9, 10, 11
1.57 (2 zone)	27, 26, 25, 24	8, 9, 10, 11	29, 28, 27, 26, 25	9, 10, 11, 12, 13
1.87 (3 zone)	27, 26, 25, 24, 23	8, 9, 10, 11, 12	29, 28, 27, 26, 25, 24	9, 10, 11, 12, 13, 14

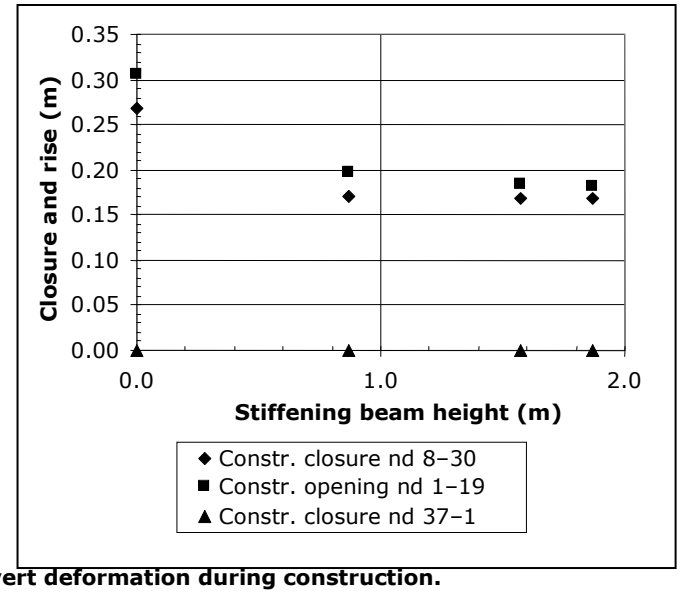

Figure 5.37 Culvert deformation during construction.

Note: Cover was 1.5 m for each test.

Stiffening beams have almost no effect on seismic deformation of the culvert (Figure 5.38). Closure between the footings reduces slightly between no stiffening beam and one 0.87 m high, but the closure with larger stiffening beams is the same as when beams are not used. The change in total racking at the crown is minor as well, when stiffening beams are added.

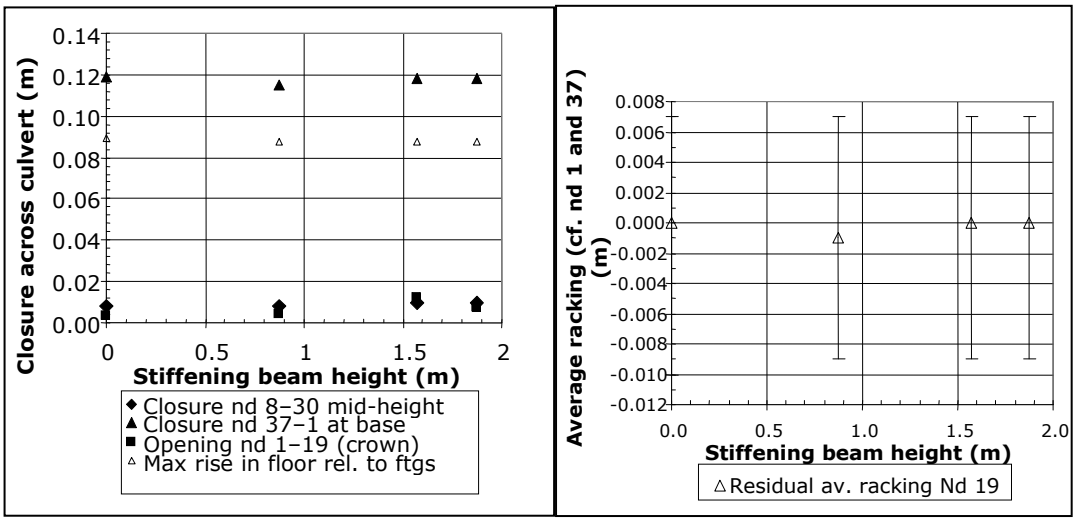

Figure 5.38 Culvert deformation as a result of earthquake shaking, as affected by stiffening beam height. Cover was 1.5 m for each test.

Note: Down error bar is maximum left racking; up error bar shows maximum right racking.

The addition of stiffening beams causes a small (less than 10%) increase in the construction footing thrust (Figure 5.39). The size of the beams has almost no effect on construction footing thrust. With seismic shaking, stiffening beams result in an increase in footing thrust by about 5% in the configuration tested. When the beam is enlarged from 0.87 to 1.57 m high, the footing thrust decreases by 2 to 3%; when the beam is enlarged to 1.87 m high, footing thrust decreases a little further to be similar to when no stiffening

beams are used. The dynamic increment in footing thrust is greatest when no stiffeners are present (about 45%) and reduces to about 35% for 1.57 and 1.87 m high stiffeners.

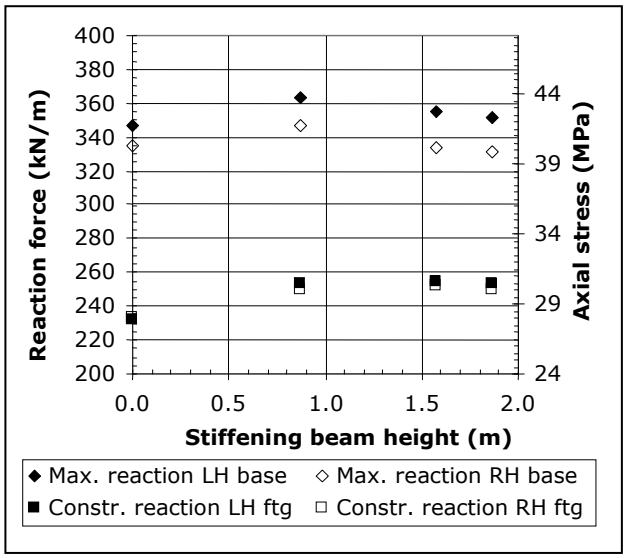

Figure 5.39 The effect on footing thrust of stiffening beam size.

The maximum construction bending stresses reduce significantly when stiffening beams are added (Figure 5.40), reflecting the reduction in peaking deformation noted above. With a one-zone (0.87 m) high beam, maximum bending is reduced (from above the first-yield stress) by approximately 30% compared to the no-beam case and a further 10% reduction occurs when the beams are 1.57 m high. No further change happens for larger stiffeners. The maximum dynamic increments of bending are similar for all cases, except for the smallest stiffeners, when it is about 20% less; the reason for this is not clear. While the maximum dynamic bending stresses follow the same pattern as the construction bending stresses, in fact, they increase relative to construction bending by 12%, 20%, 24% and 26% as the stiffener height increases.

Maximum construction and dynamic bending stresses remain near the crown in all cases (Figure 5.40). The maximum dynamic increment of bending remains around the spring line or near the footings.

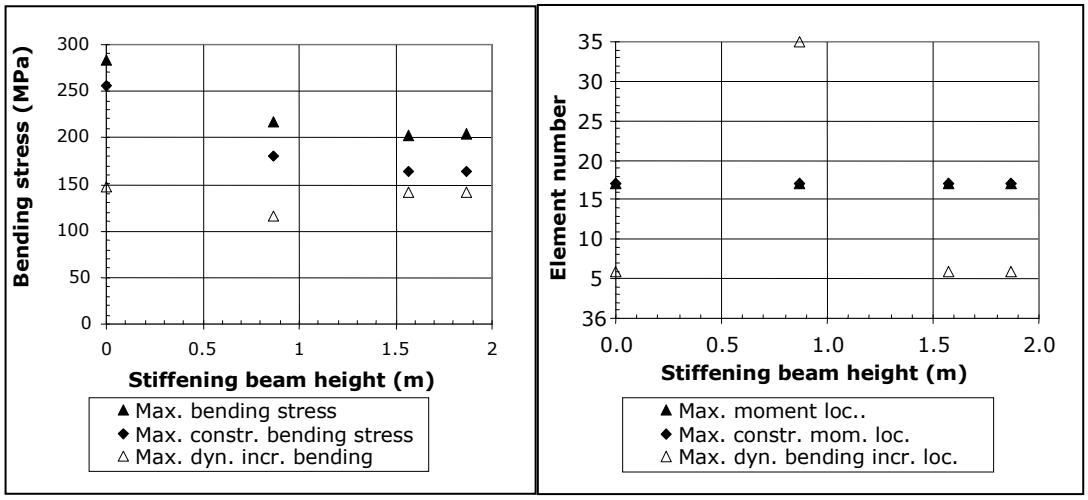

Figure 5.40 Maximum bending stresses with various stiffening beam sizes, and where they occur in the model.

Note: Elements 35 and 36 are the footings.

The addition of stiffening beams has very little effect on the magnitude and location (near the crown) of the maximum axial stress and on the maximum dynamic increment of axial stress (Figure 5.41). The maximum construction stress is also nearly unchanged, but the addition of stiffeners moves it from above the springline (where the stiffeners are located) to just below the base of the stiffener (element 28; see Figure 4.3)), using the smallest stiffener, and then further down to the spring line at the widest part of the culvert with larger stiffening beams.

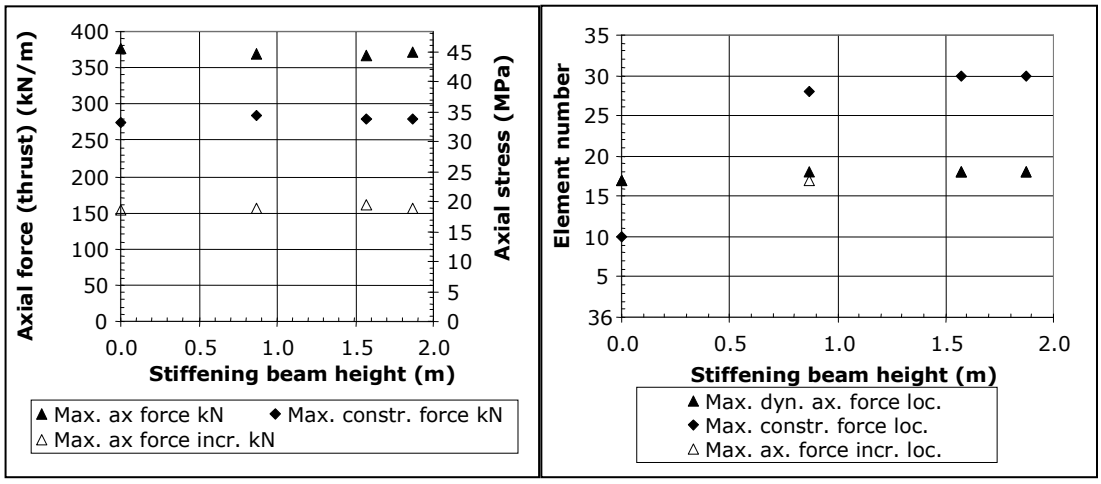

Figure 5.41 Maximum axial stresses with various stiffening beam sizes, and where they occur in the model.

Note: Elements 35 and 36 are the footings.

5.5 Interfaces

Two interface conditions were tested:

- the soil was either free to slip circumferentially around the outside of the culvert and separate from the culvert, or
- it was 'glued' to the culvert and could not slip.

The results are shown in Figure 5.42 and Figure 5.43. These tests were carried out on the base model with 1.57 m high stiffening beams and 1.5 m of cover (see Figure 4.3). The soil and the stiffening beams were effectively joined together with no interface between them.

In Figure 5.42, it is clear that the interface slip condition strongly affects construction deformations (peaking) but has almost no effect on dynamic deformations, including the amount of racking during shaking. The peaking effect is halved when no slip is allowed.

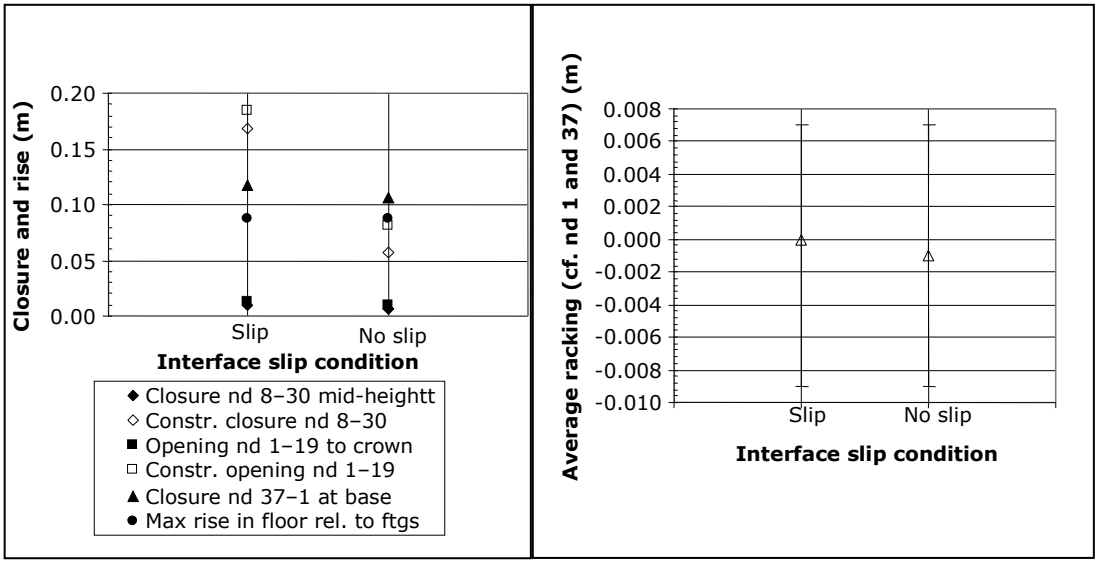

Figure 5.42 The effect on culvert deformation when the soil is allowed to slip, or not, on the outside of the culvert.

Notes to Figure 5.42:
Racking refers to the average movement of node 19 in the crown compared to the footings, nodes 1 and 37.
Down error bar is maximum left racking, up error bar is maximum right racking.

When no slip is allowed, the construction footing thrust is about 15% more than when slip is allowed (Figure 5.43). Seismic reactions are about 20% greater when slip is not allowed. The increase in no-slip seismic thrust over the construction reaction thrust is about 40%, whereas when slip is allowed, it is about 35%.

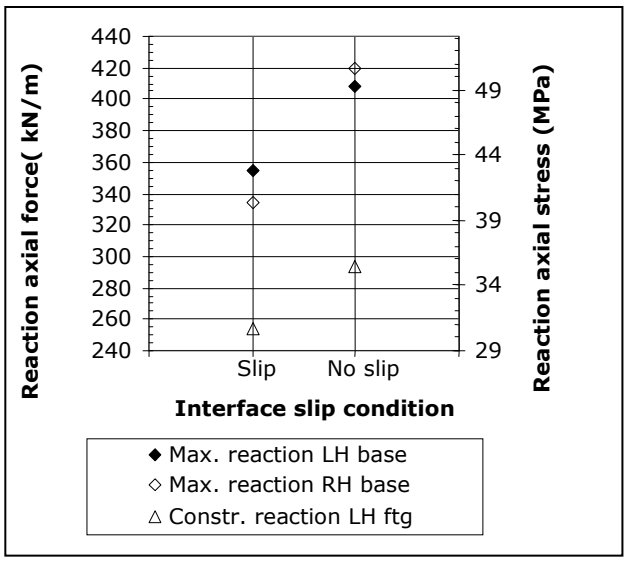

Figure 5.43 Reaction thrusts for slip and no-slip cases.

The interface slip condition has no effect on the quantum or location of maximum construction bending moments (Figure 5.44). The maximum dynamic bending moment is about 18% greater when no slip is allowed and moves from the crown (with slip) to the footing (without slip). The maximum dynamic increment is nearly 10% less without slip but moves from below the stiffener to the footing when slip is not allowed.

The maximum construction axial stress is about 10% greater when slip is not allowed (Figure 5.44) and the maximum dynamic axial stress is about 15% greater with no slip allowed. Construction maxima are located on the side wall near the spring line with slip allowed, and move towards the footings when slip is not allowed. The maximum dynamic axial stress increment also increases about 15% when no slip is allowed, and is located near the crown in both cases.

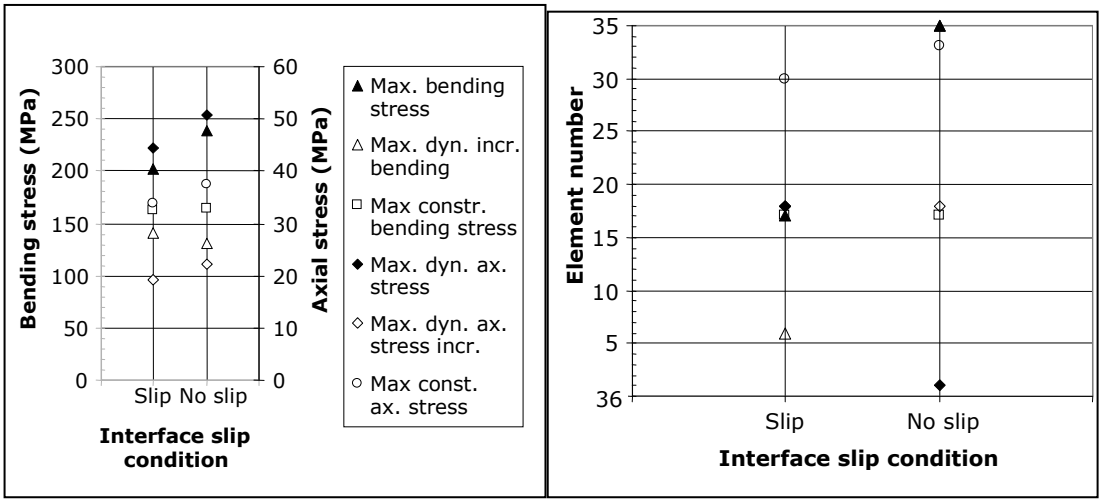

Figure 5.44 Maximum bending and axial stresses and their locations, with and without interface, and with slip and separation allowed between soil and steel culvert.

Note: Elements 35 and 36 are the footings.

5.6 Shape factor

FLAC's liner element formulation includes a property for the structural element that is called the 'shape factor'. Typical values are given for a number of usual shapes, but not for a corrugated section and the manual does not have a clear explanation of what the shape factor represents. As stated in the notes in Table 4.3, the factor for a rectangular section is given as 5/6; for an I-beam, it is the web area divided by the total area, which appears to be the shear area over the total area. The 'form factor' appears to be the inverse of the shape factor: the structural engineering literature provides several formulae for computing the form factor for a variety of cross-sectional shapes and the results can vary significantly (Charneya et al. 2005).

A comparison was done between a run with all structural elements having a shape factor value of 0.4 and one with a value of 0.833 (5/6). Very small differences were seen, so it is concluded that this property does not affect the outcome.

5.7 Earthquake

5.7.1 Introduction

The earthquakes used in the modelling were shown in Table 4.5. Horizontal components for three earthquakes (El Centro Imperial Valley Irrigation District (USA), 1940; Michoacan (Mexico), 1985; and Tabas (Iran), 1978) were chosen to match New Zealand seismic conditions. The records were scaled for periods up to about 1.5 seconds to improve the match of their 5% damped response spectrum to the Class C Site spectrum in NZS 1170.5 (2004). While no particular site was being modelled, earthquakes and scaling factors to represent sites in Wellington (Z =0.4) were used to test the effect of strong shaking on the structures. The scaling factors were calculated by GNS, using a procedure similar to that outlined in the commentary of NZS 1170.5 section C5.5.2 (2004), and received from Graeme McVerry (pers. com. 2007). Factors were used to represent earthquakes for the 500-year return period (R =1.0) and 2500-year return period (R =1.8).

The purpose of this part of the modelling was to try to find earthquake characteristic(s) that could be used in design. Variables tested were the PGA, the peak soil particle or ground velocity (PGV) and the average Arias Intensity at the footings. The Arias Intensity is defined as the integral over the earthquake record of the squares of the accelerations and is a measure of the energy contained in the earthquake. Values shown for each of the earthquake parameters were averaged between the left and right footing nodes (see Figure 4.2 and Figure 4.4).

The relationship between each of the three earthquake variables and the culvert properties discussed in previous sections are discussed below.

5.7.2 PGA

PGA is a poor characteristic with which to represent earthquakes as it only gives information about one tiny moment in the shaking. However, it is easily accessible and is used in pseudo-static analyses that include inertia forces, so it is included here. All runs were done using the base model:

- 1.5 m cover,
- 1.57 m (two zone) high stiffening beams,
- soil with a friction angle of 35°,
- cohesion of 1 Pa,
- dilation angle of 5°,
- 200 m/s shear wave velocity soil, and
- slip and separation allowed between soil and culvert, but not between soil and stiffening beams.

All of the earthquake records were used. A small number of runs were also carried out without the stiffening beams in place.

In Figures 5.46–5.57, open (unfilled) marks indicate that no beams were used in the model, while filled (solid) marks indicate that stiffening beams were present.

Culvert deformation (excluding construction deformation) is shown plotted against PGA in Figure 5.45 to Figure 5.47. For PGAs up to about 0.5 g, the culvert opens very slightly above the spring line or is unchanged, and the crown falls slightly. At larger accelerations, above about 0.55 g, the culvert is compressed laterally and the crown rises relative to the footings. The amounts are relatively small compared to the culvert span and rise. Closure between the footings occurs at all levels of shaking. The results were scattered so upper bound relationships would be suitable for design purposes. During construction, the culvert closed about 170 mm between nodes 8 and 30 and the crown rose about 180 mm relative to the footings (see Figure 5.37).

Figure 5.47 shows that seismic racking of the crown relative to the footings is 10 mm or so at PGAs of up to about 0.4g and appears to have a relatively linear upper bound relationship against PGA above that level.

Figure 5.48 shows that the axial reactions at the footings increase over the construction forces by about one-third as a result of earthquake shaking. The model is not very sensitive to the PGA, other than having a possible small increase in axial reaction (less than 10%) as PGA increases from below 0.4 g to over 0.6 g. More data are required at larger accelerations to reduce uncertainty as to whether an increase in PGA affects reaction forces.. Most of the earthquakes tested in this study were for R =1.0 (Table 4.5). The relative constancy of reaction forces at a small number of larger PGAs indicates that more testing for R =1.8 is required.

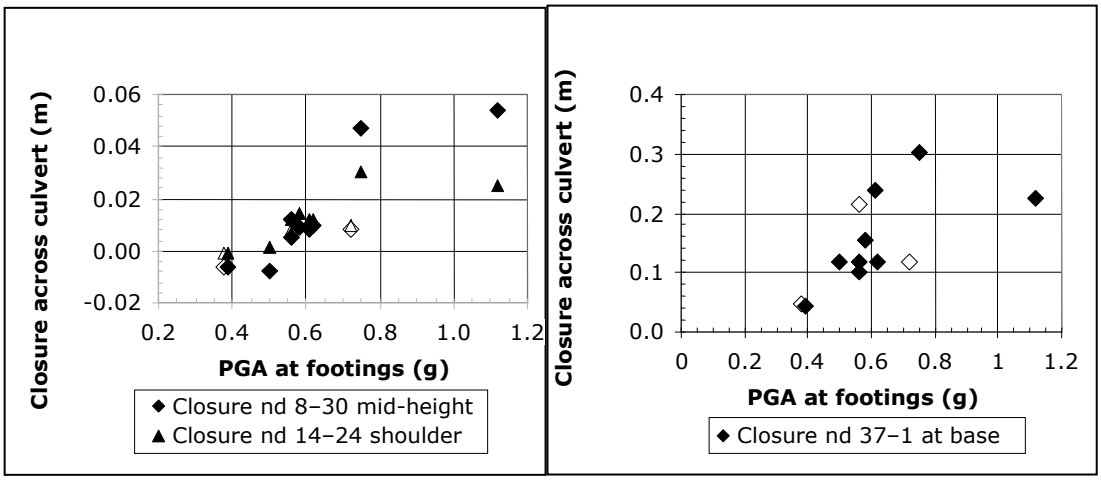

Figure 5.45 Post-construction culvert deformation related to peak ground acceleration at the footings.

Note: All models are 1.5 m cover with C_s =201 m/s soil.

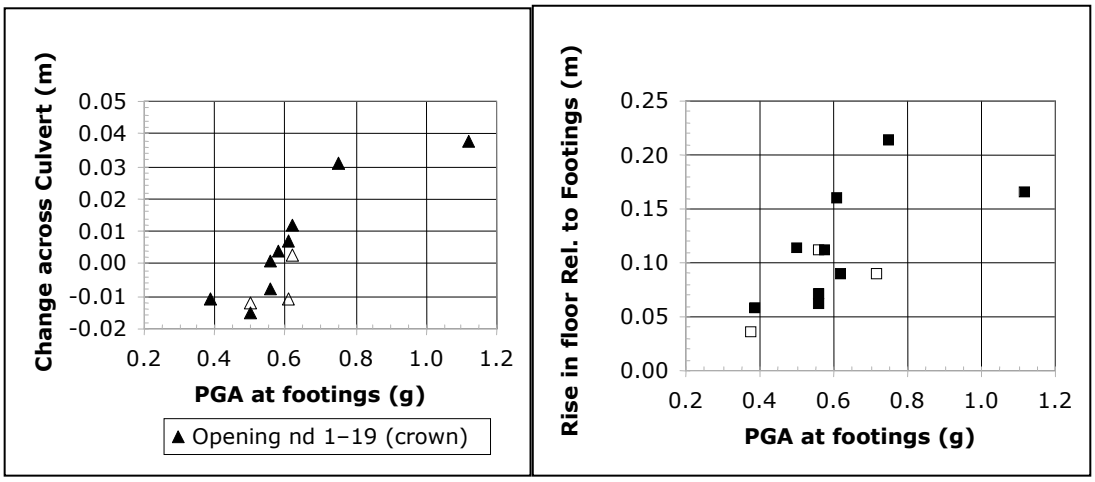

Figure 5.46 Post-construction culvert vertical deformation.

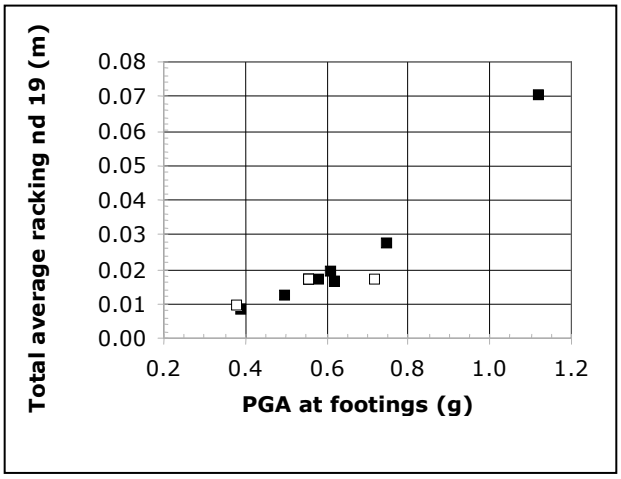

Figure 5.47 Seismic racking of node 19 in the crown compared to PGA.

Note: These are the total lengths of the 'error bar' representations of racking, shown on previous racking figures.

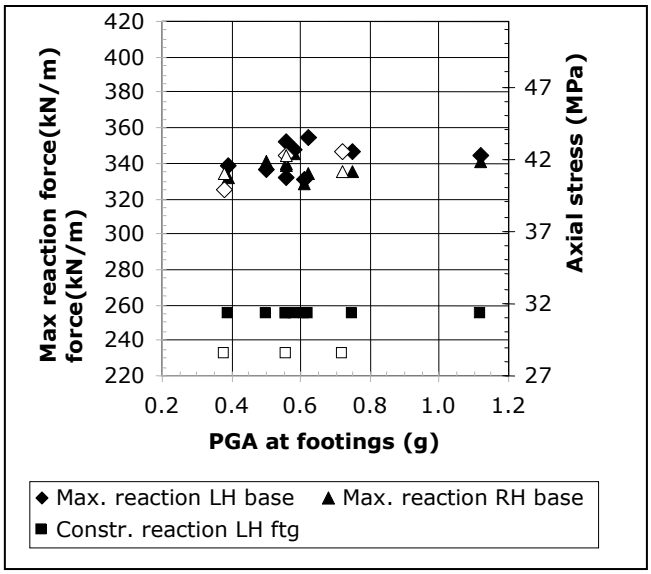

Figure 5.48 Axial reactions at the footings.

The construction thrust maxima are located around the base of the stiffening beams (nodes 10 and 30). At PGAs up to about 0.5 g, the maxima (construction and seismic) are located at or near the footings; at higher intensities of shaking, the maxima are always at the crown. The maximum dynamic increments also follow this pattern.

The maximum axial stress increases from the construction stress by about 20% with seismic shaking (Figure 5.49). Above about 0.5 g, the maximum axial stress increases about half as much again and is relatively insensitive to the PGA as it rises further. The maximum dynamic increment increases up to about 0.6 g and then appears to have little further increase as PGA continues to rise, although data are sparse above 0.8 g.

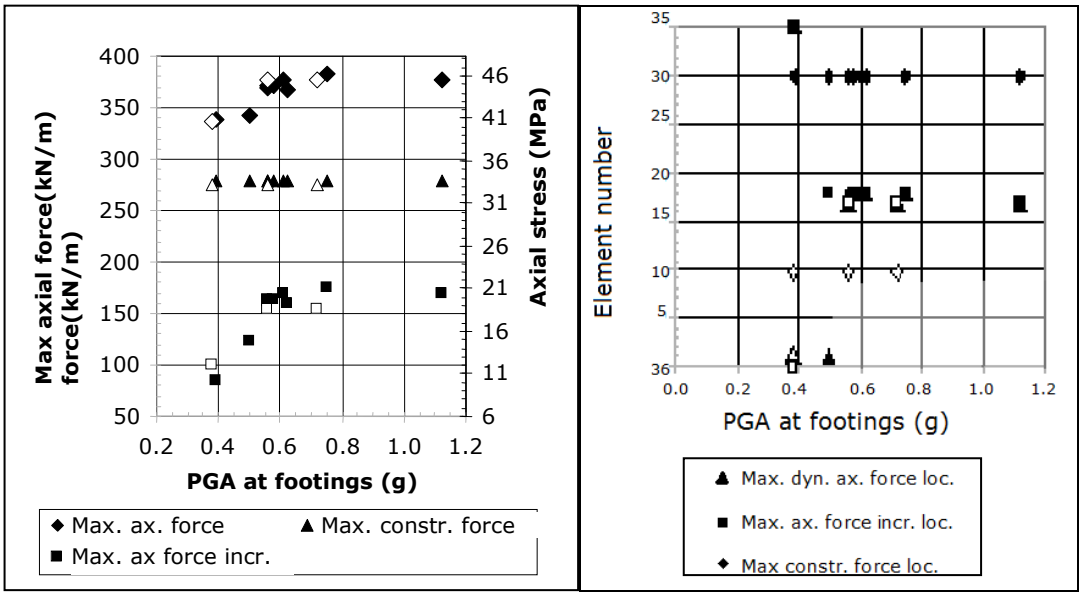

Figure 5.49 Maximum thrust (axial force) and their locations vs. peak accelerations at the footings.

Maximum bending stresses increase markedly as the PGA increases (Figure 5.50). While the data are scattered, a nearly linear upper bound relationship may exist between PGA and maximum bending stress. If the PGA is less than about 0.55 g, the bending stresses increase only slightly relative to the construction stresses. The maximum dynamic bending stress increment also increases with PGA, more rapidly than the maximum bending stress. Even at the greatest accelerations tested, the maximum moments were still less than the plastic moment when stiffening beams were present.

The maximum bending stress tends to be near the crown at lower accelerations. Above about 0.5 g, the maximum bending stress tends to move to the side walls around or below the spring line. This reflects increased closure at the footings and the greatest dynamic bending moment increment generally being in the spring line area. At the highest acceleration tested (just over 1.1 g), the maximum bending stress (350 MPa) would be near the plastic moment. This moment was located in element 7, just above the spring line and below the stiffening beam, and shows yielding of the steel with passive failure inside the footing.

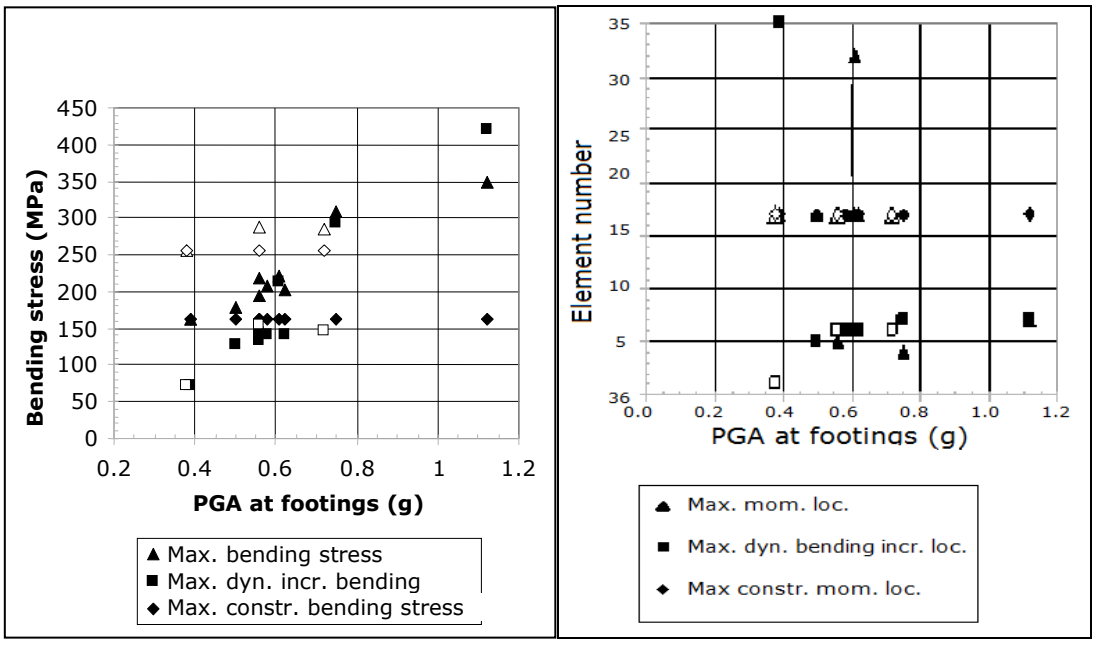

Figure 5.50 Maximum bending stresses and their locations v. peak acceleration at the footings.

Figure 5.51 shows the maximum stresses in the elements just above and below the stiffening beam locations. All the tests shown were run on the base model with 1.5 m cover and 1.57 m (two-zone) high stiffening beams. For accelerations less than about 0.5 g, both bending and axial stress maxima are greater above the beams than below. As the PGA increases beyond 0.5 g, the maximum axial stresses move to above the beams. The stresses above the beams increase by about 20% while PGA increases by about 0.1 g. Beyond about 0.65 g, the maximum axial stresses above the beams seem to remain relatively constant. Models with and without stiffening beams show no obvious

differences. The maximum stresses below the beams remain relatively constant at all acceleration levels, although the results are quite scattered.

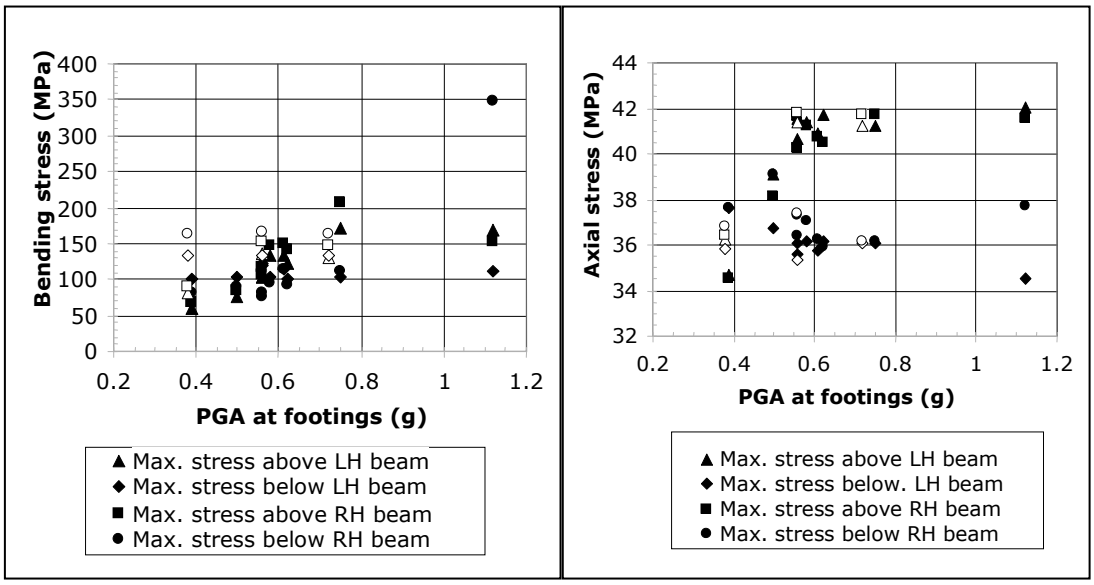

Figure 5.51 Axial and bending stresses above and below the stiffening beam locations, as affected by peak ground acceleration at the footings.

A similar effect is seen in the bending stress maxima. At accelerations below about 0.55 g, the greatest bending is below the stiffening beams. At a little more than about 0.6 g, the greatest bending moves to above the beams, although at higher PGAs, this is less clear. The very large value below the right beam at 1.12 g indicates significantly greater inward movement in that limb of the culvert, about 2.3 times the left limb.

5.7.3 PGV

Culvert deformation compared to PGV is shown in Figure 5.52 to Figure 5.54. The data for peaking (closure across the culvert and rise of the crown) are scattered and no clear relationship appears between deformation and PGV. The data for closure at the footings and rise in the floor relative to the footings are also quite scattered.

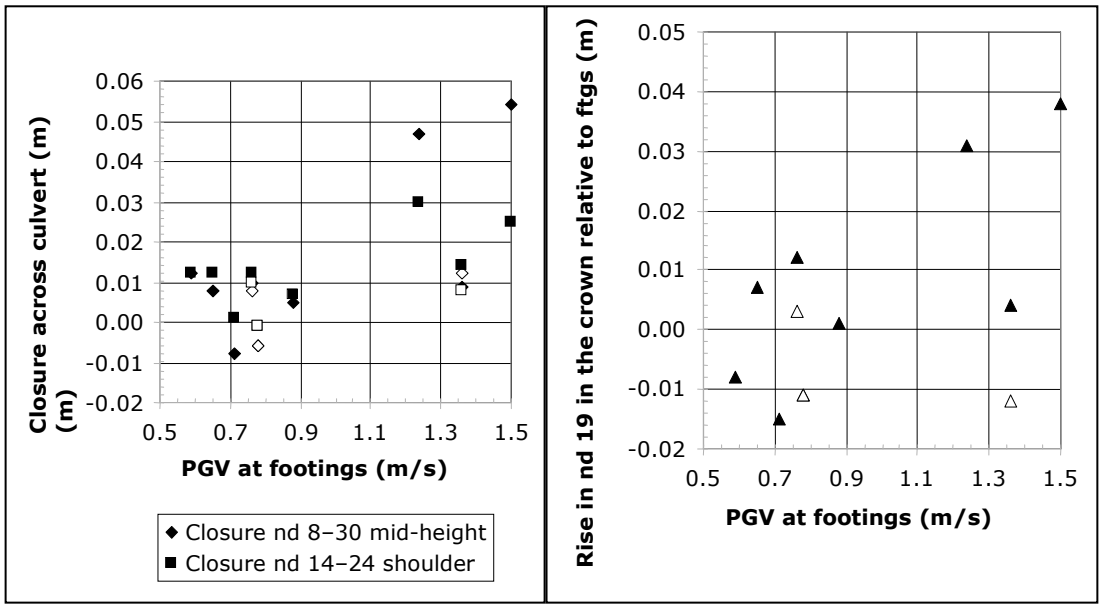

Figure 5.52 Peaking of the culvert compared to peak ground velocity at the footings.

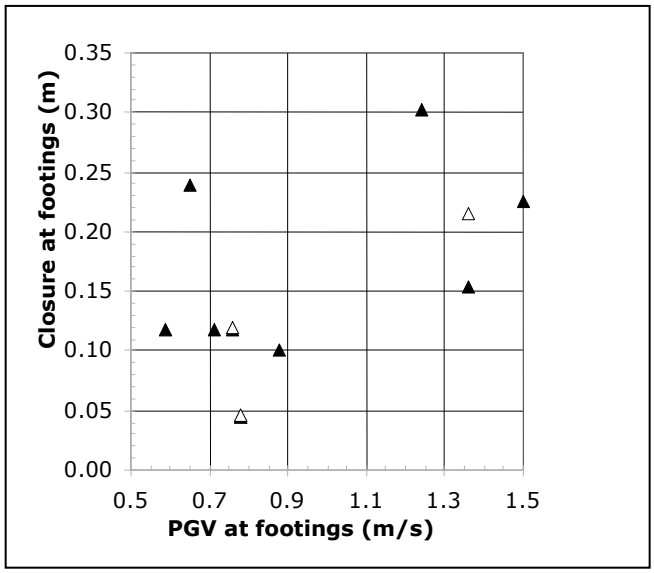

Figure 5.53 Closure at the footings and floor level rise relative to footings, compared to peak ground velocity at footings.

In Figure 5.54, only a poor correlation appears between total racking of the crown relative to the footings and PGV, for most values of PGV. The total racking for PGV of 1.5 m/s probably reflects the large displacement inwards of one footing. If one-sided transient racking is 10 mm (larger than most values in Figure 5.54), the maximum shear of the culvert is 0.01/7.29 (racking/rise) or 0.0014 radians. The maximum diametric strain

(relative to midway between the footings) is then about 7 x10^{-6}. The soil shear strain, given by V_s/C_s, would range between about 0.003 and 0.007 for the models in Figure 5.54 (C_s = 201 m/s). Using Wang's (1993) formulation for ovalling, this would be a diametric strain of 12 x10^{-6} with a full slip interface and a peak ground velocity of 0.4 m/s. A check of shear deformation in the soil halfway to the edge of the model showed that the deformation, to the left and right, over the height of the model was essentially the same as it was within the culvert and varied little as the PGV increased.

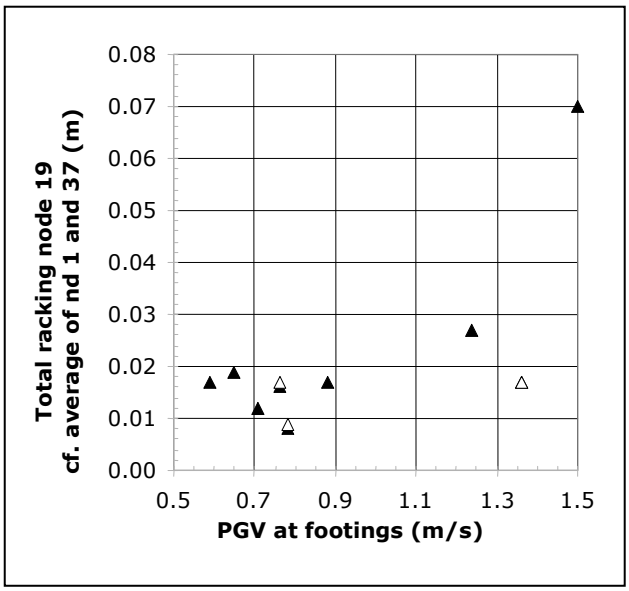

Figure 5.54 Racking of the crown (node 19) relative to the footings, compared to peak ground velocity at the footings.

Note: This shows the total left to right travel of node 19 during shaking.

PGV does not appear to be correlated well with the footing thrusts (Figure 5.55); the data are quite scattered. Maximum dynamic thrust and dynamic thrust increments (Figure 5.56) are almost unchanged through the range of PGV examined, although a little scatter appears in thrusts between 0.6 and 0.9 m/s PGV. The locations of these maxima also appear to not be related to the PGV, with essentially no changes in location as PGV increases.

Bending stresses (Figure 5.57) also appear to be poorly correlated with PGV. The maximum bending stress is generally around 200 MPa, with significant increases at some (but not all) higher PGVs. The maximum dynamic increment of bending is generally around 150 MPa, but two of the three higher PGV tests have the maximum increment at about twice and nearly three times this level. The maximum dynamic bending moment location varies between the crown (where the maximum construction moments were located) and the side walls just below the widest part of the culvert (probably reflecting the inward movement of the footings) – no pattern appears. The maximum dynamic increment of bending is almost always in the side walls just below the widest part of the culvert.

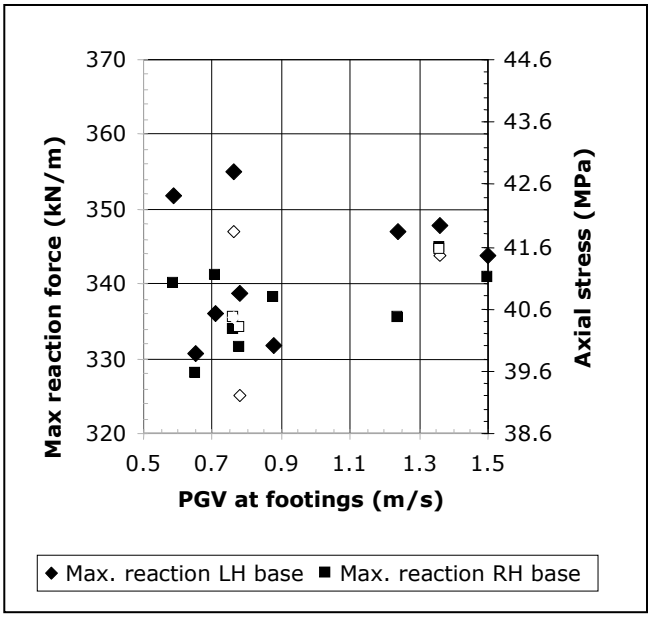

Figure 5.55 Axial thrust at the footings compared to peak ground velocity at the footings.

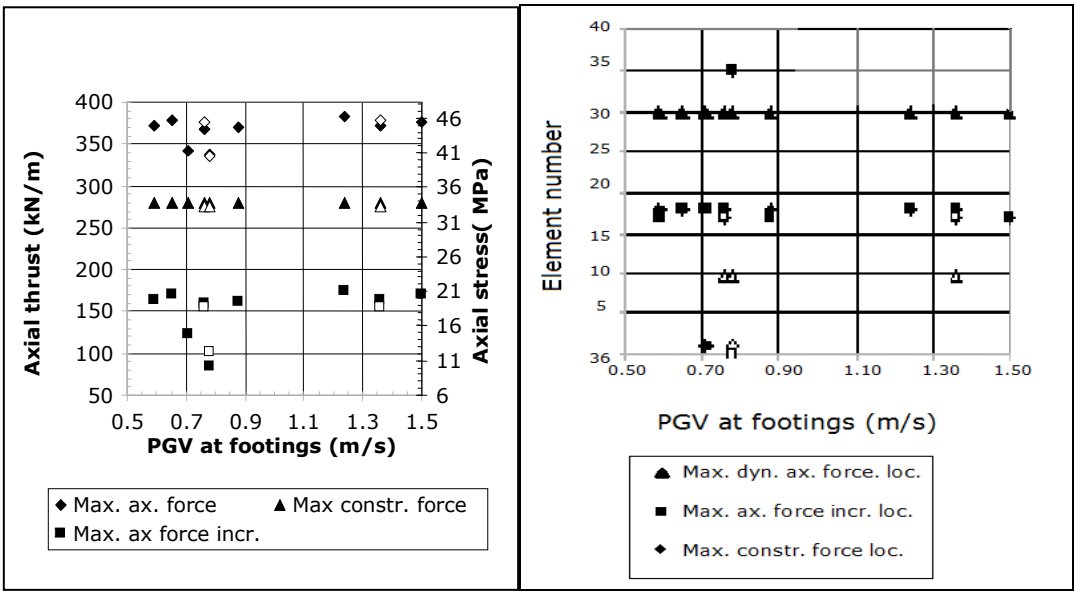

Figure 5.56 Axial thrusts and their locations compared to peak ground velocity at the footings.

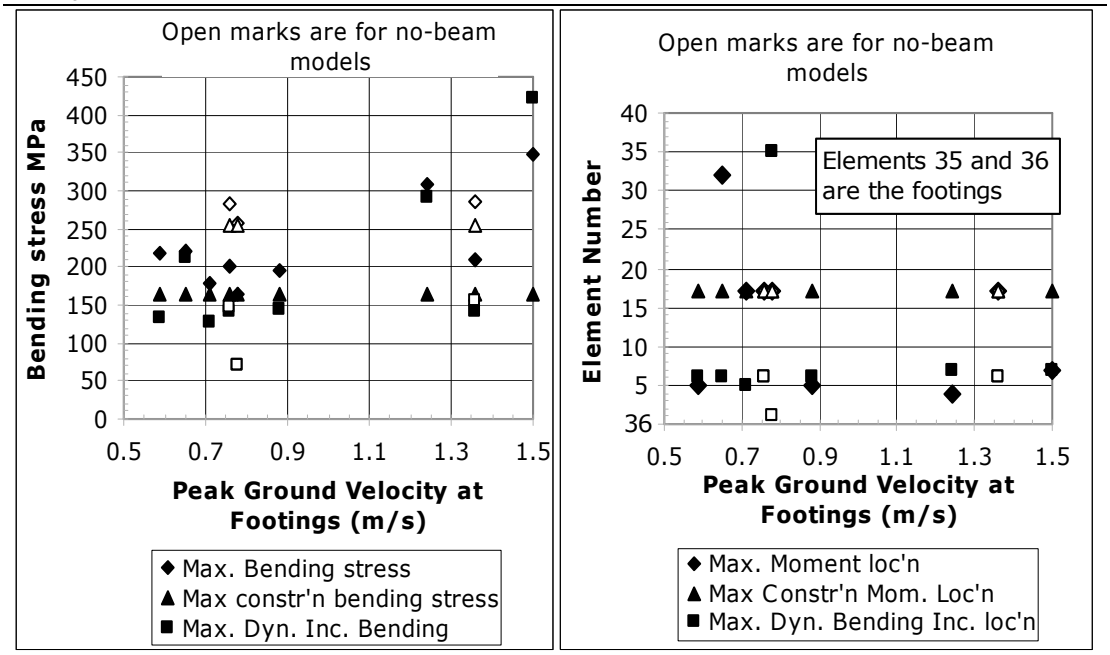

Figure 5.57 Bending stresses compared to peak ground velocity at footings.

Note: Figure 4.3 on page 38 shows structural element numbers.

The conclusion here is that PGV does not correlate well with the dynamic thrusts or dynamic bending moments in the culvert. In addition, culvert deformation is poorly correlated with PGV. It appears that PGV is not a very useful seismic design parameter for large span culverts of this type.

5.7.4 Arias Intensity: effect of soil and geometry on wave travel

5.7.4.1 General

The Arias Intensity is a measure of the energy contained in the earthquake. The seismic energy input at the base of the culvert is affected by a number of parameters, given that the earthquake record is applied at the base of the model and the shear waves travel upwards through the soil. Once the shear waves reach the culvert, the culvert' geometry is likely to have an effect, particularly in the way waves are reflected and diffracted by the opening and by the ground surface. First, we examine how the Arias Intensity is affected by values for various soil and geometric parameters, and then how the Arias Intensity affects the culvert.

The definition of the Arias Intensity is given in Section 4.8.2 on page 46. The Arias Intensity used here was calculated using accelerations normalised against gravity, so the unit is seconds^3/metre.

5.7.4.2 Effect of soil and geometry on wave travel

Figure 5.58 shows the variable effect of the depth of cover over the culvert and Figure 5.59 shows the effect of the size of the stiffness beams on the culvert. The shaking is amplified by more than 25% by the time it reaches the footings. Clearly, the geometry of the culvert system affects the acceleration of the footings to some extent.

The soil stiffness will also affect the input energy. In the Mohr-Coulomb soil model, the elastic limit is defined by a relationship that includes the greatest and least principal stress, and the cohesion and friction angle of the soil. When that limit is exceeded, the soil will flow plastically until the stresses reduce below the elastic limit, thus absorbing energy and affecting the reflection and diffraction of seismic waves around the culvert opening. The soil stiffness, which relates deformation and stress, will affect behaviour up to the elastic limit; its effect on Arias Intensity is shown Figure 5.60. The effects of soil friction and cohesion are shown in Figure 5.61 and Figure 5.62. The volumetric behaviour of the soil with shear stress also affects the input at the culvert base (Figure 5.63).

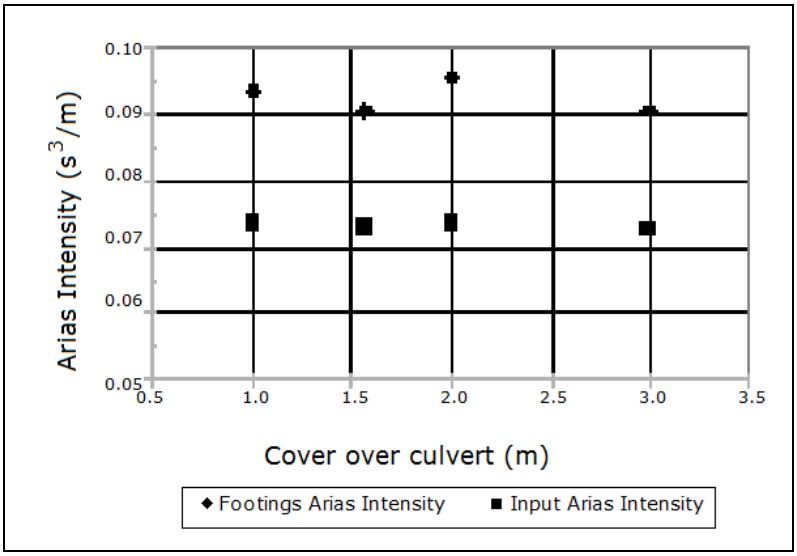

Figure 5.58 Cover over the culvert and the average Arias Intensity at footings, for El Centro 1940 S00E component scaled up 1.52 times.

Note: The difference between the greatest and the least Arias Intensity was 6%.

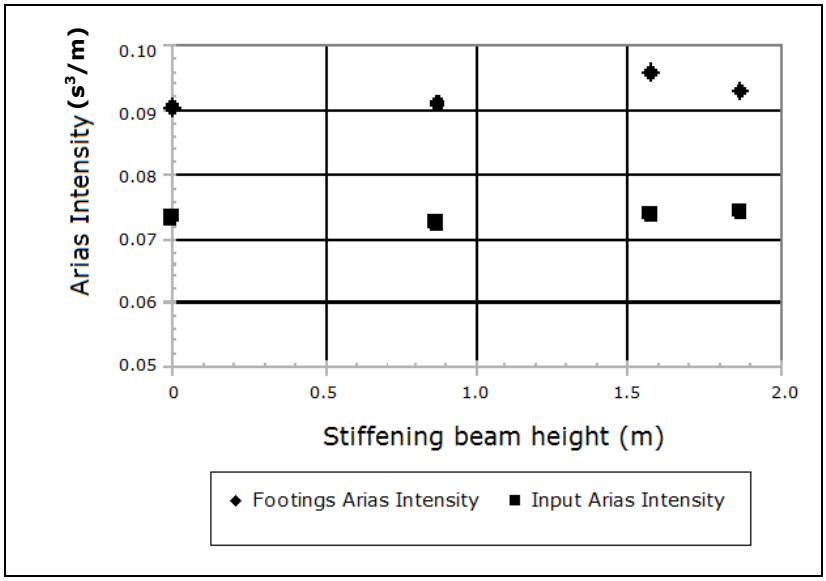

Figure 5.59 Stiffening beam height and the average Arias Intensity at footings, for El Centro 1940 S00E component scaled up 1.52 times.

Note: The greatest intensity is around 6% more than the least.

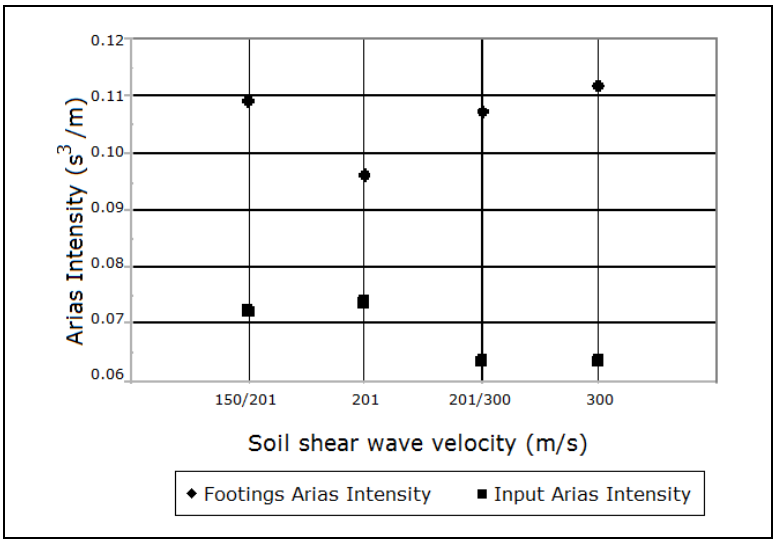

Figure 5.60 The effect of soil stiffness, measured as the shear wave velocity, on the average input energy at the culvert footings.

Note: The difference between the greatest and least Arias Intensity is 16%.

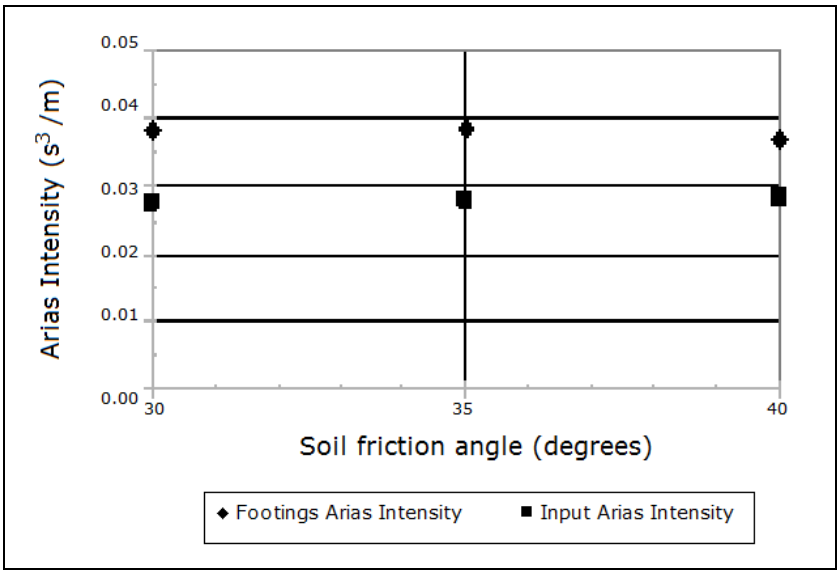

Figure 5.61 The effect of the soil friction angle on the average input energy at the culvert footings.

Note: The difference in observed Arias intensity between 30° and 40° soil is a little over 3%.

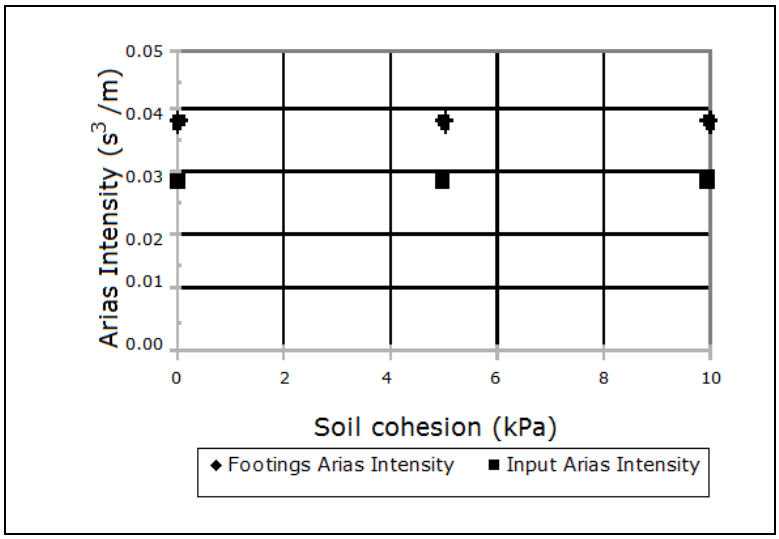

Figure 5.62 The effect of soil cohesion on the average input energy at the culvert footings.

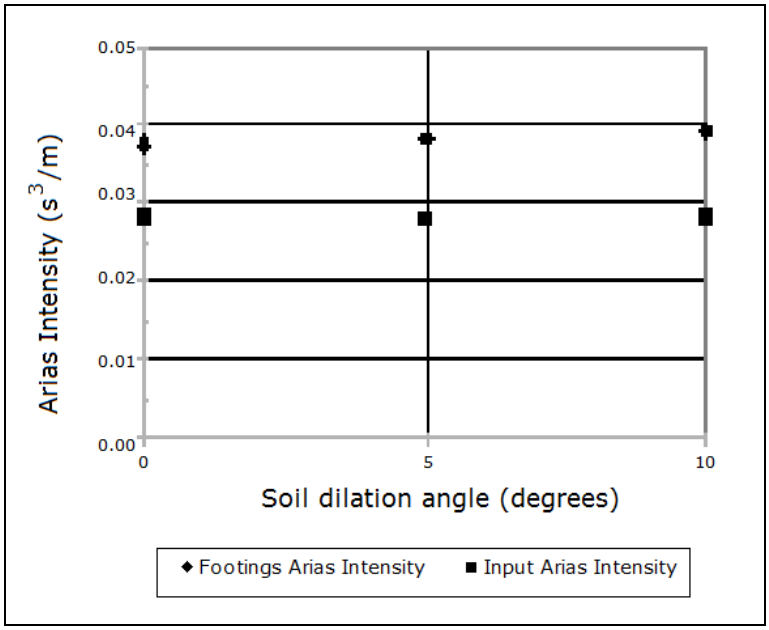

Figure 5.63 The effect of soil dilation angle on average energy input at the culvert footings.

Note: The increase from 0° to 10° is about 5%.

Another factor that will affect seismic wave travel around the culvert is whether slip is allowed at the soil–culvert interface. The effect is shown in Figure 5.64.

We note that soil stiffness has the greatest effect. This is because softer soil will attenuate the seismic shaking as it rises from the base of the model more than the stiffer soil, as well as attenuating higher frequencies more than lower frequencies. Geometry has the next greatest effect and the volumetric behaviour of the soil has an effect of similar magnitude. The effect of other soil properties and of the soil–culvert interface condition is minor.

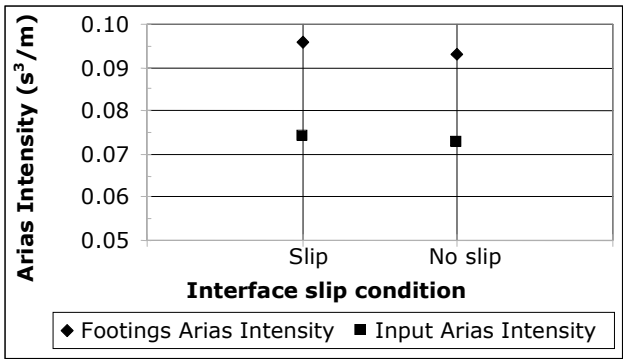

Figure 5.64 The effect on average energy input at the footings, of whether slip is allowed between the soil and the culvert.

Note: Allowing slip increases the Arias Intensity by around 3%.

Figure 5.65 to Figure 5.67 show the relationships between some of the properties of the seismic shaking. As the PGV and PA increase, their relationship with the Arias Intensity becomes more scattered. Between PGV and PGA, the data are scattered and no good correlation arises between them. Table 3.1 indicated that the relationship between PGV and PGA depends on the earthquake magnitude, the site soil conditions, and the earthquake source-to-site distance. Table 4.5 shows that the three earthquakes used in the modelling had significantly different magnitudes and source-to-site distances, so we should expect some variability in the correlation between PGA and PGV, and hence between these parameters and the Arias Intensity.

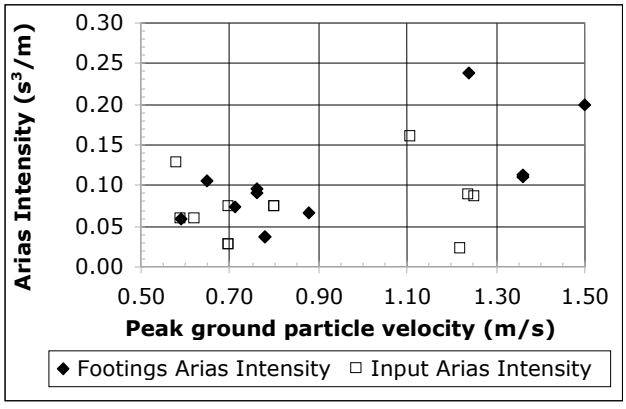

Figure 5.65 The relationship between the average Arias Intensity and the average PGV at the footings.

Note: 'Footings' are on top of the concrete footings.

5.7.4.3 Arias Intensity: effect on stresses and deformation

Here, we examine the relationships between the average Arias Intensity at the footings and the stresses and deformations in the culvert caused by seismic shaking.

Culvert deformation is shown plotted against Arias Intensity in Figure 5.68 to Figure 5.70. Overall peaking deformation has an approximate linear trend against Arias Intensity, although the data are scattered and it is unclear at which intensity the deformation changes from widening to peaking. Closure between the footings and the rise in floor level

relative to the footings is more clearly related to Arias Intensity, with less scatter. During construction, the culvert closed about 170 mm between nodes 8 and 30, and the crown rose about 180 mm relative to the footings (see Figure 5.37).

In Figures 5.67–5.73, open (unfilled) marks indicate that no beams were used in the model, while filled (solid) marks indicate that stiffening beams were present.

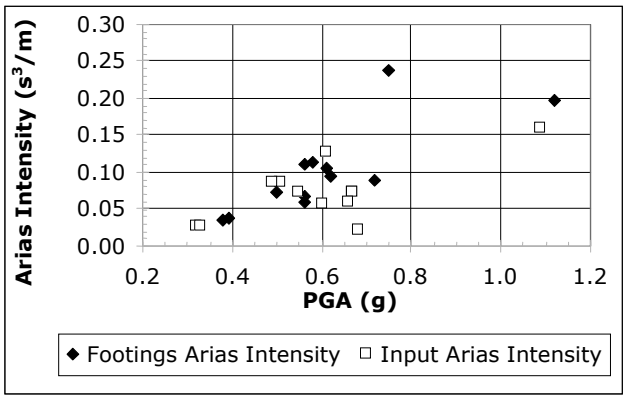

Figure 5.66 The relationship between the average Arias Intensity and the average PGA at the footings.

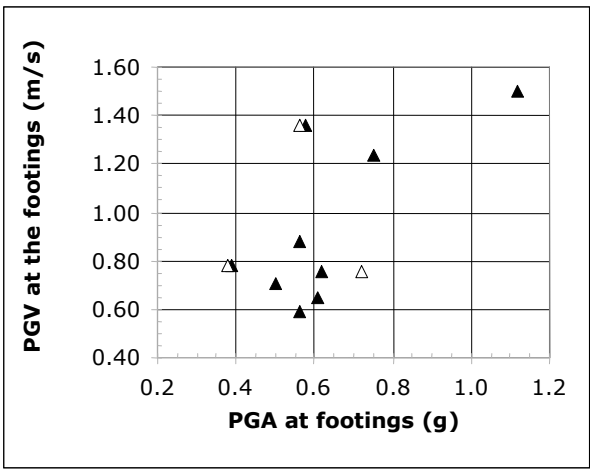

Figure 5.67 PGV v. PGA at the footings.

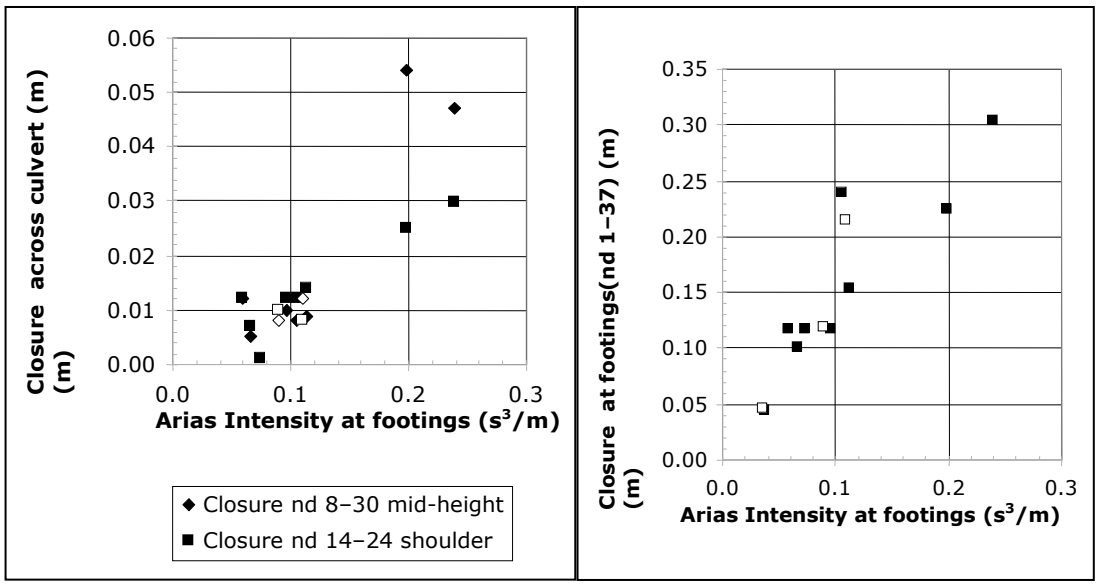

Figure 5.68 Post-construction culvert deformation related to Arias intensity at the footings.

Note: All models are 1.5 m cover with C_s=201 m/s soil.

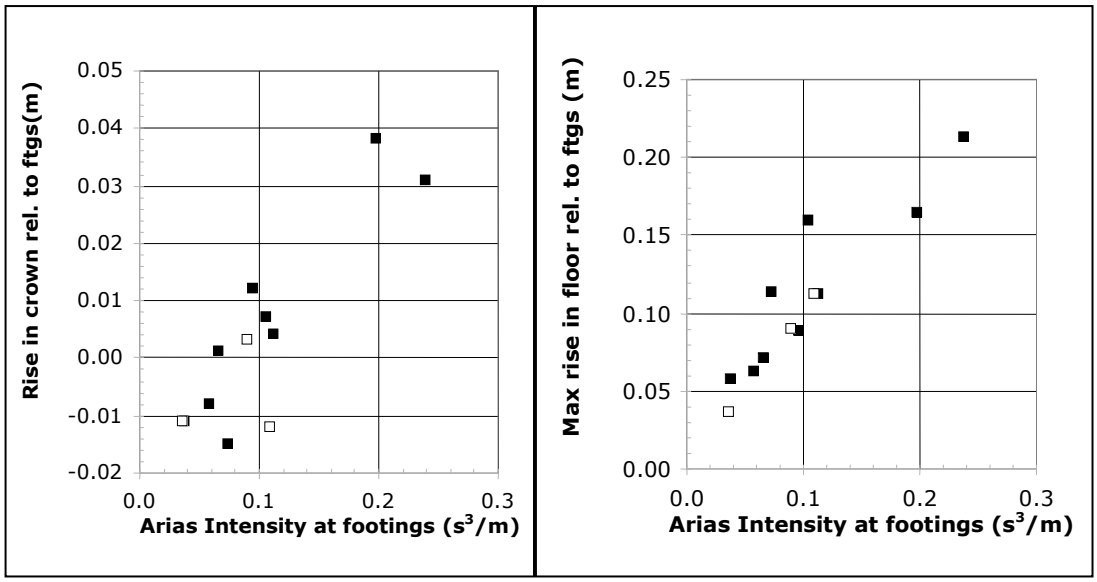

Figure 5.59 Post-construction culvert vertical deformation.

Figure 5.70 shows that racking of the crown relative to the footings is less than about 20 mm during earthquakes of up to an Arias Intensity of just over 0.1. Only two data points are for larger intensities so no conclusion can be drawn.

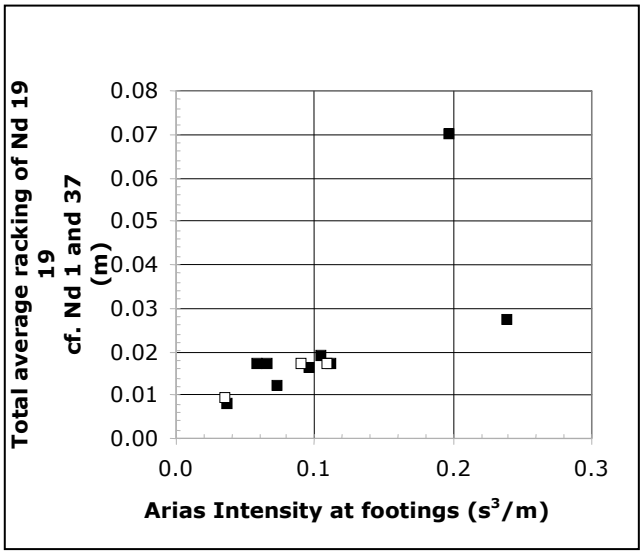

Figure 5.70 Racking of node 19 in the crown compared to Arias Intensity.

Note: These are the total lengths of the 'error bar' representations of racking, shown on previous racking figures.

Figure 5.71 shows that no clear relationship holds between Arias Intensity and the axial reactions (thrust) at the footings.

Maximum thrust and maximum dynamic thrust increment rise as the Arias Intensity rises to about 0.1 (Figure 5.72), but this rise is poorly defined. At intensities greater than that, neither of those quantities changes significantly. Both of these maxima are located at the crown for all but the lowest intensities of shaking.

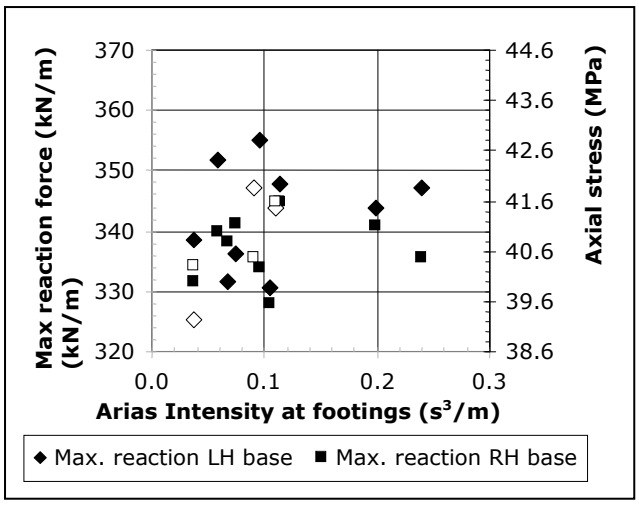

Figure 5.71 Axial reactions at the footings.

A slightly stronger relationship holds between the maximum bending stress, the maximum dynamic increment of bending stress and Arias Intensity (Figure 5.72). Both maxima appear to continue to rise as the Arias Intensity rises, although the data are scattered. The dynamic increments of bending stress increase significantly, with the

greatest value being five or six times the least. The maximum bending is in the crown, up to a little above 0.1 Arias Intensity. Beyond this intensity, the maximum bending moves to the side walls of the culvert. The maximum dynamic bending increment is always in the side walls, probably reflecting the closure between the footings.

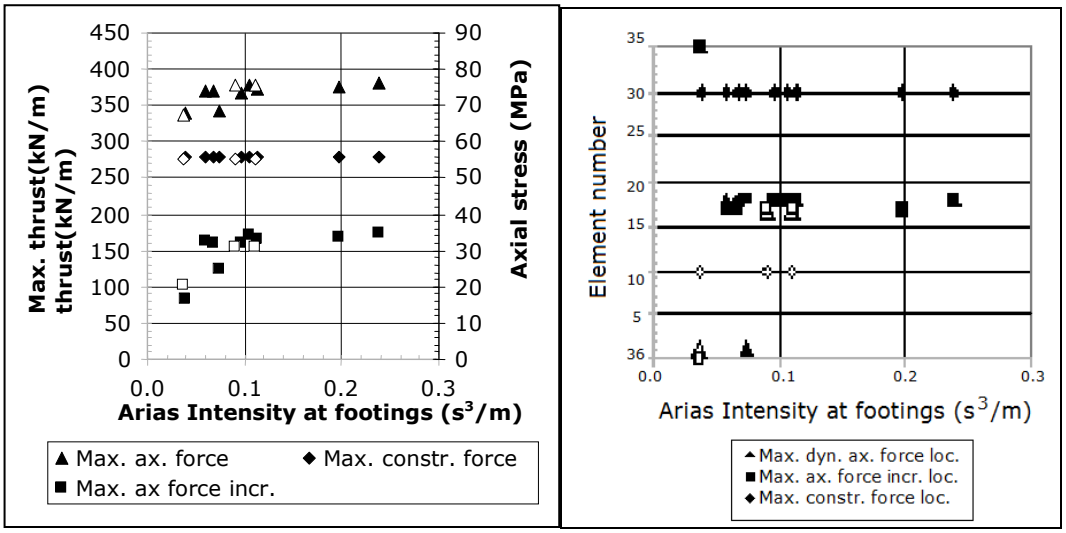

Figure 5.72 Maximum thrusts and their locations compared to average Arias Intensity.

Note: Elements 35 and 36 are the footings.

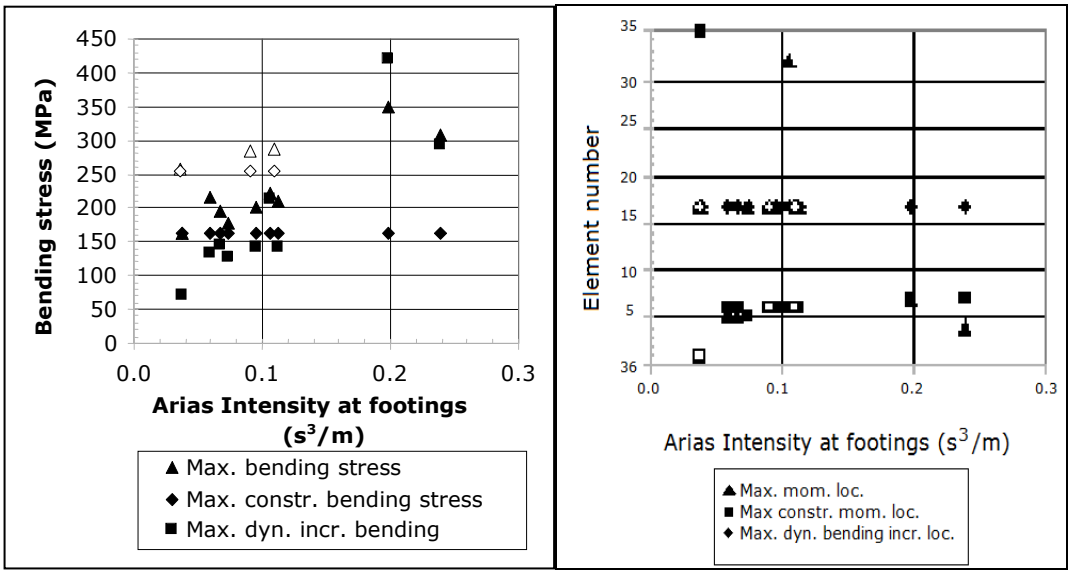

Figure 5.73 Maximum bending and its location compared to average Arias Intensity at the footings.

Note: Elements 35 and 36 are the footings

6. Conclusions

6.1 Overview

The effects of a number of culvert and model properties on construction and seismic deformations, maximum thrusts and maximum bending stresses have been examined using numerical modelling. Both horizontal components of three earthquake records, scaled for Wellington conditions for R =1 and R =1.8 (500- and 2500-year return periods), were used in the modelling. In addition, three earthquake characteristics were checked for their correlation with seismic deformations, maximum thrusts and maximum bending stresses.

This chapter presents some general conclusions, along with some more detailed conclusions about the effects of the various parameters tested.

6.2 Deformation

Permanent culvert deformation (closure at the widest point near mid-height and the rise of the crown, known as peaking) is far greater during construction (up to about 200 mm when stiffening beams are used) than as a result of seismic shaking (less than 25 mm in either direction for the configurations and earthquakes tested).

Total transient deformation of the crown from left to right relative to the footings (racking) is less than 30 mm in all cases and less than 20 mm in most cases. The maximum racking of the crown, left to right, appears to be unrelated to the peak soil particle velocity when the velocity is less than about 1 m/s (Figure 5.54), which would seem to rule out using the racking method in the design of long-span culverts. We note also that the relationship between PGV and PGA is scattered (Figure 5.67). Further study of this is required.

The greatest deformations resulted from passive failures inside the footings: closures of up to about 300 mm were found for the largest (R =1.8) earthquakes. The floor inside the culvert heaved a similar amount. Most closures were less than 200 mm. The footings used are typical of some seen in older culverts, especially circular arches over streams; more recent examples of high-profile arches have struts between the foundation beams. It is probably cheaper to put in struts between the footings than to construct footings large enough to resist passive failure. Without incompressible struts, the footings will always move slightly inwards as the passive resistance in the soil is mobilised. Such small movements should cause only small increases in bending moments in the culvert.

6.3 Site amplification

Culvert geometry – the size of the opening and the depth of cover – appears to have little effect on the intensity of seismic shaking, measured as PGV, PGA or Arias Intensity. Differences are seen between input (base of model) and culvert footing values, but the footing values do not change appreciably as the cover increases. This has been studied by others; Einstein & Schwartz (1979) mention that finite element studies have found that at shallow depths, the confining stress variation is important.

6.4 Soil arching

Soil arching, whereby the soil densifies slightly in an arch configuration, is observed when the cover is not too small. The arch reaches from above each shoulder of the culvert, downwards and outwards beside the culvert. It finishes below the widest part of the culvert. This is expected to occur as a result of the transfer of load into the soil on each side of the culvert as the steel culvert deforms under load away from the cover soil.

6.5 Bending moments and thrusts

Bending moments are usually greatest at or near the crown, as a result of peaking during construction. The maximum dynamic increase in bending moment is frequently in the side walls near the footings. At the greatest level of shaking tested, the maximum bending stress indicated that the plastic moment was approached just below the stiffening beams, reflecting the inward movement of the footings. If the footings are strutted, it is likely that these bending moment increments will be small.

Maximum dynamic increases in thrust are usually near the crown and occasionally at the footings. Maximum dynamic increases in both thrust and bending are not at the same location as the maximum values of thrust and bending recorded during the earthquake.

The maximum thrusts observed were less than half the ultimate compressive wall stress calculated using AS/NZS2041:1998 and less than about two-thirds of the ultimate stress calculated using AS3703 (1989) modified for the steel yield stress (see Note 4 in Table 4.3). The maximum bending stresses, which were assumed elastic throughout, exceeded by sometimes significant amounts the buckling stress calculated using the method of Abdel-Sayed et al. (1994), for a radius of 7.57 m and a span of 11.66 m. This aspect, and the combination of stresses caused by thrust and bending, requires further consideration. We note that the method in the standards for calculating the ultimate wall stress is based on tests of pipes up to only 1.5 m diameter.

The addition of stiffening beams significantly reduces peaking during construction, resulting in significantly lower bending moments in the crown. The stiffening beams also result in a significant reduction in seismic thrusts across the beams, between the upper (nearer horizontal) part of the culvert and the lower (near vertical) part of the culvert. This latter effect is the current purpose of using stiffening beams in design.

For this culvert, the calculated average buckling stress reaches the plastic limit at about 2.1 m of cover. The maximum moment is usually in the crown, and construction and seismic shaking cause this moment to increase, so it would seem that the depth at which the plastic limit buckling stress is reached should have an influence on the minimum allowable cover. Less cover could be used with additional stiffness across the crown. This could be done by using thicker plates there. We note also that the soil density arch was fully formed at a depth of cover of 2.0 m, which is only slightly less than the depth at which the plastic limit is reached for the buckling stress.

For culverts of larger span than considered here, the radius of the crown would be greater. This should increase the depth at which the buckling stress reaches the plastic limit.

Because deformations are small and maximum seismic (total) thrusts are well within the maximum compressive thrust, the apparently large seismic bending moment is the most critical aspect of culvert seismic design that requires further consideration.

6.6 Soil properties

Bending moments are most affected by soil properties. Soil with a high friction angle and a little cohesion gives the lowest moments. Compared to a cohesionless soil, adding a little cohesion has a very strong effect on reducing bending moments but increasing it further has little effect. Because a high friction angle and cohesion do not often appear together in soil, cohesion can perhaps be added in another way, such as using geogrids in the fill (but not attached to the culvert). Soil stiffness (measured in this work as the shear wave velocity) has significantly less effect, but stiffer soil backfill does cause reduced bending. Dilatant soil also reduces bending moments compared to non-dilatant soil, but to a lesser extent than soil stiffness. Thus to minimise bending moments in the culvert, well compacted and crushed granular soil with low to moderately cohesive fines (or perhaps geogrids) should be used in the culvert backfill.

Soil friction, cohesion and dilation have a small effect on maximum thrusts; the greatest effect is from soil stiffness (shear wave velocity), where stiffer soil has lower thrusts.

Increasing the stiffness of embedment soil (C_S) results in a decrease in construction footing thrust. Dynamic increases in footing thrust are greatest for soft soil, about a 50% increase compared to construction forces. The increase is less than 40% of the construction forces in stiffer soil. A stiffer foundation also causes a significantly greater increase in seismic footing thrust with the same embedment soil – nearly 30% greater with the stiffnesses tested. We note that a stiffer foundation also affects the intensity of shaking (see below).

Construction footing thrust reduces as the soil friction angle increases, almost linearly between friction angles of 30° and 40°. Soil cohesion causes a small reduction in construction reaction force compared to non-cohesive soil, but increasing the cohesion has almost no effect.

Maximum seismic footing thrusts are increased for higher friction soil, but they are still rarely more than 50 to 60% of the maximum compressive thrust. Increases in seismic footing thrust are 75% greater for 40° soil compared to 30° soil and can be interpolated linearly for values of friction between 30° and 40°. Whether the soil is cohesive or dilative seems to have a minor effect on dynamic changes in reaction thrust.

The greatest permanent construction deformation occurs with low-friction, low-cohesion or low-dilation soil. Soil stiffness (measured as the shear wave velocity C_S), which is mainly controlled by degree of compaction and sometimes by soil structure and suction forces, has little effect on construction deformation when the density is held constant.

Seismic deformations are affected by the soil strength parameter values in the same way as construction deformations, except for C_S, which does affect seismic deformation. The ranges of friction, cohesion and stiffness tested all reduce permanent deformations by a factor of 2 to 3 between the weaker/softer and stronger/stiffer limits. The greater dilation angle (which reflects volume increase with strain in the soil) also reduces permanent deformations by a factor of between two and three compared to when dilation is set to zero.

Total average racking is greatest for the softer (low C_S) soil, nearly four times that for the stiffer soil. Soil friction angle, cohesion and dilation do not significantly affect the seismic racking deformation of the culvert.

6.7 Soil–culvert interaction

Maximum seismic bending and thrusts were greater by 10 to 15% when no slip was allowed between the culvert and soil. For bending, this is contrary to Wang's (1993) analysis for circular tunnels, in which bending moments were up to about 20% greater with full-slip conditions; thrusts were under-estimated by 90% in some cases with full-slip conditions. Construction maximum bending was unaffected by whether slip was allowed or not; Wang's analyses found small differences. Maximum construction thrusts were a few percent greater when no slip was allowed. Construction and seismic reaction thrusts are both significantly greater when no slip is allowed.

These results seem intuitive; when the soil can slip past the steel, forces on the steel might be related to – and limited by – the friction, cohesion and adhesion between the soil and steel. When the soil is glued to the steel, any movement in either the soil or steel will cause stress in the other.

Wang commented that seismic lining distortion was greatest with full-slip interfaces, but only by very small amounts. We also found this to be true, but the differences were negligible. Construction deformations, however, were twice as great when slip was allowed compared to when it was not.

6.8 Geometry

6.8.1 Depth of cover

Total average racking is greatest for the softer (low C_S) soil, nearly four times that for the stiffer soil. Soil friction angle, cohesion and dilation do not significantly affect the seismic racking deformation of the culvert. As cover increased past about 1.75 to 2.0 m, the shape change reversed from peaking to spreading when stiffening beams were fitted. Without beams, the crown movement reversed (from rising to falling) at about the same cover level, but the culvert still closed across the widest part (by just a few millimetres). Increasing cover caused an increase in total racking of the culvert, although the total shear deformation was still small (21 mm or about 0.3% shear strain) with 3 m of cover.

Thrust at the footings was essentially linearly related to cover depth in all cases. Maximum construction thrust in the culvert was linearly related to cover (with or without stiffening beams) but the rate of increase of the maximum seismic thrust reduced as cover increased above 2.0 m. The maximum increment of seismic thrust also showed a much smaller increase above 2.0 m cover. Construction maxima were located just below the base of the stiffening beams, while seismic maxima were in the crown, moving to mid-way to the shoulder for 3 m cover with no beams.

Maximum construction moments were unaffected by cover depth. Seismic moment maxima reduced as cover increased to about 2 m and reduced only slightly further with greater cover. Maximum seismic bending without beams was usually in the crown, and moved from the crown to the footing with increasing cover when beams were fitted. Construction maxima were in the crown.

6.8.2 Beam height

The presence of stiffening beams reduced the construction peaking by about a third. The size of the beam has only a small effect on construction deformation. The presence and size of stiffening beams has almost no effect on seismic deformation, for either peaking or racking.

Construction reaction thrusts increase slightly when stiffening beams are fitted but not as the beams increase in size. Seismic reactions increase similarly when beams are fitted, but then decrease as the size of the beam increases. For the 1.87 m high beams, the seismic reaction thrust is similar to the construction value.

Construction and seismic moment maxima reduce by about a quarter when beams are fitted, then a few percent more up to the 1.57 m high beams, with no further change using the larger beams. The locations of the maxima do not change with beam size (including zero size).

Construction and seismic thrust maxima are unaffected by the presence of stiffening beams or their size.

6.9 Effect of the shaking intensity

6.9.1 General

Shaking intensity was measured at the culvert footings using three parameters: PGA, PGV and Arias Intensity, all of which were averaged for the two footing nodes (see Figure 4.2 on page 37 and Figure 4.4 on page 38). Shaking was put into the model as a stress history in the bottom row of soil elements, and PGA, PGV and Arias Intensity were measured and calculated at the culvert footings.

It was found that soil strength and stiffness, and geometry affected the intensity of shaking at the culvert footings. Intensity of shaking was measured by Arias Intensity. Most of the relationships are not clear without further study, which is beyond the scope of this study. In summary, cover has a variable effect with no clear rising or falling trend as cover increases. The effect of stiffening beam height is also variable, perhaps with a slight trend towards rising as the height increases.

Soil stiffness has a variable effect on shaking intensity at the footings. Cohesion has very minor or no effect, while the intensity seems to reduce as the soil friction angle increases. Increasing soil dilation causes an increase in shaking intensity at the footings.

Culvert design is generally based on shaking intensity at a free-field location on the ground surface. Many culverts of the type considered here are constructed in relatively flat terrain to take a highway over a railway line at a high skew. The effect of the presence of the embankment and skewed culvert on the properties of free-field shaking is beyond the scope of this work, although it is important in design.

6.9.2 PGA

At low levels of PGA (less than about 0.5 g or a little greater), the culvert spreads; while at higher PGAs, it peaks (the crown rises and the widest part narrows), although the data are scattered. Shear deformation (total average racking) increases with PGA; it may be relatively linear up to about 0.75 g and the rate of increase is greater above that level, but only one data point shows a greater PGA, so this is uncertain.

Reaction thrusts are almost unaffected by PGA. The maximum thrust anywhere in the culvert increases between about 0.4 and 0.6 g and changes very little at greater accelerations. The maximum dynamic increment of thrust increases over a similar range. The maximum thrust above the stiffening beam locations increases strongly over the 0.4–0.6 g range and is almost constant at greater accelerations. Below the beams, maximum thrust is almost unchanged with PGA.

Maximum bending moments increase almost linearly with PGA, as do the maximum dynamic increments. At higher accelerations, the bending maxima move from the crown to the shoulder, below the stiffening beams. Bending maxima in the culvert increase more at the top of the stiffening beams than at the base of the beams.

6.9.3 PGV

A number of authors have used the PGV in seismic design of openings in the ground (mainly for tunnels) where the depth of cover is greater than the span of the opening. This is because the shear deformation of the soil is related to the PGV of the shear waves in the soil.

PGV is not well correlated with the dynamic thrusts or dynamic bending moments in a culvert. In addition, culvert deformation is poorly correlated with PGV. It appears that PGV is not a very useful seismic design parameter for large-span culverts of this type.

6.9.4 Arias Intensity

Arias Intensity is a measure of the energy in the shaking at the site. It is simpler to calculate than the Fourier frequency spectrum and the power spectral density, which is a more accurate measure of the energy in the shaking.

Seismic culvert deformation (peaking or spreading) shows a correlation with Arias intensity. Both closure and spreading of the culvert occur over the same low-intensity range; at larger intensities, only closure occurs, with significant increases as the intensity rises. The range of intensities over which both rise and settlement of the crown were observed is slightly larger than for spreading. Peaking (rise) is significantly greater at greater intensities than at lower intensities. The data are scattered for both culvert closure and rise in the crown.

Closure at the footings and rise in the floor is more closely related to Arias Intensity, with a near-linear increase in both with intensity. The data are less scattered than for closure and crown rise. Ordinarily, this case should be controlled by adequate passive capacity on the inside of the footings, or by using struts between the footings.

No clear relationship was found between Arias Intensity and thrust at the footings, although the data are quite scattered.

A poorly defined and relatively small rise in maximum thrust (and the maximum dynamic increment in thrust) is seen at low values of Arias Intensity, with little or no further rise as the intensity rises further. The maximum bending stress and maximum dynamic increment appear to rise as the Arias Intensity rises, but the data are scattered. Dynamic increments of bending stress increase markedly, with the greatest value being five or six times the least.

6.9.5 General conclusions

At this stage, it appears that the PGV is not a particularly useful seismic design parameter for large-span culverts of this type. The values of the important parameters changed little as the PGV rose. Further consideration is required as to whether the passive failure of the footings has a bearing on this, because the dynamic bending moment increments and some of the maximum dynamic bending moments were greatest in the spring line area (below the stiffening beams), especially at larger PGVs. If the PGV is not so useful, the ovalling design method may not be very useful either.

Reaction axial forces (thrusts) show little change relative to values of any of the three seismic shaking measurement parameters tested.

PGA is probably the best predictor of maximum thrusts. A small increase is within the range of most earthquakes and the data are less scattered than when comparing thrusts and Arias Intensity. At accelerations greater than about 0.6 g, little further rise in maximum thrust occurs in the culvert.

Maximum bending is also more clearly related to PGA than to Arias Intensity. The upper bound of bending with PGA appears to be nearly linear.

7. References

AASHTO. 1989. *Standard Specifications for Highway Bridges, Section 12.* Washington, DC: American Association of State Highway and Transportation Officials.

Abdel–Sayed, G., Bakht, B., Jaeger, L.G. 1994. *Soil–Steel Bridges. Design and onstruction.* New York: McGraw–Hill Inc.

AFTES/AFPS. 2001. *Earthquake Design and Protection of Underground Structures. Version 1*. Guidelines prepared by a working group of the Association Française du Génie Parasismique (French Association for Seismic Engineering or AFPS) and the Association Française des Tunnels et de l'Espace Souterrain (French Tunnelling Association or AFTES). Paris: AFTES and AFPS.

AISI. 1994. *Handbook of Steel Drainage & Highway Construction Products (5th ed).* Washington, DC, USA: American Iron and Steel Institute.

Allmark, T. 2001. The observed damage to buried structures. *Newsletter of the Society. For Earthquake & Civil Engineering Dynamics (UK), Vol 14 No 4*: 2–3.

American Lifeline Alliance. 2005. Seismic guidelines for water pipelines. *www.americanlifelinesalliance.org.*

Arias, A. 1970. A measure of earthquake intensity. Pp 438–483 in *Seismic Design for Nuclear Power Plants* (ed. Hansen, R.J.). Cambridge, Massachusets, USA: MIT Press.

AS 1762. 1984. *Helical Lock-seam Corrugated Steel Pipes – Design and Installation*. Sydney: Standards Australia.

AS3703.2:1989. *Buried Corrugated Metal Structures Part 2: -Design and Installation*. Sydney: Standards Australia.

AS/NZS 1170:2005. *The Loadings Code.* Sydney and Wellington: Standards Australia & Standards New Zealand.

AS/NZS 2041: 1998. *Buried Corrugated Metal Structures.* Sydney and Wellington: Standards Australia & Standards New Zealand.

AS 3703.2. 1989. *Long-span Corrugated Steel Structures. Part 2: Design and Installation.* Sydney: Standards Australia.

Babu, G.L.S., Rao, R.S. 2003. Seismic response of buried flexible pipes. *Proceedings of Current Practices and Future Trends in Earthquake Geotechnical Engineering Conference 23–24 December 2003, Bangalore.*

Beer, F.P., Johnston, E.R. 1982. *Mechanics of Materials.* New York: McGraw-Hill.

Burns, J.Q., Richard, R.M. 1964. Attenuation of stresses for buried cylinders. *Proceedings of the Symposium on Soil/Structure Interaction, University of Arizona 8–11 June 1964.*

Byrne, P.M, Anderson, D.L., Jitno, H. 1996. Seismic analysis of large buried culvert structures. *Transportation Research Record 1541*: 133–139.

Canadian Standards Association. 2000. Canadian Highway Bridge Design Code *CAN/CSA-S6-00*. Ontario, Canada: Canadian Standards Association.

Charneya, F.A., Iyera, H., Spears, P.W. 2005. Computation of major axis shear deformations in wide flange steel girders and columns. *Journal of Constructional Steel Research V. 61, Issue 11, November*: 1525–1558.

Davis, C.A., Bardet, J.P. 1998a. Seismic analysis of buried flexible pipes. *Geotechnical Special Publication No. 75.* Seattle, Washington, USA: American Society of Civil Engineers (ASCE).

Davis, C.A., Bardet, J.P. 1998b. Seismic analysis of large-diameter flexible underground pipes. *Journal of Geotechnical and Geoenvironmental Engineering ASCE 124*:1005–1015.

Davis, C.A., Bardet, J.P. 1999. Case studies of buried corrugated metal pipes from the 1994 Northridge earthquake. *Proceedings of the 5th US Conference on Lifeline Earthquake Engineering.* Seattle, Washington, USA: ASCE.

Davis, C.A., Bardet J.P. 2000. Responses of buried corrugated metal pipes to earthquakes. *Journal of Geotechnical and Geoenvironmental Engineering ASCE 126*:28–39.

Demmin, J. 1966. Field verification of ring compression conduit design. Culverts and storm drains. *Highway Research Record 116 National Academy of Sciences; National Research Council Publication 1338*. Washington, DC: National Research Publication.

Downes, G.L. 1995. Atlas of isoseismals maps of New Zealand earthquakes. *Institute of Geological and Nuclear Sciences Monograph 11.* Lower Hutt, New Zealand: GNS.

DR04421 CP. 2004. *Draft of AS/NZS 2041.1:200X. Buried Corrugated Metal Structures. Part 1: Design Methods.* Sydney and Wellington: Standards Australia and Standards New Zealand.

Duncan, J.M. 1979. Behaviour and design of long-span metal culvert structures. *ASCE Journal of Geotechnical Engineering Division 105 (GT3)*: 399–417.

Duncan, J.M., Seed, R.B. 1986. Compaction-induced earth pressures under K0 conditions. *ASCE Journal of Geotechnical Engineering Vol. 112, No. 1*: 1–23.

Duns, C.S., Butterfield, R. 1971. Flexible buried cylinders. Part 1: static response. Part 2: dynamic response. Part 3: buckling behaviour. *International Journal of Rock Mechanics and Mining Science. Vol. 8*: 577–627.

Earthquake Engineering Research Institute (EERI). 2003. Lessons learned over time. The 1999 Turkey earthquakes: bridge performance and remedial actions. *Learning from Earthquakes Series, Vol. IV.* Oakland, California: Earthquake Engineering Research Institute.

Einstein, H.H., Schwartz, C.W. 1979. Simplified analysis for tunnel supports. *Journal of the Geotechnical Engineering Division, ASCE 105 GT4*: 499–518.

Erdik, M., Durukal, E. 2004. Strong ground motion. In: *Recent Advances in Earthquake Geotechnical Engineering and Microzonation (ed Ansal, A.)*. Berlin: Springer.

Han, Y., Sun, S., Cui, Y. 2003. Some parameters for seismic design and analysis of buried pipelines. *Pipelines 2003:* 1135–1144.

Hendron, A.J., Fernandez, G. 1983. Dynamic and static design considerations for underground chambers. *Proceedings of the Symposium on Seismic Design of Embankments & Caverns. May 1983*. Philadelphia, PA, USA: ASCE.

Höeg, K. 1968. Stresses against underground structural cylinders. *Journal of Soil Mechanics and Foundations Division ASCE 94 SM4*: 833–858.

Itasca. 2005a. *FLAC. Fast Lagrangian Analysis of Continua. User's Guide.* Minneapolis, Minnesota, USA: Itasca Consulting Group Inc.

Itasca. 2005b. *FLAC. Fast Lagrangian Analysis of Continua. Optional Features Manual: Dynamic Analysis.* Minneapolis, Minnesota, USA: Itasca Consulting Group Inc.

Kan, F, Zarghamee, M.S., Rose, B.D. 2005. *Seismic Evaluation of Buried Pipelines*. Seattle, Washington, USA: ASCE.

McCavour, T.C., Byrne, P.M., Morrison, T.D. 1998. Long-span reinforced steel box culverts. *Transportation Research Record 1624:* 184–195.

McGrath, T.J., Moore, I.D., Selig, E.T., Webb, M.C., Taleb, B. 2002. National research council. Recommended specifications for large-span culverts. *National Cooperative Highway Research Program (NCHRP) Report 473*, Washington, DC: Transportation Research Board.

Meyerhof, G.G., Baikie, L.D. 1963. Strength of steel culvert sheets bearing against compacted sand backfill. *Highway Research Record No. 30.* Washington, DC: Highway Research Board, National Academy of Science.

Ministry of Transportation of Ontario. 1992. *Ontario Highway Design Code (3rd ed).* Downsview, Ontario, Canada: Ministry of Transportation

Moore, I.D., Taleb, B. Metal culvert response to live loading. Performance of three–dimensional analysis. *Transportation Research Record 1653. Paper No. 99-0553*. Washington, DC: Transportation Research Board.

New Zealand Government. 2002. Civil Defence and Emergency Management Act 2002. *http://www.legislation.govt.nz/act/public/2002/0033/latest/DLM149789.html.*

Ogawa, Y. Koike, T. 2001. Structural design of buried pipelines for severe earthquakes. *Soil Dynamics and Earthquake Engineering 21*: 199–209.

Owen, G.N., Scholl, R.E. 1981. Earthquake engineering of large underground structures. *FHWA/RD-80/195*. Washington, DC: Federal Highway Administration.

Park, R., Paulay, T. 1975. *Reinforced Concrete Structures*. Hoboken, NJ: Wiley-InterScience.

Peck, R.B., Hendron, A.J., Mohraz, B. 1972. State of the art of soft-ground tunnelling. Pp 259–286 in *Proceedings of the 1st North American Rapid Excavation & Tunnelling Conference, Vol 1*. London, UK: Taylor & Francis Books. 527 pp.

Pineda-Porras O., Ordaz-Schroeder, M. 2003. Seismic vulnerability function for high-diameter buried pipelines: Mexico City's primary water system case. *Pipelines 2003*: 1145–1154.

Samata, S, Ohuchi, H., Matsuda, T. 1997. A study of the damage of subway structures during the 1995 Hanshin–Awaji earthquake. *Cement and Concrete Composites 19*: 223–239.

Seed, R.B., Ou, C. 1987. Measurements and analyses of compaction effects on a long–span culvert. *Transportation Research Record 1087*. Washington, DC: Transportation Research Board.

Seed, R.B., Raines, J.R. 1988. Failure of flexible long-span culverts under exceptional live loads. *Transportation Research Record 1191*. Washington, DC: Transportation Research Board.

Seed, R.B., Duncan, J. M. 1986. Compaction-induced stresses and deformation for yielding structures. *Journal of ASCE Geotechnical Engineering Division 112:1:* 23–43.

Seed, R.B., Ou, C. 1988. Compaction-induced distress of a long-span culvert overpass structure. Pp 1183-1190 (Paper No. 610) in *Second International Conference on case Histories in Geotechnical Engineering, St. Louis, MO, USA.*

St. John, C.M., Zahrah, T.F. 1987. Aseismic design of underground structures. *Tunnelling and Underground Space Technology, Vol 2, No. 2*: 165–197.

Timoshenko, S.P., Gere, J.M. 1961. *Theory of Elastic Stability (2nd ed).* New York: McGraw-Hill Book Company.

Wang, J. 1993. Seismic design of tunnels: a simple state-of-the-art design approach. *1991 William Barclay Parsons Fellowship, Parsons Brinckerhoff, Monograph 7.* New York: Jaw-Nan Wang and Parsons Brinckerhoff Inc.

Webb, M.C, Selig, E.T., Sussman, J.A., McCarthy, T.J. 1999. Field tests of a large-span metal culvert. *Transportation Research Record 1653, Paper No. 99-1425.* Washington, DC: Transportation Research Board.

Wood J.H. 2007. Earthquake design of rectangular underground structures. *Bulletin of the New Zealand Society for Earthquake Engineering, v.40, No. 1, March*: 1–6.

Youd, T., Beckman, C. 2003. Performance of corrugated metal pipe culverts during past earthquakes. Pp 294–307 in *Advancing Mitigation Technologies and Disaster Response for Lifeline Systems* (ed. Beavers, J.E.). Seattle, Washington, USA: ASCE.

Youd, T.L ., Beckman, C.J. 1996. Highway culvert performance during past earthquakes. *Rep. NCEER-96-0015.* Buffalo, NY: National Center for Earthquake Engineering Research.

Youd, T.L., Beckman, C.J. 1997. Performance of Corrugated Metal Pipe (CMP) Culverts during past earthquakes. Pp 137–151 in *Proceedings of the Workshop on Earthquake Engineering Frontiers in Transportation Facilities NCEER-97-005* (eds Lee, G.C., Friedland, I.M.). Buffalo, NY, USA: National Center for Earthquake Engineering.

Appendix A On calculating the ultimate compressive wall stress

The standards (AS/NZS2041 (1998), AS3703.2 (1989) and DR04421 (2004)) require consideration of the ultimate compressive wall stress during design. This stress takes both thrust and bending stress into consideration. Timoshenko & Gere (1961) show how a non-extensional bending moment affects the thrust by deformation of a circular ring, so a separate maximum bending moment is not required.

The ultimate compressive wall stress, f_b, in design (and Table 4.3) is determined using one of a set of three formulae:

$$f_b = f_y \quad \text{if} \quad \frac{S}{r} < 294 \qquad \text{[Equation A1]}$$

$$f_b = 302.8 - 0.613x10^{-3}\left(\frac{S}{r}\right)^2 \quad \text{if} \quad 294 < \frac{S}{r} < 500 \qquad \text{[Equation A2]}$$

$$f_b = \frac{37.35x10^6}{\left(\frac{S}{r}\right)^2} \quad \text{otherwise} \qquad \text{[Equation A3]}$$

where:

- f_y is the yield stress in MPa
- S is the span in m,
- r is the radius of gyration (in m) of the corrugations, and
- 302.8 is the tensile strength (stress) of the steel (Grade 250 in this case).

Equation A1 is the minimum yield stress of the steel, which represents crushing or yielding; Equation A2 represents the interaction zone between yielding and ring buckling; and Equation A3 represents ring buckling. These formulae are based on work carried out in 1967 to 1970 at Utah State University, Logan, Utah, USA, and sponsored by the American Iron and Steel Institute (by inference from Abdel-Sayed et al. 1994). Load tests were carried out on approximately 130 circular pipes up to 1.5 m diameter (American Iron and Steel Institute 1994). The apparent ultimate ring compression stress was plotted against the square of the ratio of the span to the radius of gyration of corrugations. The three formulae were developed to describe sections of an idealised curve on that graph, for soil compacted to at least 85% of its maximum (Proctor) density. These formulae are the same as those in AS/NZS2041 (1998) and DR04421 (2004), after appropriate conversion of units.

The change from one formula to another is by the ratio of the span to the radius of gyration of the corrugations. In AS3703.2, it is by the ratio of twice the radius of curvature of the crown to the radius of gyration of the corrugations. Using the radius is more logical when considering elastic stability (all Timoshenko & Gere's (1961) expressions use radius of

curvature). However, as these equations were derived for circular culverts, the span and twice the radius were the same. Differences in the calculated results arise when we apply the formulae to larger culverts that consist of circular segments but are not actually circular.

The two standards use different yield stresses (250 MPa in AS/NZS2041 and 230 MPa in AS3703.2) but the constants in the AS3073.2 formulae are those in AS/NZS2041 times 230/250. In addition, the ultimate wall stress determined in accordance with AS3703.2 is then corrected for the subtended angle of the top arc in accordance with elastic stability theory. The AS3703.2 formulation seems the more logical, as the top radius is the critical parameter for buckling, not span. Use of the top radius is also more general, as it provides for consideration of non-circular shapes made up of circular segments.

The ultimate compressive wall stress shown in Table 4.3 is calculated as:

$$37.35/(S_S/r_g)^2, \qquad \text{[Equation A4]}$$

which is the ring buckling equation 5.9(3) in AS/NZS2041:1998. The clear span between crests, S_S, is 11.66 m and the radius of gyration, r_g, of the corrugations is 19.8 mm, so S_S/r_g is 589.

The draft standard DR04421, which is a revision of parts of AS/NZS2041, AS3703.2 and AS1762 (1984), contains formulae for both Grade 230 and Grade 250 steel, with the appropriate constants, and uses the maximum span rather than (2*top radius). When longitudinal stiffeners are used, DR04421 also applies the correction for the angle subtended by the top arc between the stiffeners, as in AS3703.2.

AASHTO (1989) also provides a set of equations giving the buckling stress. They appear to be derived from elasticity stability theory:

$$f_b = F_u - \frac{\left(\frac{F_u.k.S}{r}\right)^2}{48.E_m} \quad \text{if } S < \left(\frac{r}{k}\right)\sqrt{\frac{24.E_m}{F_u}} \qquad \text{[Equation A5]}$$

$$f_b = \frac{12.E_m}{\left(\frac{k.S}{r}\right)^2} \quad \text{otherwise} \qquad \text{[Equation A6]}$$

where:

- F_u is the tensile strength (MPa),
- E_m is Young's modulus of the steel (MPa),
- r is the radius of gyration of corrugation (mm),
- S is the span of the structure (mm), and
- k is the soil stiffness factor, usually taken as 0.22 for well compacted soil (to at least 85% Proctor density).

Another method of calculating the buckling stress is given in Abdel-Sayed et al. (1994). The stress is affected by the soil backfill around the culvert, the cover over the location under consideration in the culvert wall and the radius of curvature of the culvert wall at that

location. The method given in Abdel-Sayed et al. considers failure of the conduit wall through instability in compression, leading to buckling waves, in an elastically supported pipe. The method includes reducing the buckling stress as recommended by Meyerhof & Baikie (1963) to account for shallow cover. The equations are given below. The values in Table 4.3 were calculated using the soil elastic modulus rather than the secant modulus as required by the formulae. As well as the type of soil, the secant modulus is definition-dependent and also depends on the state of stress in the soil, which is not modelled in this work. If the secant modulus is half of the elastic modulus, the buckling stresses are just over two-thirds of the values listed in Table 4.3.

$$\begin{aligned} \psi &= 1 \qquad \text{if} \quad \frac{h}{R} \geq 1 \\ &= \sqrt{\frac{h}{R}} \quad \text{if} \quad 0.1 < \frac{h}{R} < 1 \\ &= 0 \qquad \text{otherwise} \end{aligned} \qquad \text{[Equation A7]}$$

$$k_n = \left(1 - \left(\frac{R}{R+h}\right)^2\right) . \frac{E_S}{2.R.(1-\upsilon_S{}^2)} \qquad \text{[Equation A8]}$$

$$f_b = \frac{2.\psi}{A} . \sqrt{E_L . I . k_n} \qquad \text{[Equation A9]}$$

where:

- □ is the depth of cover reduction factor;
- h is the depth of cover;
- R is the radius of curvature at the location under consideration (usually within the top span);
- k_n is the coefficient of soil (normal) reaction and is defined as the normal pressure divided by the displacement at the pipe-soil interface;
- E_s is the secant modulus of the soil;
- u_s is Poisson's ratio of the soil;
- A is the area of lining per metre length of culvert;
- E_L is Young's modulus of the steel lining; and
- I is the second moment of area of lining per metre length of culvert.

Appendix B Transit Bridge Descriptive System output

Transit New Zealand's Bridge Descriptive System database was searched in August 2006 to find records with 'arch' in the Type field or 'multiplate' in the material field. The 188 records discovered are on the following pages.

The database is maintained by the NZTA with input supplied by the Bridge Management Consultants.

The tables in this appendix have been reformatted from the original output for space reasons.

Table B1 Results 1–8 of the search of the BDS using 'arch' and 'multiplate' as search keywords.

Feature	Result number							
	1	2	3	4	5	6	7	8
Structure ID	32363	32394	32412	32420	32450	32509	32544	32559
BSN	287	1079	–	1816	2414	–	–	–
SH[a]	2	2	2	2	2	2	2	2
RS[b]	18	99	156	180	232	406	516	577
Distance	10.75	8.98	0.75	1.64	9.37	7.29	13.8	12.31
Direction	1 – two way	1 – two way	2 – increasing	1 – two way	1 – two way	1 – two way	1 – two way	1 – two way
Name	Heaven's Twin Culvert	Ross Stock Underpass 1.8 diameter	Hairini Pedestrian Underpass (increasing)	Raymonds Drain Culvert (3.3. ARMCO)	Te Rahu Canal Pipe Arch Culvert 4.3/2.7 m	Dymock's Culvert	Waiatai Culvert	McKenzie"s Rail Culvert
Function	SH over waterway	SH over stock underpass	SH over combination of stream, road, railway or other	SH over waterway	SH over waterway	SH over waterway	SH over waterway	SH over railway
Year built	1979	1965	?	1956	1994	1965	1983	1975
Design loading	HN_HO_72	–	–	HN_HO_72	–	H20_S16	HN_HO_72	other
Drawings	SR1806	2/31/21/7204	–	2/37/1/7234	BBO 124400/31	–	3/19/1/7304	PWN 6701
No. Drawings	–	–	_	–	_	–	0	0
Drawings held at	–	–	–	–	–	–	–	–
Drawings comment	Pipe arch 3.0m x 4.0m	ARMCO 1.8 dia	–	–	Pipe arch ARMCO 4.3 m x 2.7 m	–	–	–
Cost ($)	34,478	?	?	?	120,000	?	207,900	?
Structure type	culvert	stock underpass	pedestrian subway	culvert	culvert	culvert	culvert	culvert
Foundations	spread footings	spread footings	spread footings	spread footings	spread footings	spread footings	spread footings	spread footings
Fill depth (m)	1	0.9	0.7	2	1.2	1.2	1.5	1.8
Length of structure (m)	28.6	15.2	20	32	36	21	34.1	32.9
Type	multiple pipe	pipe	pipe	pipe arch	pipe arch	pipe	pipe arch	arch
Invert lining	none	concrete	concrete	none	none	other	other	other

Notes to Table B1:

a SH = state highway

b RS = Route Station, or distance in kilometres along a state highway.

Table B2 Results 9–16 of the search of the BDS using 'arch' and 'multiplate' as search keywords.

Feature	Result number							
	9	10	11	12	13	14	15	16
Structure ID	32591	32592	32597	32598	32599	32624	32634	32638
BSN	7243	–	7534	–	–	–	8230	8391
SH[a]	2	2	2	2	2	2	2	2
RS[b]	721	721	751	751	751	788	808	825
Distance	3.28	6.82	2.37	2.71	3.09	8.56	14.94	14.09
Direction	1 – two way	1 – two way	1 – two way	1 – two way	1 – two way	1 – two way	1 – two way	1 – two way
Name	Sanitorium Hill Culvert No. 1	Sanitorium Hill Culvert No. 4	Butcher's Creek Culvert	Murphy's Underpass (stock)	Hayes' Underpass (stock)	Papatawa Stream Culvert	Warren's Creek Culvert	Newman Factory Creek Culvert
Function	SH over waterway	SH over waterway	SH over waterway	SH over stock underpass	SH over stock underpass	SH over waterway	SH over waterway	SH over waterway
Year built	1986	1986	1992	1992	1992	1993	1993	1993
Design loading	HN_HO_72	HN_HO_72	–	–	–	HN_HO_72	HN_HO_72	HN_HO_72
Drawings	3/33/8/7304	3/33/8/7304	–	–	–	4/125/1/7404/ 1-2	5/10/19/7504/ 1-7	5/11/9/7504/ 1-7
No. Drawings	–	–	–	–	–	–	–	–
Drawings held at	–	–	–	–	–	–	–	–
Drawings comment	–	–	–	–	–	–	–	–
Cost ($)	64,250	80,420	?	?	?	104,000	140,000	90,000
Structure type	culvert	culvert	culvert	stock underpass	stock underpass	culvert	culvert	culvert
Foundations	spread footings	spread footings	–	other	other	spread footings	spread footings	spread footings
Fill depth (m)	0.9	3.2	–	1	0.9	1.6	1.8	9.5
Length of structure (m)	27.6	37.7	–	15	15	16.8	32.7	43.5
Type	pipe	pipe	–	pipe	pipe	pipe arch	pipe arch	pipe
Invert lining	concrete	concrete	–	concrete	concrete	concrete	–	–

Notes to Table B2:
a SH = state highway
b RS = Route Station, or distance in kilometres along a state highway.

Table B3 Results 17–24 of the search of the BDS using 'arch' and 'multiplate' as search keywords.

Feature	Result number							
	17	18	19	20	21	22	23	24
Structure ID	32643	32644	32645	32646	32647	32650	32677	35555
BSN	–	–	–	–	–	–	–	–
SH[a]	2	2	2	2	2	2	2	3
RS[b]	842	842	842	842	842	842	946	16
Distance	6.96	7.11	7.46	8.02	8.38	14.95	6.62	10.42
Direction	1 – two way	1 – two way	1 – two way	1 – two way	1 – two way	1 – two way	1 – two way	1 – two way
Name	Todd's Underpass No. 1 (stock)	Todd's Underpass No. 2 (stock)	McClaren's Underpass No. 1 (stock)	McClaren's Underpass No. 2 (stock)	Hansen's Underpass (stock)	Tankersley's Creek Culvert	Gibbons Street Culvert	Mangaohoi Stream ARMCO pipe arch
Function	SH over stock underpass	SH over stock underpass	SH over stock underpass	SH over stock underpass	SH over stock underpass	SH over waterway	SH over waterway	SH over waterway
Year built	1992	1992	1992	1992	1992	?	?	2000
Design loading	HN_HO_72	HN_HO_72	HN_HO_72	HN_HO_72	HN_HO_72	–	unknown	HN_HO_72
Drawings	5/12/15/7504/8	5/12/15/7504/8	5/12/15/7504/7	5/12/15/7504/5	5/12/15/7504/4	–	–	MO1 03, 28, &
No. Drawings	–	–	–	–	–	–	–	3
Drawings held at	–	–	–	–	–	–	–	BBO[c]
Drawings comment	–	–	–	–	–	–	–	–
Cost ($)	111,000	99,000	112,000	137,000	125,000	?	?	?
Structure type	stock underpass	stock underpass	stock underpass	stock underpass	stock underpass	culvert	culvert	culvert
Foundations	spread footings	spread footings	spread footings	spread footings	spread footings	–	spread footings	spread footings
Fill depth (m)	1.2	1.1	1.3	1.3	1.5	10	1	1
Length of structure (m)	32.3	29.5	32.6	39.7	36.1	42	28	27.4
Type	arch	arch	arch	arch	arch	pipe	multiple pipe	pipe arch
Invert lining	asphalt	concrete	concrete	asphalt	concrete	concrete	other	none

Notes to Table B3:
a SH = state highway
b RS = Route Station, or distance in kilometres along a state highway.
c BBO = Bloxham Burnett and Olliver Ltd, Hamilton

Table B4 Results 25–32 of the search of the BDS using 'arch' and 'multiplate' as search keywords.

Feature	Result number							
	25	26	27	28	29	30	31	32
Structure ID	32970	32982	32983	33039	33043	33046	33360	33364
BSN	1222	–	–	–	–	–	–	–
SH[a]	3	3	3	3	3	3	4	4
RS[b]	118	176	176	279	310	310	77	94
Distance	4.46	0.47	0.62	4.18	5.98	9.93	12.24	13.68
Direction	1 – two way	1 – two way	1 – two way	1 – two way	1 – two way	1 – two way	1 – two way	1 – two way
Name	Auld's Stock Underpass 5.0 x 3.1 m	Mangapepeki No. 1	Mangapepeki No. 2	Ngaere Overbridge	Ballantine Stock Underpass	Rawson Stock Underpass	Otapouri Stream Culvert	Pukerimu Stream Culvert
Function	SH over stock underpass	SH over waterway	SH over waterway	SH over railway	SH over stock underpass	SH over stock underpass	SH over waterway	SH over waterway
Year built	1975	1963	1965	1998	1994	1993	1977	1965
Design loading	–	H20_S16_T16	H20_S16_T16	HN_HO_72	HN_HO_72	HN_HO_72	HN_HO_72	H20_S16_T16
Drawings	–	NP6798	NP6975	PWD 95806 4/32/7/7424	–	–	WG9462 TM3703	TM2802
No. Drawings	–	–	–	5	–	–	–	–
Drawings held at	–	–	–	BBO[c]	–	–	–	–
Drawings comment	–	–	–	original drawings	–	–	–	–
Cost ($)	15,300	8,900	15,240	900,000	29,000	42,000	129,000	?
Structure type	stock underpass	culvert	culvert	culvert	stock underpass	stock underpass	culvert	culvert
Foundations	spread footings	–	other	–	–	–	–	spread footings
Fill depth (m)	1.1	1.2	2.4	1	–	–	4.9	1.3
Length of structure (m)	20	20.2	30.5	112	17	14	46.9	39.6
Type	arch	pipe	arch	arch	arch	arch	pipe arch	pipe
Invert lining	concrete	–	–	none	concrete	concrete	concrete	none

Notes to Table B4:
a SH = state highway
b RS = Route Station, or distance in kilometres along a state highway.
c BBO = Bloxham Burnett and Olliver Ltd, Hamilton

Table B5 Results 33–39 of the search of the BDS using 'arch' and 'multiplate' as search keywords.

Feature	Result number						
	33	34	35	36	37	38	39
Structure ID	35590	35591	33571	33572	33581	33583	33585
BSN	–	–	918	943	–	–	–
SH[a]	4	4	5	5	5	5	5
RS[b]	206	206	77	77	190	190	204
Distance	9.2	9.3	14.86	17.29	9.63	11.37	12.8
Direction	1 – two way	1 – two way	1 – two way	1 – two way	1 – two way	1 – two way	1 – two way
Name	Waimatao No. 1 ARMCO	Waimatao No. 2 ARMCO	Mangahoanga Pipe Arch Culvert 4.1W x 2.2H	Mangakara Culvert Pipe Arch 4.1W x 2.2H	Stoney Creek Culvert (SH5)	Baker's Culvert (extension)	Stock Underpass
Function	SH over waterway	SH over waterway	SH over waterway	SH over waterway	SH over waterway	SH over waterway	SH over combination of stream, road, railway, or other
Year built	1997	1997	1976	1976	1966	1987	1988
Design loading	HN_HO_72	HN_HO_72	HN_HO_72	HN_HO_72	H20_S16_T16	HN_HO_72	HN_HO_72
Drawings	Payne Sewell 2400073 sheet 16	Payne Sewell 2400073 sheet 16	RO5557/1-4843	RO5557/2-4843	PWN 4853	3/42/32/7304	3/43/13/7304
No. Drawings	1	1	–	–	–	6	2
Drawings held at	–	–	–	–	–	Opus Napier	Opus Napier
Drawings comment	6.3 m diameter	6.3 m diameter	–	–	–	–	–
Cost ($)	234,000	234,000	?	?	?	?	53,000
Structure type	culvert	culvert	culvert	culvert	culvert	culvert	stock underpass
Foundations	spread footings	spread footings	other	other	spread footings	spread footings	spread footings
Fill depth (m)	9.7	5.8	4	5	10	3	1
Length of structure (m)	56	47	28.7	38.4	55.5	17	40
Type	pipe	pipe	pipe arch	pipe arch	pipe	pipe	arch
Invert lining	none	none	none	none	concrete	none	other

Notes to Table B5:
a SH = state highway
b RS = Route Station, or distance in kilometres along a state highway.

Table B6 Results 40–46 of the search of the BDS using 'arch' and 'multiplate' as search keywords.

Feature	Result number						
	40	41	42	43	44	45	46
Structure ID	33589	33835	33842	33872	33895	33897	33908
BSN	–	–	–	4279	4708	4730	4977
SH[a]	5	6	6	6	6	6	6
RS[b]	233	336	363	416	463	471	489
Distance	11.16	4.58	4.99	11.85	7.82	2.01	8.69
Direction	1 – two way	1 – two way	1 – two way	1 – two way	1 – two way	1 – two way	1 – two way
Name	Northland Stock Underpass	Mary's Creek Culvert	Whitehorse Creek Culvert	Coal Creek Stock Underpass	Hokitika River (N Channel) Culvert	Fisherman's Creek Culvert	Totara River Overflow Culvert
Function	SH over stock underpass	SH over waterway	SH over waterway	SH over stock underpass	SH over waterway	SH over waterway	SH over waterway
Year built	1996	1981	1974	?	1991	1992	1994
Design loading	HN_HO_72	HN_HO_72	–	HN_HO_72	HN_HO_72	HN_HO_72	HN_HO_72
Drawings	3/45/30/7304/13	6/40/5/7604	HCH 3399/2	6/46/5	WKS 6/49/17/7604	WKS 6/49/22/7604	6/51/10/7604
No. Drawings	0	–	_	_	–	–	–
Drawings held at	–	–	_	_	_	–	–
Drawings comment	–	–	_	_	_	–	–
Cost ($)	91,000	?	2,656	?	62,000	90,000	120,000
Structure type	stock underpass	culvert	culvert	stock underpass	culvert	culvert	culvert
Foundations	spread footings	spread footings	spread footings	spread footings	spread footings	spread footings	spread footings
Fill depth (m)	1	6	7	0.5	4	0.6	2.3
Length of structure (m)	21	52.9	40.8	19	37	25	26.7
Type	arch	arch	arch	pipe	pipe arch	pipe arch	pipe arch
Invert Lining	other	concrete	concrete	concrete	other	none	none

Notes to Table B6:
a SH = state highway
b RS = Route Station, or distance in kilometres along a state highway.

Table B7 Results 47–54 of the search of the BDS using 'arch' and 'multiplate' as search keywords.

Feature	Result number							
	47	48	49	50	51	52	53	54
Structure ID	33932	34076	34088	34089	34090	34125	34131	34165
BSN	5574	7802	7906	–	7955	–	–	###
SH[a]	6	6	6	6	6	6	6	6
RS[b]	551	767	783	783	783	866	918	1095
Distance	6.39	13.15	7.63	10.13	12.46	0	8.6	8.66
Direction	1 – two way	1 – two way	1 – two way	1 – two way	1 – two way	1 – two way	1 – two way	1 – two way
Name	Hercules Creek Culvert	18 Mile Culvert	Solitude No. 2 Culvert	Douglas Falls Culvert	Big Creek Culvert	Dinner Creek Culvert	Tinwald Burn Culvert	Ramhill Stream Culvert
Function	SH over waterway	SH over waterway	SH over waterway	SH over waterway	SH over waterway	SH over waterway	SH over waterway	SH over waterway
Year built	1980	?	1954	?	?	1980	1980	1979
Design loading	HN_HO_72	other	other	–	–	HN_HO_72	HN_HO_72	–
Drawings	6/55/3/7604	GR7463	GR 7463|6/71/7	GR7463	GR7463	7/40/2/7704	7/44/2/7714	–
No. Drawings	–	–	–	–	–	–	–	–
Drawings held at	–	–	–	–	–	–	–	–
Drawings comment	–	–	–	–	–	–	–	–
Cost ($)	?	?	?	?	?	19,024	18,260	?
Structure type	culvert	culvert	culvert	culvert	culvert	culvert	culvert	culvert
Foundations	spread footings	spread footings	driven piles, steel	driven piles, steel	spread footings	other	–	other
Fill depth (m)	4.3	0.3	0.8	1.4	0.8	5	1	3
Length of structure (m)	31.8	7.7	12.5	12.4	7.7	31	14.6	20
Type	arch	arch	arch	arch	arch	arch	pipe	pipe
Invert Lining	concrete	none	none	none	concrete	–	none	other

Notes to Table B7:
a SH = state highway
b RS = Route Station, or distance in kilometres along a state highway.

Table B8 Results 55–61 of the search of the BDS using 'arch' and 'multiplate' as search keywords.

Feature	Result number						
	55	56	57	58	59	60	61
Structure ID	34431	34661	34662	34663	34664	34665	34666
BSN	2431	–	–	–	–	–	–
SH[a]	7	8	8	8	8	8	8
RS[b]	239	271	297	297	297	297	297
Distance	4.07	17.46	1.12	2.92	8.29	9.75	10.55
Direction	1 – two way	1 – two way	1 – two way	1 – two way	1 – two way	1 – two way	1 – two way
Name	Callaghan's Creek Culvert No. 1	Quartz Reef Creek Culvert	Firewood Creek Culvert	Brewery Creek Culvert	Nine Mile Creek No. 2 Culvert	Sonora Creek Culvert	No. 6 Creek Culvert
Function	SH over waterway	SH over waterway	SH over waterway	SH over waterway	SH over waterway	SH over waterway	SH over waterway
Year built	1978	1983	1982	1982	1982	1988	1988
Design loading	HN_HO_72	HN_HO_72	HN_HO_72	HN_HO_72	HN_HO_72	HN_HO_72	HN_HO_72
Drawings	6/88/8/7604	–	–	WCS7/75/13	WCS7/75/19	WCS7/75/26	WCS7/75/26
No. Drawings	–	–	–	–	–	–	–
Drawings held at	–	–	–	–	–	–	–
Drawings comment	–	6.3 m diameter	–	–	–	–	–
Cost ($)	?	?	?	?	?	?	?
Structure type	culvert	culvert	culvert	culvert	culvert	culvert	culvert
Foundations	spread footings	–	–	–	other	–	–
Fill depth (m)	6	3	5	2	2	7	15
Length of structure (m)	37.3	40	32	176	29	60	81
Type	arch	pipe	pipe	pipe	pipe arch	pipe arch	pipe
Invert Lining	concrete	concrete	concrete	concrete	concrete	concrete	concrete

Notes to Table B8:
a SH = state highway
b RS = Route Station, or distance in kilometres along a state highway.

Table B9 Results 62–68 of the search of the BDS using 'arch' and 'multiplate' as search keywords.

Feature	Result number						
	62	63	64	65	66	67	68
Structure ID	34667	34668	34669	34671	34672	35233	32230
BSN	–	–	–	–	–	88	800
SH[a]	8	8	8	8	8	12	12
RS[b]	297	297	297	310	310	0	74
Distance	10.96	11.84	12.69	1.2	3.55	8.77	5.95
Direction	1 – two way	1 – two way	1 – two way	1 – two way	1 – two way	1 – two way	1 – two way
Name	No.5 Creek Culvert	Leaning Rock Creek Culvert	No. 4 Creek Culvert	Champagne Gully Culvert	Robertson's Creek Culvert	Wairoro Stream Culvert	Rumsey's Stock Underpass
Function	SH over waterway	SH over waterway	SH over waterway	SH over waterway	SH over waterway	SH over waterway	SH over stock underpass
Year built	1988	1988	1987	1987	1985	1999	1994
Design loading	HN_HO_72	HN_HO_72	HN_HO_72	HN_HO_72	HN_HO_72	HN_HO_72	HN_HO_72
Drawings	WCS7/75/26	WCS7/75/26	WCS7/75/27	–	–	9/41/16/7914/16	1/46/15/7114/26
No. Drawings	–	–	–	–	–	1	1
Drawings held at	–	–	–	–	–	Opus Whangarei	Opus, Whangarei
Drawings comment	–	–	–	–	–	–	–
Cost ($)	?	?	?	?	?	?	–
Structure type	culvert	culvert	culvert	culvert	culvert	culvert	stock underpass
Foundations	–	–	–	–	–	spread footings	spread footings
Fill depth (m)	12	7	4	2	3	1.2	1.2
Length of structure (m)	48	49	36	36	34	23	22.1
Type	pipe	pipe	pipe	pipe arch	pipe	arch	arch
Invert lining	concrete	concrete	concrete	concrete	–	other	other

Notes to Table B9:
a SH = state highway
b RS = Route Station, or distance in kilometres along a state highway.

Table B10 Results 69–75 of the search of the BDS using 'arch' and 'multiplate' as search keywords.

Feature	Result number						
	69	70	71	72	73	74	75
Structure ID	32234	32238	32244	32301	32320	35715	35716
BSN	934	1001	1366	483	235	142	143
SH[a]	12	12	12	14	16	18	18
RS[b]	89	89	132	44	19	0	0
Distance	4.39	11.1	4.58	4.3	4.45	1.42	1.43
Direction	1 – two way	1 – two way	1 – two way	1 – two way	1 – two way	1 – two way	1 – two way
Name	Waikohatu Stream Culvert 617	Merowharara Stream Culvert 1401	Dacker's Culvert 1859	Te Wharau Railway Overbridge No. 130	Brigham's Creek Culvert	Alexander Stream Culvert	SH 18 Pedestrian Underpass
Function	SH over waterway	SH over waterway	SH over waterway	SH over railway	SH over waterway	SH over waterway	SH over waterway
Year built	1982	1984	1967	1980	1984	1998	1994
Design loading	HN_HO_72	HN_HO_72	H20_S16_T16	HN_HO_72	HN_HO_72	HN_HO_72	HN_HO_72
Drawings	1/47/2/7104	1/47/4/7104	WR-9955	1/58/2/7104	1/60/2/7104/ 1-4	–	–
No. Drawings	3	2	1	7	–	–	–
Drawings held at	Opus, Auckland	Opus, Auckland	Opus, Whangarei	Opus, Whangarei	–	–	–
Drawings comment	–	–	–	–	–	–	–
Cost ($)	?	?	?	90,000	300,000	?	?
Structure type	culvert	culvert	culvert	culvert	culvert	culvert	pedestrian subway
Foundations	spread footings	spread footings	spread footings	spread footings	other	–	–
Fill depth (m)	1.2	4	1.1	1	3.5	5	1
Length of structure (m)	27.4	11.1	18.3	32.2	37.5	70	41
Type	pipe	arch	arch	arch	arch	pipe	pipe
Invert Lining	none	none	concrete	none	none	none	none

Notes to Table B10:
a SH = state highway
b RS = Route Station, or distance in kilometres along a state highway.

Table B11 Results 76–83 of the search of the BDS using 'arch' and 'multiplate' as search keywords.

Feature	Result number							
	76	77	78	79	80	81	82	83
Structure ID	32713	32775	32776	32779	32846	32857	32875	32895
BSN	12	1068	1103	1198	–	–	–	–
SH[a]	23	25	25	25	26	26	26	27
RS[b]	0	99	99	113	17	35	80	16
Distance	1.2	7.84	10.84	6.66	7.25	8.11	6.73	0
Direction	1 – two way	1 – two way	1 – two way	1 – two way	2 – increasing	1 – two way	1 – two way	1 – two way
Name	Dinsdale ARMCO pipe arch 5 m x 3 m	Mapauriki Stream Culvert	Pitoone Stream Culvert	Ake Ake Stream Culvert	Morrinsville West Extension (incr. lane)	Waiwhero St Pipe Arch 4.9 x 3.3	Smith Stock Underpass 3.0 dia	Takos Drain ARMCO Culvert 4.35 x 2.95 m
Function	SH over waterway	SH over waterway	SH over waterway	SH over waterway	SH over waterway	SH over waterway	SH over stock underpass	SH over waterway
Year built	1975	1978	1979	2003	1980	1978	1982	1974
Design loading	–	HN_HO_72	–	–	–	HN_HO_72	–	HN_HO_72
Drawings	2/71/1/9924	2/81/2 RAB	2/81/3/ RAB	–	2/94/9/7204 RAB	2/96/3/7204 RAB	2/99/2/7214	HDO13666
No. Drawings	0	0	0	0	0	–	–	0
Drawings held at	–	–	–	–	–	–	–	–
Drawings comment	–	Pipe arch 5 x 3 m	Pipe arch 4.4 x 3 m	Pipe ARMCO 3 m diameter	–	–	–	–
Cost ($)	?	71,800	38,000	?	?	78,000	24,000	?
Structure type	culvert	culvert	culvert	culvert	culvert	culvert	stock underpass	culvert
Foundations	spread footings	other	other	other	spread footings	other	other	spread footings
Fill depth (m)	1.2	0.5	0.6	0.7	1	2	0.6	1.1
Length of structure (m)	92.7	25	18.3	7.7	5	19	14.6	19.5
Type	pipe arch	pipe arch	pipe arch	pipe	pipe	pipe arch	pipe	pipe arch
Invert Lining	none	concrete	concrete	none	none	other	concrete	none

Notes to Table B11:
a SH = state highway
b RS = Route Station, or distance in kilometres along a state highway.

Table B12 Results 84–90 of the search of the BDS using 'arch' and 'multiplate' as search keywords.

Feature	Result number							
	84	85	86	87	88	89	90	91
Structure ID	35570	35569	33105	33106	33108	33110	33112	
BSN	–	184	32	66	140	258	334	
SH[a]	27	27	30	30	30	30	30	
RS[b]	16	16	0	0	14	14	30	
Distance	2.45	2.46	3.24	6.65	0	11.81	3.43	
Direction	1 – two way	1 – two way	1 – two way	1 – two way	1 – two way	1 – two way	1 – two way	
Name	Waikaka Stock Underpass	Waikaka Stream Culvert	Waiteti Stream Pipe Arch Culvert 3.9 x 2.5 m	Hawker's Pipe Arch Culvert 2.8 x 2.0 m	Puketutu Rail Overpass	Slaughterhouse Pipe Arch Culvert 6.3 x 4.0 m	Benneydale Pipe Arch Culvert 4.0 x 2.6 m	
Function	SH over stock underpass	SH over waterway	SH over waterway	SH over waterway	SH over railway	SH over waterway	SH over waterway	
Year built	2003	2003	1962	?	1987	1982	1962	
Design loading	–	–	–	–	HN_HO_72	other	–	
Drawings	–	–	TK261	–	2/114/8	2/114/3/7914	TK-262	
No. Drawings	0	0	–	–	–	–	–	
Drawings held at	–	–	–	–	–	–	–	
Drawings comment	–	–	–	–	–	–	–	
Cost ($)	?	?	?	?	275,000	130,000	?	
Structure type	stock underpass	culvert	culvert	culvert	culvert	culvert	culvert	
Foundations	spread footings	spread footings	other	other	spread footings	other	other	
Fill depth (m)	1.2	1.2	0.8	3	1.2	0.9	1.2	
Length of structure (m)	20	20	15.2	20	30	26.9	14.6	
Type	pipe	pipe	pipe arch	pipe arch	arch	pipe arch	pipe arch	
Invert Lining	concrete	none	none	none	none	none	none	

Notes to Table B12:
a SH = state highway
b RS = Route Station, or distance in kilometres along a state highway.

Table B13 Results 91–98 of the search of the BDS using 'arch' and 'multiplate' as search keywords.

Feature	Result number							
	91	92	93	94	95	96	97	98
Structure ID	33120	33121	33124	33127	33137	33144	33145	33164
BSN	–	–	–	–	2138	54	72	–
SH[a]	30	30	30	30	30	31	31	32
RS[b]	115	115	115	131	206	0	0	45
Distance	0.55	1.83	14	11.52	6.5	5.37	7.17	6.63
Direction	1 – two way	1 – two way	1 – two way	1 – two way	1 – two way	1 – two way	1 – two way	1 – two way
Name	Camel Road Pipe Arch 3.1 x 2.1 m	Zebra Road Pipe Arch 3.1 x 2.1 m	Waikaukau Pipe Arch Culvert 4.0 x 6.3 m	Tureporepo Pipe Arch ARMCO 4.8 x 3.2	Jacksons Pipe Arch 2.4 x 3.6	Mangamahoe ARMCO pipe culvert 3.0 diameter	Owaikura Stream Pipe Arch Culvert	Mangakowiriwiri Stream Culvert
Function	SH over waterway	SH over waterway	SH over waterway	SH over waterway	SH over waterway	SH over waterway	SH over waterway	SH over waterway
Year built	1959	1959	1973	1976	1975	1979	1979	1965
Design loading	–	–	HN_HO_72	H20_S16_T16	HN_HO_72	–	–	HN_HO_72
Drawings	–	–	RO 5339	RO 5036	5302/4	2/129/1/7924 RAB	2/129/4/7924 RAB	RO 4340
No. Drawings	–	–	–	–	–	–	–	–
Drawings held at	–	–	–	–	–	–	–	–
Drawings comment	–	–	–	–	–	3.0 diameter	–	ARMCO culvert 3.2 m diameter
Cost ($)	?	?	?	?	?	?	?	?
Structure type	culvert	culvert	culvert	culvert	culvert	culvert	culvert	culvert
Foundations	other	other	other	other	other	other	other	spread footings
Fill depth (m)	3.7	2.3	6.4	2.4	1	2.5	0.8	2.7
Length of structure (m)	26.8	27	40	25.9	22.4	17.5	21.3	19.5
Type	pipe arch	pipe arch	pipe arch	pipe arch	pipe	pipe	pipe arch	pipe
Invert Lining	none	none	none	none	none	none	none	none

Notes to Table B13:
a SH = state highway
b RS = Route Station, or distance in kilometres along a state highway.

Table B14 Results 99–105 of the search of the BDS using 'arch' and 'multiplate' as search keywords.

Feature	Result number						
	99	100	101	102	103	104	105
Structure ID	33189	33191	33237	33255	33276	33283	33287
BSN	431	528	1883	–	–	–	–
SH[a]	35	35	35	35	35	35	35
RS[b]	41	49	180	225	263	274	289
Distance	2.09	3.76	8.29	5.86	7.37	11.21	3.12
Direction	1 – two way	1 – two way	1 – two way	1 – two way	1 – two way	1 – two way	1 – two way
Name	Callaghan's ARMCO 3.5 x 2.1	Waiora ARMCO 4.2 x 3.0	Pepere Culvert	Te Matai Culvert	Mangapeka Culvert	Makatote	Mangaone Culvert
Function	SH over waterway	SH over waterway	SH over waterway	SH over waterway	SH over waterway	SH over waterway	SH over waterway
Year built	1970	1975	1984	1990	1974	1958	1985
Design loading	H20_S16_T16	HN_HO_72	HN_HO_72	HN_HO_72	H20_S16_T16	H20_S16	HN_HO_72
Drawings	PWG7125	PWN 6677	3/62/1/7304	3/66/24/7304	PWN 6545	PWG 4829	3/71/2/7304
No. Drawings	–	–	–	–	–	–	–
Drawings held at	–	–	–	–	–	–	–
Drawings comment	–	–	–	–	–	–	–
Cost ($)	?	?	?	114,000	?	?	?
Structure type	culvert	culvert	culvert	culvert	culvert	culvert	culvert
Foundations	spread footings	spread footings	spread footings	spread footings	spread footings	spread footings	spread footings
Fill depth (m)	2.4	6.4	0.8	1.1	2	3	2.5
Length of structure (m)	15.2	39.6	18.1	20	28.3	31.7	35.5
Type	pipe arch	arch	arch	pipe arch	multiple pipe	pipe arch	pipe
Invert Lining	other	none	concrete	none	asphalt	other	none

Notes to Table B14:
a SH = state highway
b RS = Route Station, or distance in kilometres along a state highway.

Table B15 Results 106–112 of the search of the BDS using 'arch' and 'multiplate' as search keywords.

Feature	Result number						
	106	107	108	109	110	111	112
Structure ID	33291	33293	35705	33302	33322	33324	33325
BSN	–	–	391	217	–	–	–
SH[a]	35	35	36	38	38	38	38
RS[b]	300	300	28	17	161	161	179
Distance	2.91	4.79	11.14	4.7	12.34	17.74	0.7
Direction	1 – two way	1 – two way	1 – two way	1 – two way	1 – two way	1 – two way	1 – two way
Name	Wallis Hill South Culvert	Glenroy	Hauraki Stream Culvert	Forestry ARMCO Underpass	Matai Culvert	Titirangi Culvert	Mahanga Culvert
Function	SH over waterway	SH over waterway	SH over waterway	SH over combination of stream, road, railway or other	SH over waterway	SH over waterway	SH over waterway
Year built	1960	1984	?	1995	1992	1993	1993
Design loading	H20_S16	HN_HO_72	–	HN_HO_72	HN_HO_72	HN_HO_72	HN_HO_72
Drawings	PWG 5297	3/72/1/7304	–	FGA 43/1	3/87/24/7304	3/87/26/7304	3/88/15/7304
No. Drawings	–	–	–	–	–	–	–
Drawings held at	–	–	–	–	–	–	–
Drawings comment	–	–	Taken over from Rotorua District Council 2005. No drawings available	7.5 diameter	–	–	–
Cost ($)	?	?	?	300,000	178,291	207,900	291,100
Structure type	culvert	culvert	culvert	culvert	culvert	culvert	culvert
Foundations	spread footings	spread footings	–	spread footings	spread footings	spread footings	spread footings
Fill depth (m)	2.2	2.4	–	1	5.1	5	19.8
Length of structure (m)	21.9	45.7	–	7.5	27	38	73
Type	pipe arch	pipe	pipe arch multiplate	pipe	pipe	pipe	pipe
Invert Lining	other	none	none	other	none	none	none

Notes to Table B15:
a SH = state highway
b RS = Route Station, or distance in kilometres along a state highway.

Table B16 Results 113–119 of the search of the BDS using 'arch' and 'multiplate' as search keywords.

Feature	Result number						
	113	114	115	116	117	118	119
Structure ID	33327	33422	33424	33426	33434	33435	33437
BSN	–	–	–	–	–	–	–
SH[a]	38	41	43	43	43	43	43
RS[b]	179	56	0	0	32	32	51
Distance	4.24	2.03	10.65	13.64	2.89	3.71	2.71
Direction	1 – two way	1 – two way	1 – two way	1 – two way	1 – two way	1 – two way	1 – two way
Name	Double Crossing Culvert	Hangareto Stream ARMCO Pipe Culvert 3.5 diameter	Manawawiri Stream	Toko Stream Tributary	Katuatua Stream	Mangaotuku No. 5 Culvert	Pohokura Stream
Function	SH over waterway	SH over waterway	SH over waterway	SH over waterway	SH over waterway	SH over waterway	SH over waterway
Year built	1980	1965	1974	1963	1969	1978	1979
Design loading	HN_HO_72	–	HN_HO_72	H20_S16_T16	H20_S16_T16	HN_HO_72	HN_HO_72
Drawings	3/88/3/7304	–	NP 8362	NP 6933	NP 7680	4/82/2/7924/ 1-4	4/83/5/7924/ 1-2
No. Drawings	–	–	–	–	–	–	–
Drawings held at	–	–	–	–	–	–	–
Drawings comment	–	3.5 m diameter; RP corrected from old 52/6.03	–	–	–	–	–
Cost ($)	90,400	?	30,000	8,800	8,000	30,000	50,000
Structure type	culvert	culvert	culvert	culvert	culvert	culvert	culvert
Foundations	spread footings	spread footings	–	–	–	–	–
Fill depth (m)	8	4	2.5	2.5	2.1	0.9	1.6
Length of structure (m)	48.2	70	30.5	25.6	26.8	20	21.5
Type	pipe	pipe	arch	multiple pipe	pipe	arch	arch
Invert Lining	other	none	none	–	–	–	–

Notes to Table B16:
a SH = state highway
b RS = Route Station, or distance in kilometres along a state highway.

Table B17 Results 120–126 of the search of the BDS using 'arch' and 'multiplate' as search keywords.

Feature	Result number						
	120	121	122	1123	124	125	126
Structure ID	33438	33442	33443	33444	33456	33477	35277
BSN	600	–	–	–	1066	–	–
SH[a]	43	43	43	43	43	45	45
RS[b]	57	65	65	80	111	15	15
Distance	2.97	15.13	15.15	0.05	5.59	1.8	4.25
Direction	1 – two way	1 – two way	1 – two way	1 – two way	1 – two way	1 – two way	1 – two way
Name	Awahou Stream Culvert	Tahora Railway Underpass	Tahora Culvert (Waiau)	Tahora Paroa	Nevin's Hill Culvert	Telford Stock Underpass	Stock Underpass
Function	SH over waterway	SH over railway	SH over waterway	SH over waterway	SH over waterway	SH over stock underpass	SH over combination of stream, road, railway or other
Year built	1979	1980	1980	1980	1972	1997	1997
Design loading	HN_HO_72	HN_HO_72	HN_HO_72	HN_HO_72	HN_HO_72	HN_HO_72	HN_HO_72
Drawings	4/83/4/7924/1-3	4/84/2/7404/1-5	4/84/2/7404/1-5	4/85/6/7924/1-2	–	–	–
No. Drawings	–	–	–	–	–	–	–
Drawings held at	–	–	–	–	–	–	–
Drawings comment	3.6m x 2.3 m	–	–	–	–	–	–
Cost ($)	40,000	?	?	23,000	?	40,000	?
Structure type	culvert	culvert	culvert	culvert	culvert	stock underpass	stock underpass
Foundations	–	spread footings	–	other	spread footings	–	–
Fill depth (m)	0.7	1.7	7.9	0.7	1	–	–
Length of structure (m)	19.2	39.6	46.3	20.1	14	–	20
Type	arch	arch	arch	pipe	pipe arch	arch	arch
Invert Lining	–	–	–	–	asphalt	concrete	concrete

Notes to Table B17:
a SH = state highway
b RS = Route Station, or distance in kilometres along a state highway.

Table B18 Results 127–133 of the search of the BDS using 'arch' and 'multiplate' as search keywords.

Feature	Result number						
	127	128	129	130	131	132	133
Structure ID	33481	33491	33601	33643	33654	33662	34307
BSN	–	–	178	–	–	–	–
SH[a]	45	45	50	54	57	57	67
RS[b]	15	28	12	38	0	26	30
Distance	9.24	12.89	5.77	8.02	11.03	7.6	14
Direction	1 – two way	1 – two way	1 – two way	1 – two way	1 – two way	1 – two way	1 – two way
Name	Shorrock Stock Underpass	Kapoaiaia Stream	Mill Stream Culvert	Baxter's Underpass (Stock)	Waoku Stream Culvert	Tokomaru Pedestrian Underpass	McMaster's Creek Culvert
Function	SH over stock underpass	SH over waterway	SH over waterway	SH over stock underpass	SH over waterway	SH over combination of stream, road, railway, or other	SH over waterway
Year built	1997	1982	1987	1994	1995	1995	1958
Design loading	HN_HO_72	HN_HO_72	HN_HO_72	–	–	–	–
Drawings	–	40/90/7/7404/1	3/90/18/7304	–	–	95/6 S1	–
No. Drawings	–	–	–	–	–	–	–
Drawings held at	–	–	–	–	–	–	–
Drawings comment	–	–	–	–	–	–	–
Cost ($)	105,000	335,000	137,000	?	?	?	?
Structure type	stock underpass	culvert	culvert	stock underpass	culvert	pedestrian subway	culvert
Foundations	–	spread footings	spread footings	other	–	other	spread footings
Fill depth (m)	–	2.3	0.8	1.5	–	0.6	1.5
Length of structure (m)	19	43.9	24.5	16.1	20	12.7	13
Type	arch	arch	arch	arch	pipe	arch	arch
Invert Lining	concrete	–	concrete	concrete	–	concrete	none

Notes to Table B18:
a SH = state highway
b RS = Route Station, or distance in kilometres along a state highway.

Table B19 Results 134–140 of the search of the BDS using 'arch' and 'multiplate' as search keywords.

Feature	Result number						
	134	135	136	137	138	139	140
Structure ID	34475	34713	34728	34733	34801	34803	34813
BSN	1081	278	153	420	–	–	–
SH[a]	73	80	82	82	87	87	90
RS[b]	107	17	0	42	82	82	17
Distance	1.09	10.8	15.3	0	5.86	10.3	3.08
Direction	1 – two way	1 – two way	1 – two way	1 – two way	1 – two way	1 – two way	1 – two way
Name	Manson's Creek Culvert	Stock Underpass	Arno Culvert	Grassy Hills Stream Culvert	Annett's Creek Culvert	Scrubburn Culvert	Black Gully Stream Culvert
Function	SH over waterway	SH over combination of stream, road, railway or other	SH over waterway	SH over waterway	SH over waterway	SH over waterway	SH over waterway
Year built	1990	?	1982	1975	1996	1986	1981
Design loading	HN_HO_72	–	HN_HO_72	H20_S16_T16	HN_HO_72	HN_HO_72	HN_HO_72
Drawings	6/141/9/7604	–	6/168/6/7904/2	6/171/1/7624	WCS 7/112/10	7/112/3/7714	7042/1 to 7042/5
No. Drawings	–	–	–	–	–	0	–
Drawings held at	–	–	–	–	–	–	–
Drawings comment	–	–	–	–	–	–	–
Cost ($)	140,000	?	30,000	?	?	130,000	37,300
Structure type	culvert	stock underpass	culvert	culvert	culvert	culvert	culvert
Foundations	spread footings	spread footings	spread footings	spread footings	–	spread footings	-
Fill depth (m)	1	4	1.5	0.8	7	4.6	0.9
Length of structure (m)	25.3	37	23.3	20.7	24	33	9.2
Type	pipe arch	pipe arch	arch	arch	pipe	arch	pipe
Invert Lining	concrete	other	other	–	concrete	none	–

Notes to Table B19:
a SH = state highway
b RS = Route Station, or distance in kilometres along a state highway.

Table B20 Results 141–147of the search of the BDS using 'arch' and 'multiplate' as search keywords.

Feature	Result number						
	141	142	143	144	145	146	147
Structure ID	34852	34853	34856	35190	35203	31476	31482
BSN	–	–	–	83	383	228	494
SH[a]	94	94	94	1A	1A	1N	1N
RS[b]	163	163	177	0	0	20	44
Distance	3.85	4.66	6.74	0.83	3.83	2.79	5.4
Direction	1 – two way	1 – two way	1 – two way	1 – two way	1 – two way	1 – two way	1 – two way
Name	Swamp Creek Culvert	Mistletoe Creek Culvert	Boyd Creek Culvert	Weiti Stream Culvert	Orewa Deep Gully Culvert	Karatia Creek Culvert No. 170	Wairahi No. 2 Culvert No. 182
Function	SH over waterway	SH over waterway	SH over waterway	SH over waterway	SH over waterway	SH over waterway	SH over waterway
Year built	1966	1966	1979	1999	1999	1977	1977
Design loading	H20_S16_T16	H20_S16_T16	–	–	–	HN_HO_72	HN_HO_72
Drawings	EIN 2916	EIN 2962	7/149/7	–	–	9/60/2/7114	9/61/4/7114
No. Drawings	–	–	–	–	–	1	1
Drawings held at	–	–	–	–	–	Opus, Whangarei	Opus, Whangarei
Drawings comment	–	–	–	–	–	–	–
Cost ($)	?	?	?	?	?	?	?
Structure type	culvert	culvert	culvert	culvert	culvert	culvert	culvert
Foundations	other	other	other	spread footings	spread footings	spread footings	spread footings
Fill depth (m)	1	1.5	2.2	6	12	1.5	1.8
Length of structure (m)	10	10	20	120	200	13.6	19
Type	arch	pipe	pipe	pipe	pipe	pipe arch	pipe arch
Invert Lining	other	none	none	concrete	concrete	concrete	none

Notes to Table B20:
a SH = state highway
b RS = Route Station, or distance in kilometres along a state highway.

Table B21 Results 148–154 of the search of the BDS using 'arch' and 'multiplate' as search keywords.

Feature	Result number						
	148	149	150	151	152	153	154
Structure ID	31483	31485	31496	31580	31589	35187	35204
BSN	498	569	842	2883	3057	3977	3983
SH[a]	1N	1N	1N	1N	1N	1N	1N
RS[b]	44	44	83	273	303	386	398
Distance	5.8	12.91	1.21	15.27	2.68	11.68	0.32
Direction	1 – two way	1 – two way	1 – two way	1 – two way	1 – two way	1 – two way	1 – two way
Name	Waiarahi No. 1 Culvert No. 183	Ngataki Stream Culvert No. 185	Big Flat Outfall Culvert No. 195	Halse's Stock Underpass	Robert's Stock Underpass	John's Creek Culvert No. 1	John's Creek Culvert No. 2
Function	SH over waterway	SH over waterway	SH over waterway	SH over stock underpass	SH over stock underpass	SH over waterway	SH over waterway
Year built	1977	1975	1975	1994	1994	1999	1999
Design loading	HN_HO_72	HN_HO_72	H20_S16_T16	HN_HO_72	HN_HO_72	–	–
Drawings	9/61/5/7114	9/62/1/7114 and 9/62/7/7114	–	9/16/24/7914	9/17/32/7914	1/23/98/7104	1/23/98/7104
No. Drawings	1	3	0	1	1	–	–
Drawings held at	Opus, Whangarei	Opus, Whangarei	–	Opus, Whangarei	Opus, Whangarei	–	–
Drawings comment	–	–	Ex-FNDC structure. No drawings exist. Construction date estimated by RBC 03/05	–	–	–	–
Cost ($)	?	?	?	82,000	80,000	?	?
Structure type	culvert	culvert	culvert	stock underpass	stock underpass	culvert	culvert
Foundations	spread footings	spread footings	spread footings	spread footings	spread footings	spread footings	spread footings
Fill depth (m)	0.75	0.5	0.4	0.6	0.6	7	2
Length of structure (m)	15.4	15.2	17.4	24	21	137	120
Type	pipe arch	arch	pipe	arch	arch	pipe	pipe
Invert Lining	none	none	concrete	other	other	none	none

Notes to Table B21:
a SH = state highway
b RS = Route Station, or distance in kilometres along a state highway.

Table B22 Results 155–98 of the search of the BDS using 'arch' and 'multiplate' as search keywords.

Feature	Result number						
	155	156	157	158	159	160	161
Structure ID	35211	35212	35213	31710	35548	31733	31752
BSN	4065	4069	4078	5502	6546	6997	7759
SH[a]	1N	1N	1N	1N	1N	1N	1N
RS[b]	398	398	398	543	638	695	763
Distance	8.53	8.94	9.78	7.19	16.6	4.74	12.93
Direction	2 – increasing	2 - increasing	2 – increasing	1 – two way	1 – two way	1 – two way	1 – two way
Name	Wright Rd Culvert (Southbound)	Wright Lonely Culvert (Southbound)	Lonely Track Culvert (Southbound)	Waitawhiriwhiri Pipe Arch Culvert	3.6 Dia ARMCO Culvert	Waipouwerawera Stream ARMCO Culvert	Makahikatoa Stream ARMCO 2.7 m diameter
Function	SH over waterway	SH over waterway	SH over waterway	SH over waterway	SH over waterway	SH over waterway	SH over waterway
Year built	1999	1999	1999	1973	1995	1966	1985
Design loading	HN_HO_72	–	–	–	HN_HO_72	–	–
Drawings	1/23/99/7104	1/23/99/7106 R1	1/23/99/7104 R1	HCC SW/S	122891/ 301-303	RO 4431	4/3/2/7004
No. Drawings	–	–	–	–	3	–	–
Drawings held at	–	–	–	–	BBO[c]	–	–
Drawings comment	–	–	–	RP corrected from 533/17.19 3.8.05	–	–	–
Cost ($)	?	?	?	?	?	?	634,000
Structure type	culvert	culvert	culvert	culvert	culvert	culvert	culvert
Foundations	spread footings	–	–	spread footings	spread footings	spread footings	–
Fill depth (m)	5	3	12	11	8	22	22
Length of structure (m)	87	106	136	113.7	70	97	89.4
Type	pipe	pipe	pipe	pipe arch	pipe	pipe	pipe
Invert Lining	none	none	none	asphalt	concrete	none	none

Notes to Table B22:
a SH = state highway
b RS = Route Station, or distance in kilometres along a state highway.
c BBO = Bloxham Burnett and Olliver Ltd, Hamilton

Table B23 Results 162–169 of the search of the BDS using 'arch' and 'multiplate' as search keywords.

Feature	Result number							
	162	163	164	165	166	167	168	169
Structure ID	35583	31764	31707	31777	31779	31780	31781	31782
BSN	8174	8302	5400	8559	8572	8587	8593	8604
SH[a]	1N	1N	1N	1N	1N	1N	1N	1N
RS[b]	815	828	855	855	855	855	855	855
Distance	2.35	2.23	0.17	0.91	2.18	3.68	4.29	5.41
Direction	1 – two way	1 – two way	1 – two way	1 – two way	1 – two way	1 – two way	1 – two way	1 – two way
Name	Waiouru Rail Overpass	Turangarere Culvert	Arch Culvert	Culvert 2.1 m diameter	Stock Underpass	Stock Underpass	Mangaweka Stream Culvert 4.27 m Diameter	Arch Culvert 2.41 x 3.81 m
Function	SH over railway	SH over waterway	SH over waterway	?	SH over stock underpass	SH over combination of stream, road, railway or other	SH over waterway	SH over waterway
Year built	1999	1986	1959	?	?	?	?	?
Design loading	HN_HO_72	HN_HO_72	HN_HO_72	–	–	–	–	–
Drawings	Payne Swell Ltd. 2400162 sht 16–20	4/8/9/7404/1	HDO8802	–	–	–	–	–
No. Drawings	5	–	–	–	–	–	–	–
Drawings held at	–	–	–	–	–	–	–	–
Drawings comment	ARMCO Type 46EA13	–	2.1 m H x 1.8 m W	2.9 m diameter	2.9 m diameter	2.9 m diameter	–	–
Cost ($)	1,600,000	?	?	?	?	?	?	?
Structure type	culvert	culvert	culvert	culvert	stock underpass	stock underpass	culvert	culvert
Foundations	spread footings	spread footings	spread footings	spread footings	spread footings	spread footings	spread footings	–
Fill depth (m)	1.2	2.5	4	–	0.7	1	4	4
Length of structure (m)	107.3	37.8	70	100	20	25	50	50
Type	pipe arch	pipe	pipe	pipe	pipe	pipe arch multiplate	pipe arch multiplate	pipe arch multiplate
Invert Lining	other	concrete	concrete	none	concrete	concrete	concrete	concrete

Notes to Table B23:
a SH = state highway
b RS = Route Station, or distance in kilometres along a state highway.

Table B24 Results 170–176 of the search of the BDS using 'arch' and 'multiplate' as search keywords.

Feature	Result number						
	170	171	172	173	174	175	176
Structure ID	31783	35584	35586	35585	31801	31802	31815
BSN	8605	–	8885	8886	9053	9076	9868
SH[a]	1N	1N	1N	1N	1N	1N	1N
RS[b]	855	885	885	885	901	901	985
Distance	5.42	3.25	3.47	3.48	4.32	6.62	1.83
Direction	1 – two way	1 – two way	1 – two way	1 – two way	1 – two way	1 – two way	1 – two way
Name	Stock Underpass	Vinegar Hill Rail Overpass	Porewa Stream Culvert	Porewa Stream Overflow	Maungaraupi Stream Culvert	Maungaraupi Stock Underpass	Ohau Pedestrian Underpass
Function	SH over combination of stream, road, railway or other	SH over railway	SH over waterway	SH over waterway	SH over waterway	SH over combination of stream, road, railway or other	SH over combination of stream, road, railway or other
Year built	?	1999	1999	1999	1991	1991	1992
Design loading	–	HN_HO_72	HN_HO_72	HN_HO_72	HN_HO_72	HN_HO_72	–
Drawings	–	Payne Sewell Ltd 2400103 sheet 29–30	Payne Sewell Ltd 2400103 sheet 31	Payne Sewell 2400103 sheet 31	4/13/13/7404/13	4/13/13/7404/18	–
No. Drawings	–	2	1	1	–	–	–
Drawings held at	–	–	–	–	–	–	–
Drawings comment	2.9 m diameter	ARMCO model 42EA12	5.34 m span; 3.4 m rise	5.34 m span; 3.4 m rise	–	–	–
Cost ($)	?	300,000	187,000	187,000	650,000	82,000	?
Structure type	stock underpass	culvert	culvert	culvert	culvert	stock underpass	pedestrian subway
Foundations	spread footings	spread footings	spread footings	spread footings	spread footings	spread footings	other
Fill depth (m)	2	2	6.8	6.8	6.7	1	1.5
Length of structure (m)	25	35.8	53	53	48	30.2	37.3
Type	pipe arch multiplate	pipe arch	pipe arch	pipe arch	pipe	arch	arch
Invert Lining	concrete	other	none	none	concrete	concrete	concrete

Notes to Table B24:
a SH = state highway
b RS = Route Station, or distance in kilometres along a state highway.

Table B25 Results 177–183 of the search of the BDS using 'arch' and 'multiplate' as search keywords.

Feature	Result number						
	177	178	179	180	181	182	183
Structure ID	31829	36002	31944	35295	35297	31967	–
BSN	###	29	1969	2067	2085	2510	–
SH[a]	1N	1S	1S	1S	1S	1S	1S
RS[b]	1012	0	195	195	195	247	601
Distance	7.53	2.91	1.9	10.6	12.4	3.96	15.11
Direction	1 – two way	1 – two way	1 – two way	1 – two way	1 – two way	1 – two way	1 – two way
Name	Muaupoko ARMCO Culvert	Elevation Crossing Rail Overpass	Buntings Creek Culvert	Homestead Gully Culvert	Hawkswood Stream No. 1 Culvert	Cobbolds Creek Culvert	Wainakarua Overbridge
Function	SH over waterway	SH over railway	SH over waterway	SH over waterway	SH over waterway	SH over waterway	SH over railway?
Year built	1957	2005	1995	2001	2001	1983	?
Design loading	H20_S16	HN_HO_72	HN_HO_72	HN_HO_72	HN_HO_72	HN_HO_72	–
Drawings	P1386/ Sheet 1	C003, C116 + Turbosider Drawing 8497	ROYDS 69220/C12	MW69762.02	MW69762.02 6/8/5/7604	6/11/9/7604	–
No. Drawings	–	18	–	–	0	–	–
Drawings held at	–	Connell Wagner	–	–	–	–	–
Drawings comment	–	–	–	–	–	–	7.1 span x 5.4 height
Cost ($)	?	?	?	?	?	135,000	–
Structure type	culvert	culvert	culvert	culvert	culvert	culvert	–
Foundations	other	–	spread footings	–	–	spread footings	–
Fill depth (m)	0.5	3.2	1.1	18.5	15.1	5	1.5
Length of structure (m)	23	60.3	23	101	95	32.5	–
Type	pipe	multiplate arch	pipe arch	pipe	pipe	arch	horseshoe arch
Invert Lining	concrete	none	concrete	concrete	concrete	concrete	–

Notes to Table B25:
a SH = state highway
b RS = Route Station, or distance in kilometres along a state highway.

Table B26 Results 184–188 of the search of the BDS using 'arch' and 'multiplate' as search keywords.

Feature	Result number				
	184	185	186	187	188
Structure ID	35244	32068	32069	32144	33003
BSN	–	–	–	8814	–
SH[a]	1S	1S	1S	1S	MIS
RS[b]	618	618	618	872	229
Distance	10.21	15.12	15.13	9.42	9.4
Direction	1 – two way	1 – two way	1 – two way	1 – two way	1 – two way
Name	Ngutukaka Creek Culvert	Trotter's Subway	Trotter's Creek Culvert	Ota Creek Culvert	Northgate Railway Tunnel (under SH3)
Function	SH over waterway	SH over waterway	SH over waterway	SH over waterway	SH over railway
Year built	2000	1995	1995	1984	1982
Design loading	HN_HO_72	HN_HO_72	HN_HO_72	HN_HO_72	HN_HO_72
Drawings	MW801/47426	–	–	7/392/9/7934	4/195/3
No. Drawings	–	–	–	–	–
Drawings held at	–	–	–	–	–
Drawings comment	–	–	–	–	Runs under SH3
Cost ($)	?	?	?	?	900,000
Structure type	culvert	culvert	culvert	culvert	tunnel
Foundations	–	–	–	other	other
Fill depth (m)	12	3.5	3	1.4	0.8
Length of structure (m)	90	36	44	26.8	106.3
Type	pipe	pipe	pipe	arch	arch
Invert Lining	none	concrete	none	none	concrete

Notes to Table B26:
a SH = state highway
b RS = Route Station, or distance in kilometres along a state highway.

Appendix C Abbreviations and acronyms

ν:	Poisson's ratio
ψ:	soil dilation angle
ϕ':	soil friction angle (effective stress)
ΔL:	maximum element size in the model
γ_{max}:	maximum free-field shear strain in the soil
3D:	three-dimensional
AASHTO:	American Association of State Highway and Transportation Officials
AFPS:	*Association Française du Génie Parasismique* (French Association for Seismic Engineering)
AFTES:	*Association Française des Tunnels et de l'Espace Souterrain* (French Tunnelling Association)
AS:	Australian Standard
BBO:	Bloxham Burnett and Olliver Ltd, Hamilton
BDS:	Bridge Descriptive System
BS:	British Standard
c:	soil cohesion in kiloPascals (kPa)
CMP:	Corrugated metal pipe
C_S:	shear wave velocity in the soil
E:	Young's modulus, GPa
EERI:	Earthquake Engineering Research Institute
f'_C:	concrete compressive strength, MPa
FLAC:	Fast Lagrangian Analysis of Continua, software from Itasca
F_N:	maximum normal force on culvert at culvert-soil interface
F_{Smax}:	maximum shear force on culvert-soil interface in the Coulomb shear strength criterion
F_V:	ground coefficient, a scaling factor depending on the site and ground class
g:	(preceded by a number) proportion of acceleration caused by gravity
G:	soil shear modulus (small strain) MPa
GNS:	Geological and Nuclear Science Ltd
GPa:	gigaPascals
H:	thickness of soil layer
Hz:	frequency in Hertz
I:	second moment of inertia, m^4, although usually per metre of culvert in this work, m^3
K:	soil bulk modulus (small strain) MPa
LRFD:	load and resistance factor design
mE:	metres east
MM:	Modified Mercalli intensity
mN:	metres north
MPa:	megaPascals
N16W:	16 degrees west of north, direction of earthquake component recording
N74E:	74 degrees east of north, direction of earthquake component recording

N90E: ninety degrees east of north, direction of earthquake component recording
N90W: ninety degrees west of north,
NIMT: North Island Main Trunk railway
NZMG: New Zealand map grid
NZS: New Zealand Standard
NZTA: The NZ Transport Agency
PGA: Peak ground acceleration
PGV: Peak ground velocity
PI: plasticity index
r_g: radius of gyration of the corrugations
RP: Route Position
RS: Route Station
S00E: zero degrees east of south, direction of earthquake component recording
SA_1: spectral acceleration in g at 1 second period for 5% damping at rock sites
SH: State Highway
SIMT: South Island Main Trunk railway
S_S: maximum clear span of the culvert between corrugation crests
Su: undrained shear strength of the soil
UT: universal time, used for earthquake recording times
V_S: soil particle velocity as shear wave passes
w: moisture content of the soil
Z: section modulus, m^3, although usually per metre of culvert in this work, m^2
κ: the crown moment coefficient
ρ: soil density, kN/m^3

Earthquake Performance of Long Span Arch Culverts

NZ Transport Agency
Research Report 366